A GOLD DECORATION STUDY OF THE SUZUKI PHASE $6NaCl\text{-}MnCl_2$ in NaCl

ALFREDO GOMEZ

A DISSERTATION SUBMITTED FOR THE DEGREE OF DOCTOR OF PHILOSOPHY

UNIVERSITY OF WARWICK
DEPARTMENT OF PHYSICS

DECEMBER 1978

DECLARATION

This dissertation is submitted in support of my application for admission to the degree of Doctor of Philosophy.

It contains an account of the research I undertook at the Department of Physics of the University of Warwick during the period October 1974 - June 1977 under the supervision of Mr. G. A. Bassett. No part of this thesis has been previously submitted by me to any other University. Except where otherwise stated, the work described is my own.

A. Gómez
Department of Physics
University of Warwick
October 1978

ABSTRACT

In this research the gold decoration technique has been used to study the Suzuki phase precipitates $6NaClMnCl_2$ in Mn doped crystals slowly cooled from 650°C.

The size distribution of the precipitates has been analyzed and found not to conform to the simple predictions of the Lifschitz Wagner theory for Ostwald Ripening; although in some instances a good fit was obtained to the theoretical distribution curves for bulk - diffusion and dislocation diffusion controlled processes, in disagreement with earlier treatments. Most precipitates have been found to be cubes in agreement with previous observations (9).

Irregular structures, composed exclusively of steps, having an overall square shape and being highly localized are reported. These structures are believed to be the result of the interaction of the cleavage crack with precipitates close but not on the cleavage surfaces.

The interrelations between the cleavage and slip structures with the precipitates have also been studied and a simple model that explains qualitatively the observed features is proposed. According to this model the peculiar decoration features of the Mn doped crystals arise as a result of different propagation speeds for the cleavage crack on the surface and on the precipitate areas.

ACKNOWLEDGEMENTS

I wish to thank to Mr. C.A. Bassett for his help and encouragement which made the present work possible. I would like to thank Prof. A.J. Forty for making available to me the facilities of the laboratory. I also thank the British Council and the National Council for Science and Technology of México for providing financial support.

I am grateful to Dr. M.L. Lewis and Dr. C.R. Hall for their hospitality at the ceramics research group; to the technical staff of the Department of Physics, in particular to Mr. G. Smith, and to Dr. M. J. Yacaman for many valuable discussions.

My thanks are also due to my wife Yolanda for typing the manuscript and to P. Gómez for assistance with the drawings.

Special thanks are due to Dr. O. Cano and A. Cordero for permission to use their unpublished X-ray data on NaCl-$InCl_2$ crystals, and to the crystal growth group (UNAM) for providing the crystals used. The impurity contents determinations were made by Dr. D.M. Evans (Birmingham) and E. Camarillo (UNAM) whose assistance is kindly acknowledged.

I am also grateful to Miss S. Callanan for typing the final corrections.

TABLE OF CONTENTS

FIGURES

Chapter 3

3-7 Same sample as in figure 3-6, showing an example of the structures described in the text as "irregular structures". (84000X) 23

3-8 Sample 105; region of the crystal surface close to the point where cleavage was started. The slip steps present confirm the fact that the square structures (Suzuki precipitates) are aligned along 100 (84000 X). 25

3-9 A sample of type II (chapter 2). The nuclei of manganese oxide can be appreciated in the lower part of this picture, they correspond to the surface exposed to air during the heating (linear cooling at 11°C/h from 650°C). The upper part shows the vacuum cleaved and decorated surface. The boundary between the two surfaces is also shown. The precipitates (not shown in this figure) are aligned with their sides parallel to this boundary (14000 X). 25

3-10 The diffraction pattern of sample 98, showing the preferential orientations for gold onto NaCl. The central figure is the image of the same region from which the diffraction pattern was taken. Camera length = 76 cm, magnification on plate 66000 X, on print 110000 X. The diffraction pattern-image angle at this setting is 129°. From the plate the angle between the side of the precipitate and a (200) spot is 35° which compares favourably with expected $39^{\circ} \equiv 129^{\circ}$ (mod. 90°). 25

TABLES

CHAPTER 1

INTRODUCTION AND REVIEW

1.1 Introduction

The problem of the properties of doped crystals has received considerable attention and is regarded as one of the most important in the fields of metallurgy and materials science.

The reasons for this are manifold: firstly, the fact that the impurities within a crystal control largely its electronic properties shows that an understanding of the effect of the dopant is of both scientific and technological importance; secondly, the mechanical properties of the materials are also affected by the impurities present. As a matter of fact nearly all the properties of solid materials depend to some extent on the nature and amount of foreign species present, a list of such properties should include the Ionic Conductivity, the optical properties, magnetic properties and many others.

All the properties mentioned depend considerably on the "state" in which the impurities are, that is on whether they are forming a solid solution or diverse phases.

Among those the materials in which the state and effect of the impurities have been studied, the alkali halides occupy a special place. There are several factors contributing to the suitability of these materials, among them are:

1°) These materials are relatively easy to grow as single crystals.

2°) Impurities can be incorporated into their lattices, either substitutionally or interstitially.

3°) They are well characterized.

4°) They can be studied by a great variety of techniques such as Electron

paramagnetic resonance (E.P.R.), ionic conductivity (I.C.), ionic thermocurrents (I.T.C.), electron microscopy (replication, decoration or direct), scanning electron microscopy, X-ray analysis and many others.

In this research some aspects of the formation of the so called "Suzuki" phases in NaCl doped with Mn ($NaCl:MnCl_2$ system) are studied, the primary technique used being transmission electron microscopy of Gold decorated surfaces.

Sections 1-2, 1-3, and 1-4 of this chapter are devoted to a review of the field of Suzuki phases in alkali-halides, and in section 1-5 the plan of the present research is presented.

1.2 Suzuki Phases, Their Existence and Structure.

While studying by X-ray diffraction methods NaCl crystal grown with $CdCl_2$ (about 10% mol) Suzuki, (1) found that a metastable phase precipitates out of the $NaCl-CdCl_2$ solid solution. This phase has the stoichiometry $6NaCl\,CdCl_2$ and a f.c.c. structure with a lattice parameter a_s twice as large as the corresponding parameter a_n of the NaCl. The unit cell of the $6NaCl\,CdCl_2$ has the structure shown schematically in figure 1-1 from which it can be seen that it consists of alternating layers of two kinds on (100) planes, one layer being similar to (100) planes of NaCl and the other similar to (100) planes of NaCl in which some Na ions have been replaced by Cd ions and vacancies. This phase grows in an orientation parallel to that of the NaCl, i.e.

$$[100]_{NaCl} \,//\, [100]_{6NaCl\,CdCl_2} \text{ and } (001)_{NaCl} \,//\, (001)_{6NaCl\,CdCl_2}$$

Figure 1-2 shows the phase diagram for the $NaCl:CdCl_2$ system obtained by Suzuki in the low $CdCl_2$ concentration region. It is interesting to

Figure 1-1 Schematic representation of the structure of Suzuki phases. The two illustrations shown represent the two different kinds of (100) layers. The arrows illustrate the displacement of the anions.

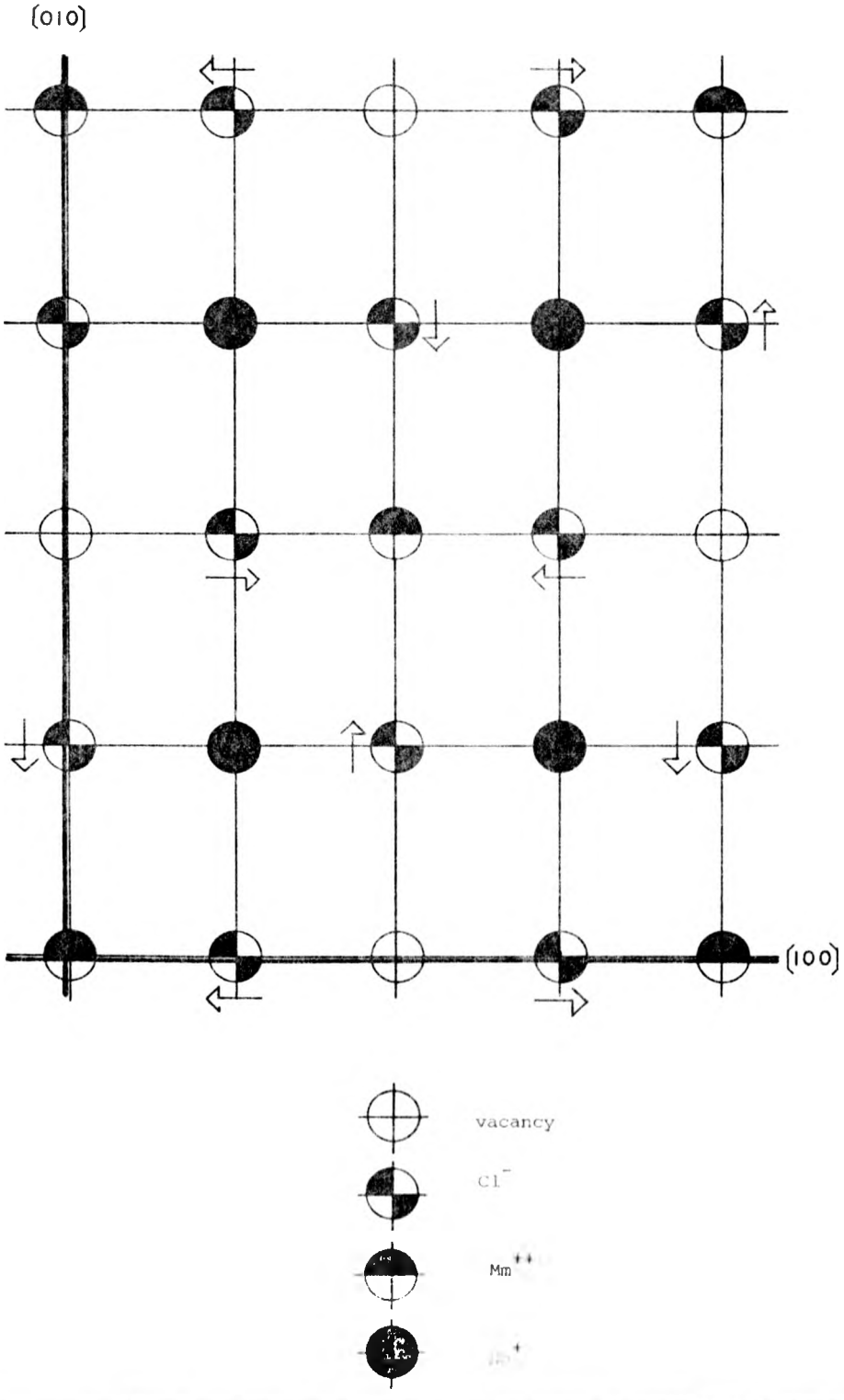
(010)
(100)
vacancy
Cl^-
Mn^{++}
Fe^{++}

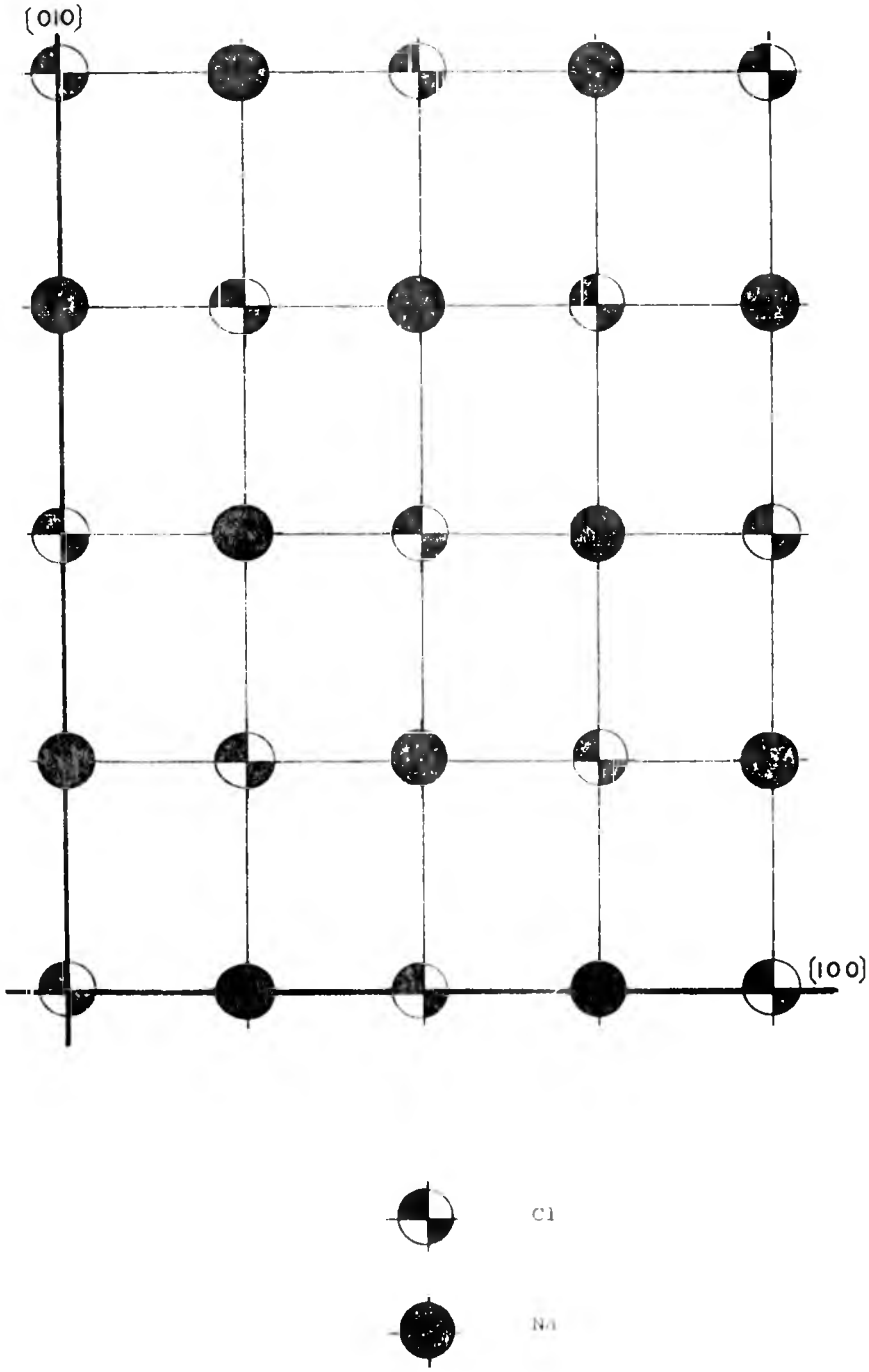
(010)
(100)
Cl
Na

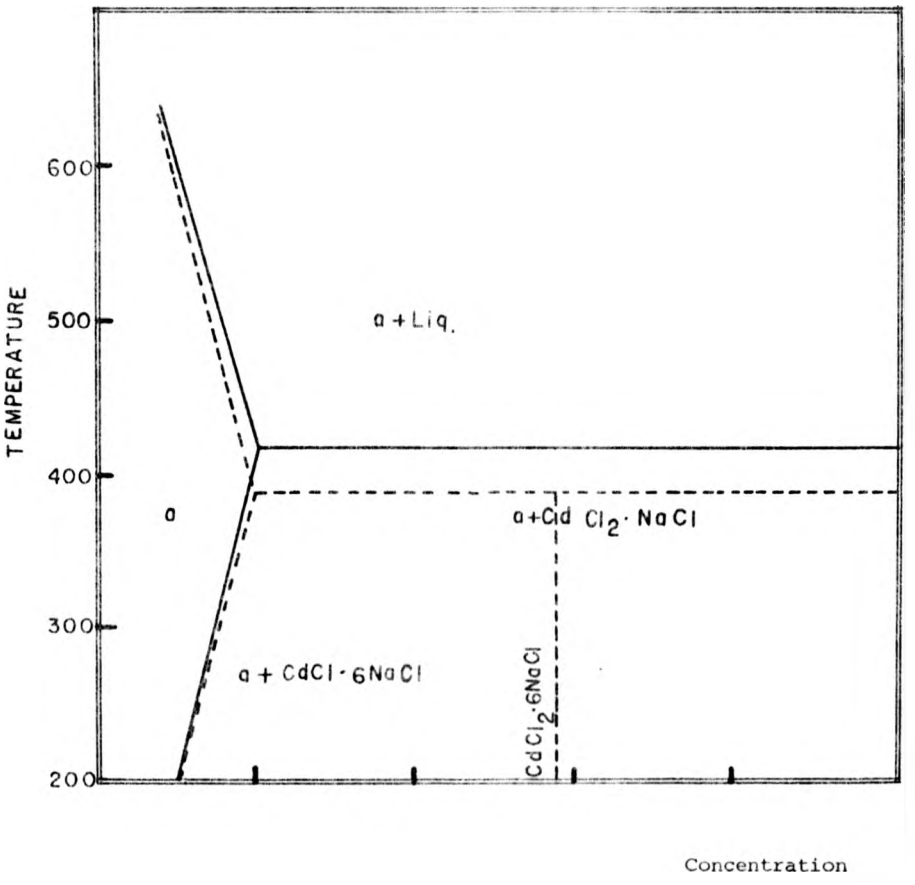

Figure 1-2 The phase diagram for NaCl: $CdCl_2$ as determined by Suzuki (1). The dotted line represents the metastable "Suzuki" phase.

notice that these observations were carried out in two kinds of crystals, one of them consisted of samples with the phases α ($NaCl-CdCl_2$ solid solution) $6NaClCdCl_2$ and $2NaClCdCl_2$ and the other consisted of $6NaClCdCl_2$ single crystals.

Similar phases have been found to precipitate in other systems such as $NaCl:MnCl_2$ (2), $LiF:MgCl_2$ (3), $NaCl:MgCl_2$ (4), $LiF:ZnF_2$ (5) and $NaCl:FeCl_2$ (6). These phases have all the stoichiometry $6MXNX_2$ where M represents the alkali metal ion, X the halogen ion and N the cationic divalent ion; and they have a structure analogous to that shown in figure 1-1 for the $6NaClCdCl_2$. For this reason they are collectively referred to as Suzuki Phases. In the case of some alkali halides doped with divalent impurities, phases can precipitate which are not Suzuki phases; examples of this are the systems $NaCl-CaCl_2$ (7), $NaCl-BaCl_2$ (8) and $NaCl-ZnCl_2$ (9) where the precipitates have been found to be the corresponding chloride NX_2. The precipitates in the system $NaCl-SrCl_2$ have been reported to be $SrCl_2$ (8) although there is a study suggesting that they might be Suzuki precipitates (10). There is some evidence that the precipitates in the systems $NaCl-NiCl_2$ (11) $KCl-PbCl_2$ (12,13), $LiF-MnCl_2$, $KCl-MnCl_2$, $LiCl-MnCl_2$ $NaBr-MnCl_2$ and $NaCl-CoCl_2$ (14) are Suzuki phases.

The detailed crystallographic nature of the Suzuki phases has been analyzed by several authors. Suzuki (1), Sors (5) and Toman (15) studied the $NaCl:CdCl_2$ system (by X-ray methods), Chapman and Lilley (2) and Sors (5) and Van Loon and Idjo (16) studied the $NaClMnCl_2$ system (these last authors used X-ray and neutron diffraction methods on Suzuki Phase crystals), Lilley and Newkirk (3) and Sors (5) studied the $LiF-MgF_2$ system, and the systems $NaCl:FeCl_2$ and $NaCl:MgCl_2$ have been analyzed by Van Loon and Idjo (16). In these works it has been established that in the Suzuki phases the anions next to a vacancy are displaced with

respect to the positions they would occupy in a perfect NaCl lattice; these anion displacements are shown in figure 1-1. In table 1-1 the positions of the different ions in a Suzuki phase are presented (the coordinates are relative to the Suzuki phase unit cell, the position "X" of some of the anions depends on the system in which they occur). Table 1-2 shows the positions of the anions in terms of the displacement parameter defined as $\delta = |\frac{1}{4} - X|$ (in other words, δ is the displacement of the anion with respect to the position it would have in the perfect NaCl lattice), the measured values for a_S (Suzuki phase unit cell side) and the values for a_S calculated on a theoretical basis (to be discussed later) are also presented.

Sors and Lilley (17) and Boswarva (18) have calculated the displacement of the anions and the lattice energies for several Suzuki phases using the Born polarizable point-ion model of an ionic solid obtaining values in good agreement with those experimentally measured.

In table 1-3 the lattice parameters of the various Suzuki phases $6MXNX_2$ and of the corresponding MX matrix are compared. In all cases the lattice parameter for the Suzuki phases is approximately equal to twice the corresponding MX parameter, the difference has been quantified in terms of the Λ parameter defined as $\Lambda = (a_S - 2a_{MX})/2a_S$ (where the subscripts S and MX refer to the Suzuki phase and the matrix MX respectively).

The morphology of the Suzuki phase precipitates has been studied by optical microscopy (8), direct transmission electron microscopy (19) and gold decoration of the precipitates (20, 21, 9, 22, 6, 23). All these studies indicate that the Suzuki precipitates are in the form of rectangular prisms, usually cubes, whose faces are parallel to (001) planes of the matrix; so the growth habits are fully consistent with the

TABLE 1-1

M	0	1/4	1/4
X_1	1/4	1/4	1/4
X_2	x	0	0
N	0	0	0

x = 0.2287 in $6NaClCdCl_2$ (10)

Coordinates of the various ions in a $6'MNX_2$ Suzuki phase (M = cation, X = anion, N = divalent cation) X_1 represents the undisplaced anions and X_2 the displaced ones.

TABLE 1 - 2

System	a_s		$\delta_{exp.}$		$\delta_{calc.}$	
$NaCl:MnCl_2$	11.2274	(16)	0.021? 0.028 0.020	(16) (5) (2)	0.032 0.030	(18) (17)
$NaCl:FeCl_2$	11.181	(16)	- - -		- - -	
$NaCl:CdCl_2$	11.248	(16)	0.028 0.014 0.020	(1) (15) (5)	0.022 0.023	(18) (17)
$NaCl:MgCl_2$	11.200	(16)	- - -		0.039	(18)
$LiF:MgF_2$	8.20	(3)	0.01 0.005 to 0.010	(3) (5)	0.025	(18)
$LiF:ZnF_2$	- - -		- - -		0.016	(18)

Suzuki lattice parameter a_s, anion displacement $\delta_{exp.}$ (measured) and anion displacement $\delta_{calc.}$ (calculated) for various systems. Numbers within brackets indicate the reference from which values were taken.

TABLE 1 - 3

System	a_n	a_s	Δ
$NaCl:MnCl_2$	5.639 A	11.2274 A (16)	0.0045
$NaCl:FeCl_2$	5.639 A	11.181 A (16)	0.0860
$NaCl:CdCl_2$	5.639 A	11.243 A (16)	0.0027
$NaCl:MgCl_2$	5.639 A	11.200 A (16)	0.0069
$LiF:MgF_2$	4.14 A	8.2 A (3)	0.0097

Lattice misfit for several Suzuki phases in alkali halide crystals. a_n is the lattice parameter of the matrix, a_s the lattice parameter of the Suzuki phase and Δ = misfit. Numbers in brackets indicate the references.

Crystalline structure.

1.3 The Formation of Suzuki Phases.

The Suzuki phase forming systems have several common characteristics; these will be presented here using the $NaCl:MnCl_2$ system as a model case; the reason for this choice being that this system is the most thoroughly studied and understood.

At $MnCl_2$ concentrations of the order of 100-600 mppm and temperatures between 200°C and 800°C the $NaCl:MnCl_2$ system presents an α (solid solution) phase. That it is a substitutional solution has been determined by E.P.R techniques (28). In this range of temperatures and concentrations the Ionic Conductivity of the crystal shows (27, 21, 31) that for T (temperature) $T \geq 350°C$ the conduction is determined by the charge-compensating vacancies introduced by the foreign species Mn^{++} (extrinsic range) and that for $200 < T \leq 350$ the Mn ions and vacancies undergo reactions of the general type:

Mn + vacancy $\rightleftharpoons$ Complex of Ions and Vacancies (association region).

There has been considerable disagreement concerning the detailed nature of the association reactions (32,33 and references quoted there). Of special interest are the studies by Strutt and Lilley (34,33) who based on ideas developed by Crawford (35) proposed a mechanism for the association which leads to the formation of a Suzuki phase. The mechanism is of the form

$$A_1 + A_1 \rightleftharpoons {}^{L}A_2$$

$${}^{L}A_2 \rightleftharpoons {}^{4}A_2$$

$$^4A_2 \rightleftharpoons {}^4A_2^*$$

$$4A_2^* + A_1^* \rightarrow {}^4A_3^*$$

$$4A_3^* + A_1^* \rightarrow {}^4A_3^*$$

$$\cdots$$

$$4A_n^* + A_1^* \rightarrow {}^4A_{n+1}^*$$

$$4A_{n+1}^* + A_1^* \rightarrow \text{Suzuki phase}$$

where A represents a Mn-vacancy complex, the superscript L indicates a loosely coupled dimmer, the superscript 4 indicates that impurity ions are separated four nearest neighbour distances and the subscript n (n = 1,2...) indicates the number of dipoles in A. The symbol A_1^* means a next nearest neighbour dipole, A_{n+1}^* a critical Suzuki phase precipitate and A_2^*, A_3^* and A_4^* represent unstable complexes.

The precipitation of the Suzuki phase occurs at about 200°C (9, 21); and the precipitates can then be observed under the electron microscope directly (19) or by means of Gold decoration (9, 20, 21, 6, 14). Using the latter technique, the thermal evolution of the precipitates has been observed (21). The analysis of the temperature and concentration limits for the precipitation has led to the determination of the phase diagram for this system in the low concentration region (figure 1.3); this has been done by electron microscopy (9, 21) Ionic Conductivity (21,31) and X-rays (31). As it can be appreciated from figure 1-2 the Suzuki Phase is metastable.

After precipitation has taken place (induced by a linear cooling from some 600°C); the volume fraction of the precipitate and the Mn contents of the original solid solution are related by (21)

$$(1) \qquad \frac{V_s}{V_t} = 8C + C_o$$

where V_s is the volume occupied by the [illegible] of the Mn concentration. The factor "8" comes from the fact that $A_s \simeq 2a_{NaCl}$; and C_o has been interpreted as due to some Mn being in a state different from a Suzuki phase, for instance the remaining Mn could be bound to a "chemical impurity" (27, 28, 29, 30). The data by Kirk et. al. are reproduced in figure 1-4.

Both the mean size and the spread in sizes have been found to increase with the Mn concentration (9, 21).

The size distribution of the precipitates has been studied by Kahn, (9) and by Kirk et.al. (21) whose data are reproduced on figure 1-5. Jain and Hughes (25) have analyzed this size distribution graphs and found, for the one representing the lowest concentration of Mn, ($\simeq$ 225 mppm) that it could be explained in terms of a Lifschitz-Wagner-Shlezov (59, 60) distribution for a surface-controlled process; but the other published size distribution histograms do not conform to this distribution.

1.4 Electron Microscopy of Suzuki Phases and the Structure of the NaCl-precipitate interface.

Kahn (9) has shown that, the gold decoration technique (24) is capable of revealing the presence of Suzuki precipitates (figure 1-6), and this fact has been used in various studies (9, 20, 21, 6, 22, 14, 26). However, the question of why is it that the precipitates affect the gold nucleation, in such a way that the precipitates are revealed as square or rectangular regions inside of which the nuclei are smaller and appear with a higher density than elsewhere, has received little attention. It is acknowledged that the main reason for this enhanced nucleation lies in the fact

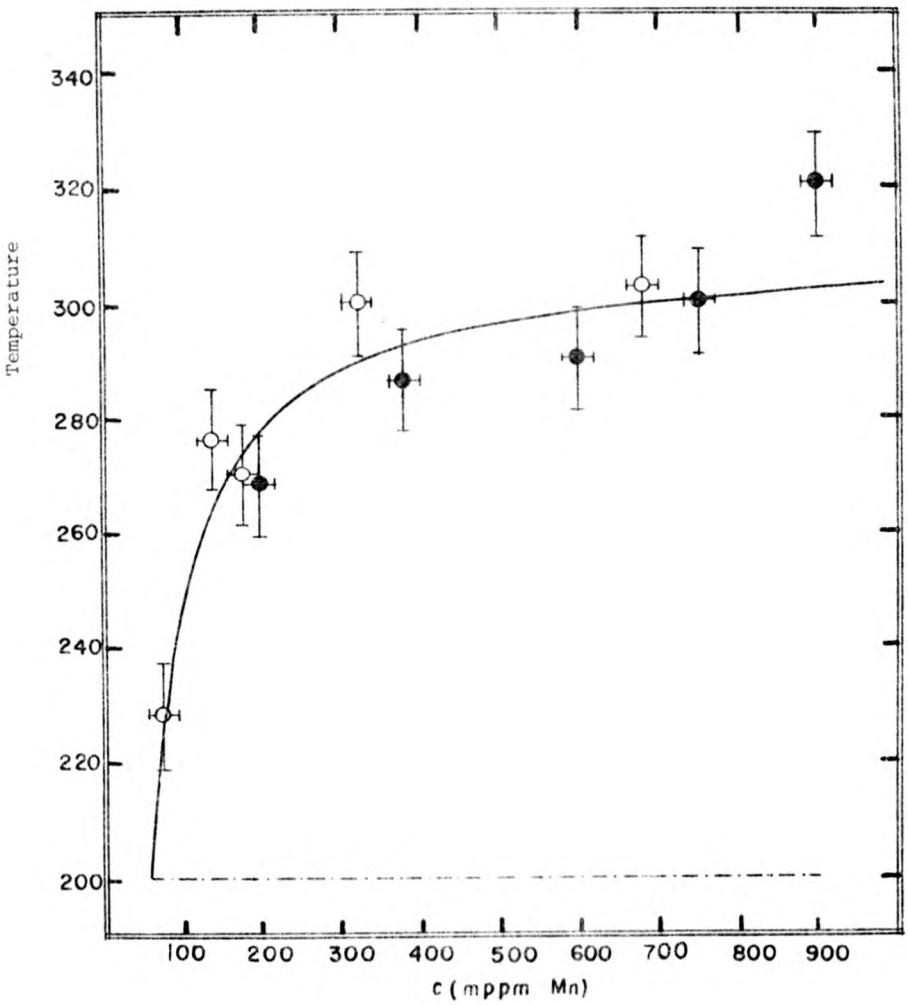

Figure 1-3: Phase diagram for the NaCl: $MnCl_2$ system in the low concentration region as determined by Kirk Kahn and Pratt (21).

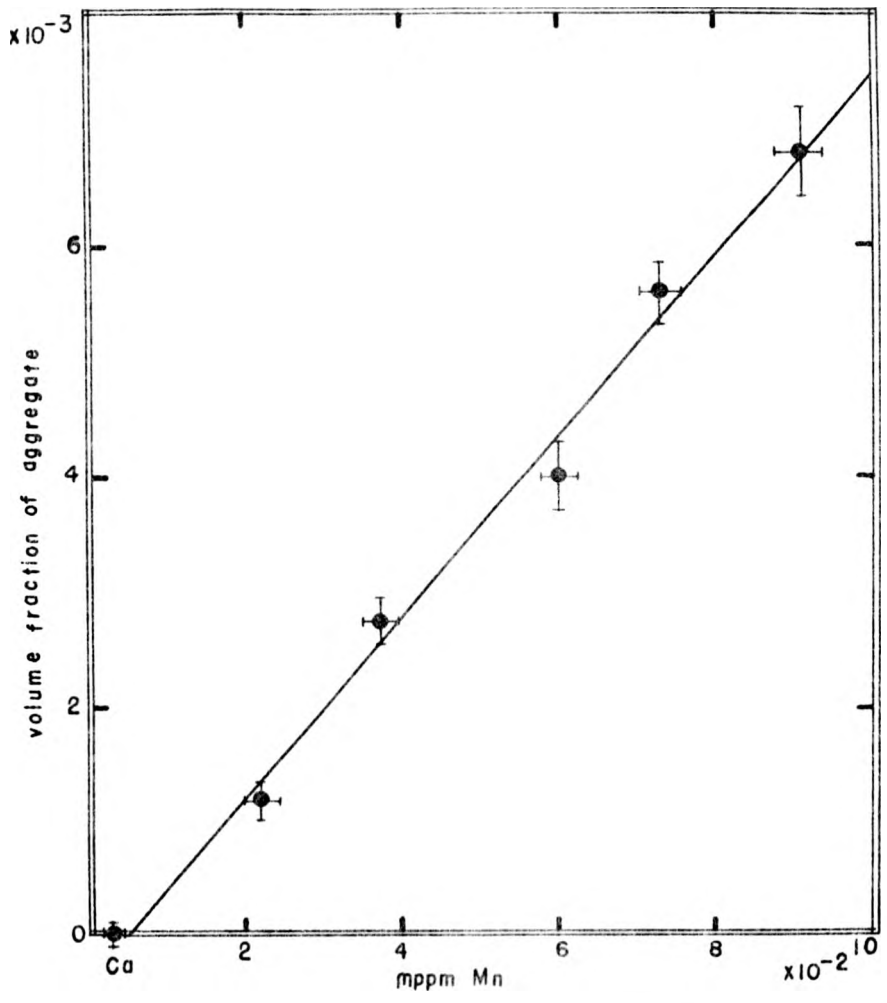

Figure 1-4: Dependence of the volume fraction with area fraction for Suzuki precipitates in NaCl: $MnCl_2$ (taken from 21).

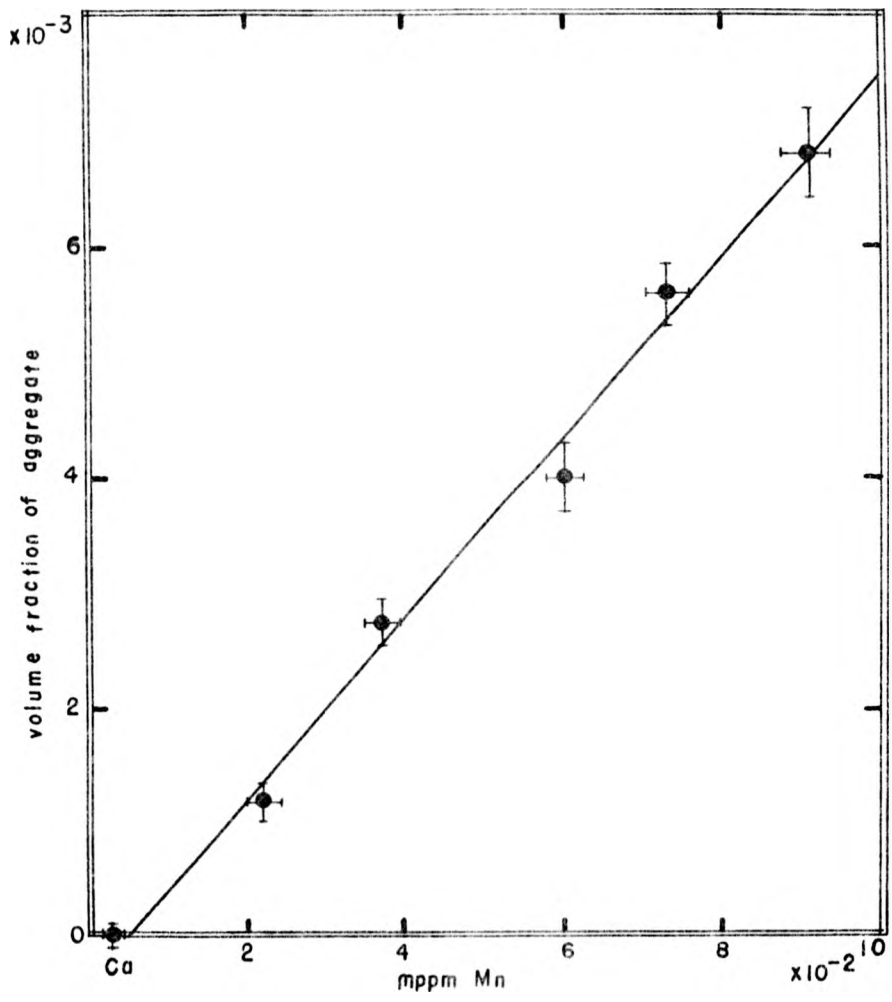

Figure 1-4: Dependence of the volume fraction with area fraction for Suzuki precipitates in NaCl: $MnCl_2$ (taken from 21).

that the Suzuki phases are ordered arrays of charged defects (20, 23); Yacaman and Hirth (23) have suggested that the location of Suzuki phases might be understood in terms of the calculation by Chernov and Trusov (36) which indicate that even a single unit of charge close to the surface decreases strongly the work of formation of an Au nucleus, increasing the nucleation rate.

At the same time these authors have remarked that a great variety of defects can affect the nucleation kinetics such as dislocation-surface intersections, steps, surface layers produced by water dissolution, surface vacancies, surface kinks and impurities (23 and references quoted there).

Recently Niedermayer (37) has proposed a model explaining the differences in nucleation inside and outside the precipitate areas. The model is based on the assumption that the activation energies for the surface diffusion in both kinds of areas are different. The predictions of this model are:

1) that for constant temperature, the ratio (n_S/n_{NaCl}) of the (saturation) nuclei densities inside and outside the precipitate areas should remain constant for varying deposition rates (J).
2) that for constant deposition rate, $(n_S/n_{NaCl}$ should vary as $exp(\frac{2}{3}\frac{\Delta E}{KT})$ where ΔE is the difference in activation energies for surface diffusion.

This model is being currently tested (62) and preliminary results show that the dependence of the saturation density upon deposition rate is as predicted.

Using the fact that the Gold decoration permits the study of dislocation structures (38, 39, 40), Kahn (9) and Yacaman and Hirth (23) have investigated the nature of the interface between NaCl and

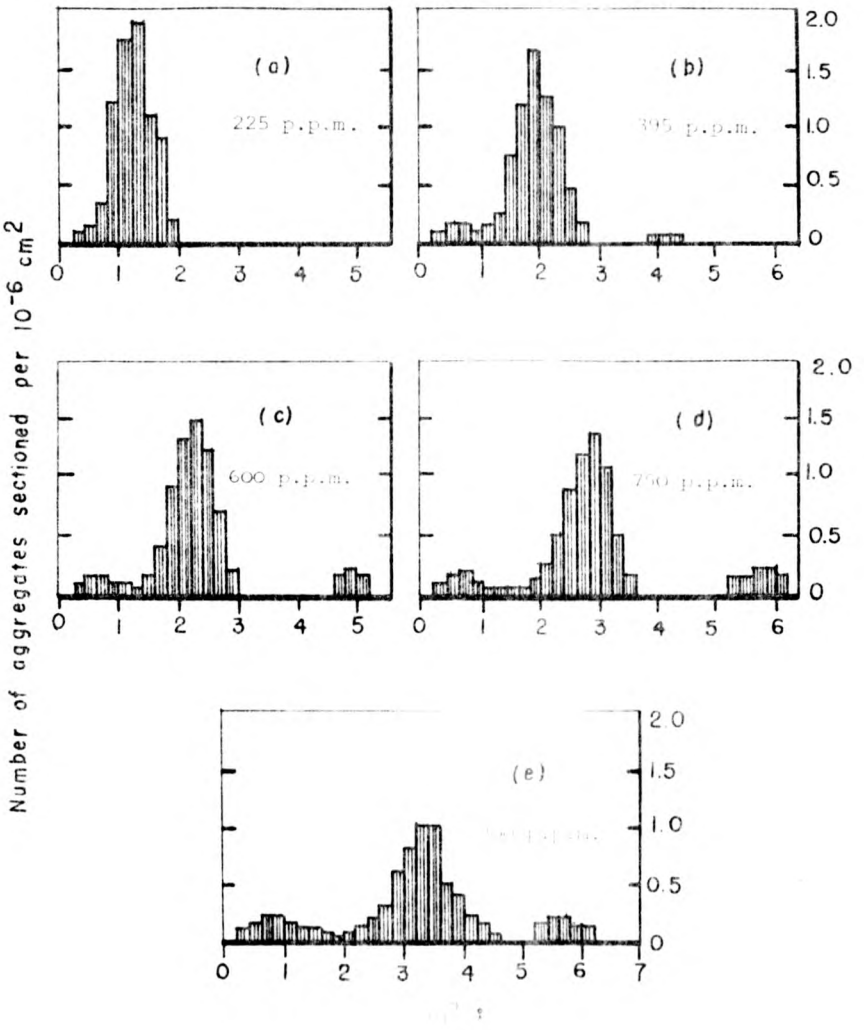

Figure I-5: Size distribution in I stage for Suzuki precipitates in NaCl: MoO_3 as determined by Kirk Kahn and Pratt (11).

the Suzuki precipitates. Kahn (9) noticed that a profusion of steps is formed around the precipitates and interpreted it as an indication of incoherency at the interface (figure 1-6). According to Yacaman and Hirth (23) this interface is formed by an ordered array of dislocations, the role of these dislocations being to relieve the misfit stress between the two phases; the spacing between the dislocations is, then, determined by the lattice parameters of both NaCl and the Suzuki phase. This hypothesis gives good agreement with the measured spacing between steps in the precipitate regions (23).

Other characteristics of the Suzuki phases that have been studied by Gold decoration are:

a) the orientation of the precipitates and their habit (9)

b) their spatial distribution (9, 26); in particular it has been reported that the precipitates are frequently aligned over low angle boundaries.

c) their size distribution (9)

d) the volume fraction precipitated (9, 26)

e) the thermal resolution of the precipitates (9, 21).

The direct observation of Suzuki phases in the electron microscope has been reported by Yacaman et.al.(19). They found two kinds of dislocation structures around the precipitates; the first one consisted of loops surrounding the precipitate and with large line segments running parallel to ⟨100⟩ directions. The number of loops was found to increase with decreasing precipitate size and they have been interpreted as being interface mismatch dislocations since their spacing agrees well with those expected under the assumption that they relieve the stress caused by the lattice misfit. The other kind consisted of irregular lines at the interface, their number was found

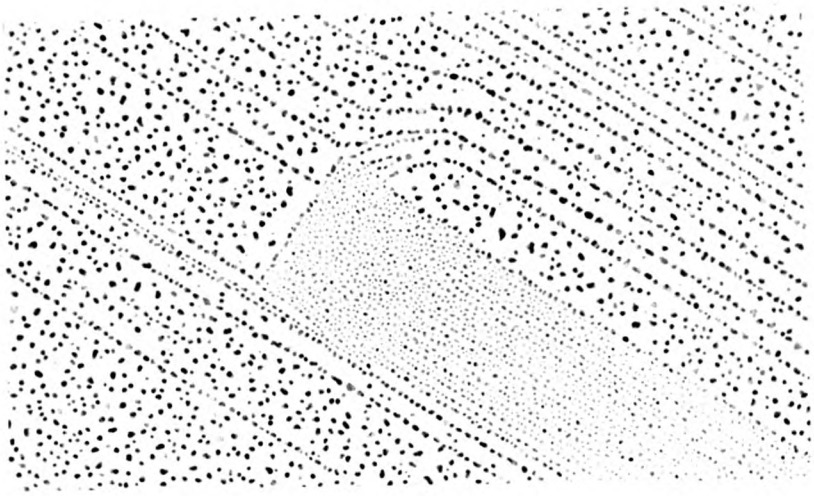

1-6 The appearance of a decorated NaCl:$MnCl_2$ surface showing a Suzuki precipitate.

to increase with precipitate size; no explanation for them was found.

At present a group at the Imperial College (London) is doing direct microscopy of the precipitates and preliminary results show the presence of grain boundary ledges.

1.5 Plan of Present Research

The purpose of this investigation is to study, using the gold decoration technique, the Suzuki phase $6NaCl.MnCl_2$ in Mn doped NaCl crystals. This system was chosen because it is the one most thoroughly studied and hence the best characterized because it has been investigated by most of the techniques mentioned in the introduction.

The gold decoration technique has been used bearing in mind that it can yield information concerning the presence, sizes, size distributions, and thermal behaviour of the precipitates and the dislocation structures associated with them. This technique has been preferred to that of direct transmission microscopy because the alkali halides are extremely sensitive to damage by the electron beam (41) rendering systematic observation and photography of the precipitates very difficult.

Chapter two is devoted to a discussion of the experimental techniques used, the results are presented in chapter three and they are discussed in chapter four. Finally in chapter five the conclusions are summarized and suggestions for further work are discussed.

CHAPTER 2

EXPERIMENTAL PROCEDURE

2.1 Introduction

In this chapter a detailed account of the experimental techniques employed is presented. The procedure followed can be summarized as follows:

Starting with a single crystal of NaCl:$MnCl_2$ small pieces were cut by cleavage in air; these pieces were subjected to a thermal treatment which, in general, consisted in an anneal at 650°C for 2 hours followed by a linear cooling to room temperature. These heat-treated crystals were decorated with gold in the standard (24) way and after dissolution of the crystal the carbon supported gold was mounted into electron microscope grids. The cleavage for the decoration was carried out under high vacuum conditions (better than 1.10^{-5}torr) and one of the pieces left by cleavage was kept for the impurity contents determination. The decorated samples were observed in a Jeol 100-C transmission electron microscope.

2.2 The NaCl:Mn Crystals

The Mn doped NaCl crystals for these experiments were provided by the Instituto de Física (Universidad Nacional Autónoma de México) and were grown by the Kyropoulos method in an argon atmosphere. The Mn was added as $MnCl_2$ to the melt in 1% weight. Both the NaCl and the $MnCl_2$ were of analytic reagent purity.

In a few experiments, nominally pure NaCl single crystals were used; these were purchased form the Harshaw Chemical Co.

The as grown single crystals (of 120 gr. each approximately)

were cut into pieces of about 1 x 1 x 1 cm. by means of cleavage in air. These pieces were subjected to the thermal treatments as described in section 2-3.

Each piece was labeled stating the larger crystal from which it was cut and its approximate location with respect to the growth axis; in this way it was possible to have beforehand an idea of which samples were likely to have similar impurity contents. The actual impurity levels were known only after the analysis described in section 2.5.

2.3 The Heat Treatments.

All the heat treatments, unless otherwise stated, consisted of an anneal at 650°C for two hours followed by a linear cooling to room temperature. The cooling rates used were α_1 = 11 C°/h α_2=6.9C°/h α_3=4.1C°/h ($\pm$ 3%)

For these treatments a tubular furnace was used. It had a hot zone of approximately 4 cm long, in figure 2-1 the dependence of the temperature as function of position is presented. The maximum difference of temperatures (between locations inside the hot zone) found was of 10°C when the centre was at the highest temperature used (650°C). One end of the furnace was blocked with a refractory brick to prevent air currents from entering the furnace, for it was found that without this precaution the temperature fluctuated by amounts up to 20°C.

The temperature was measured by means of a platinum-platinum 13% rhodium thermocouple whose cold junction was at room temperature (20°C). The thermocouple in turn fed an Ether 1290 temperature controller fitted with a programme temperature unit Ether 12-94. The readings from the controller were compared against the temperature obtained by measuring the thermocouple output directly with a

Figure 2-1 Dependence of temperature with position in the tubular furnace.

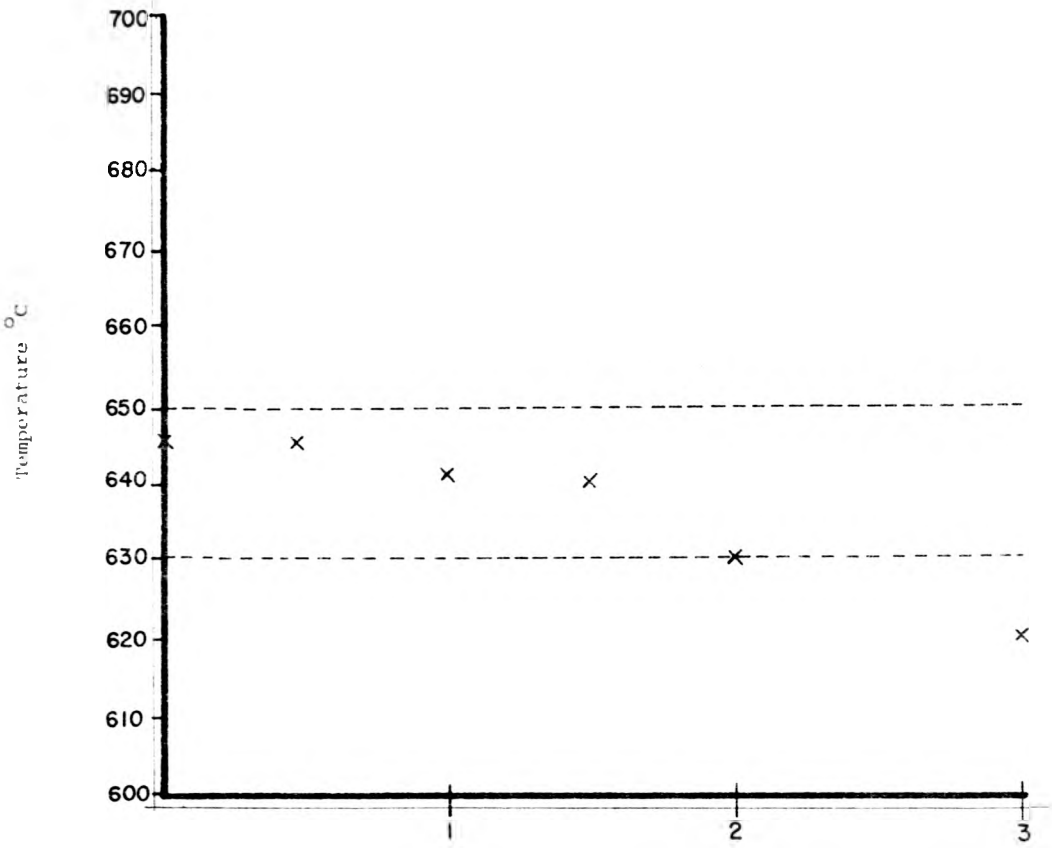
Temperature °C
700
690
680
670
660
650
640
630
620
610
600
1
2
3
Position from centre of furnace (cm)

potentiometer and both sets of measurements were found in good agreement, as shown in figure 2-2. Figure 2-3 shows the variation of temperature with time during cooling; verifying that the cooling was indeed linear.

The thermal treatment used was chosen with a view to inducing the precipitation of the manganese (21).

After this treatment, a change in the colour and transparency of the crystals was evident. Upon cleaving new faces the original appearance was restored showing that the material responsible for the change was at the surfaces exposed to air during the heat treatment. By dissolving the crystal in water the surface material could be removed from the crystal. This phenomenon (which has been called Diffusion to the Surface) has been previously reported (42) and it is known that a thin film of manganese oxide is formed at the surfaces.

2.4 Gold Decoration

The gold decoration of the crystals was carried out as described by Bassett (24). A NGN 12" coating unit was used and the pressure inside the bell jar during the decoration process was always less than 10^{-5} torr.

A specimen holder with a heating stage was constructed, and the temperature was monitored by means of a chromel-alumel thermocouple placed in contact with the crystal. The gold deposition was carried out with the specimen at 100°C. The gold was evaporated from a "V" shaped tungsten wire, and the amount of gold was adjusted so that (assuming an homogeneous isotropic evaporation from the source) it corresponded to a thin film of 8Å mean thickness.

The crystals were transferred from the furnace into the coating

Figure 2-2 Comparison of the temperature readings from an Ether programme controller with the reading a from a Pt-Rh 13% Pt thermo couple.

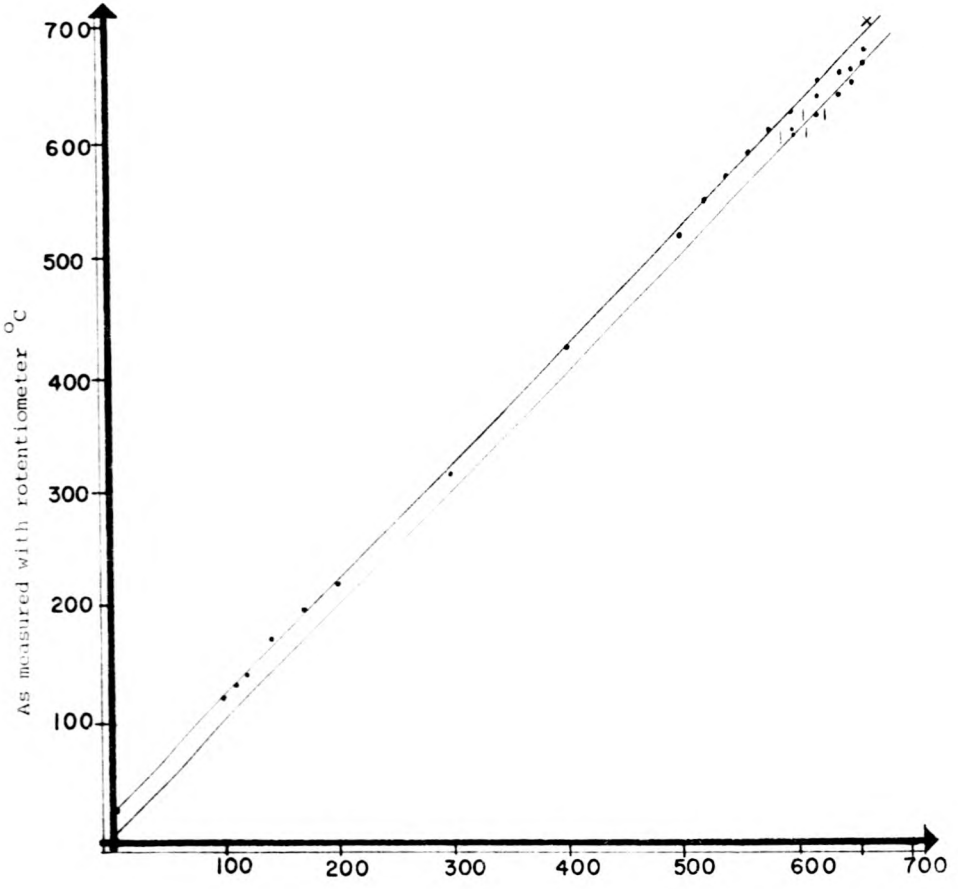
700
600
500
400
300
200
100
As measured with rotentiometer °C
100
200
300
400
500
600
700
As measured with controller °C

Figure 2-3 Dependence of temperature in the furnace with time verifying the linearity of the cooling.

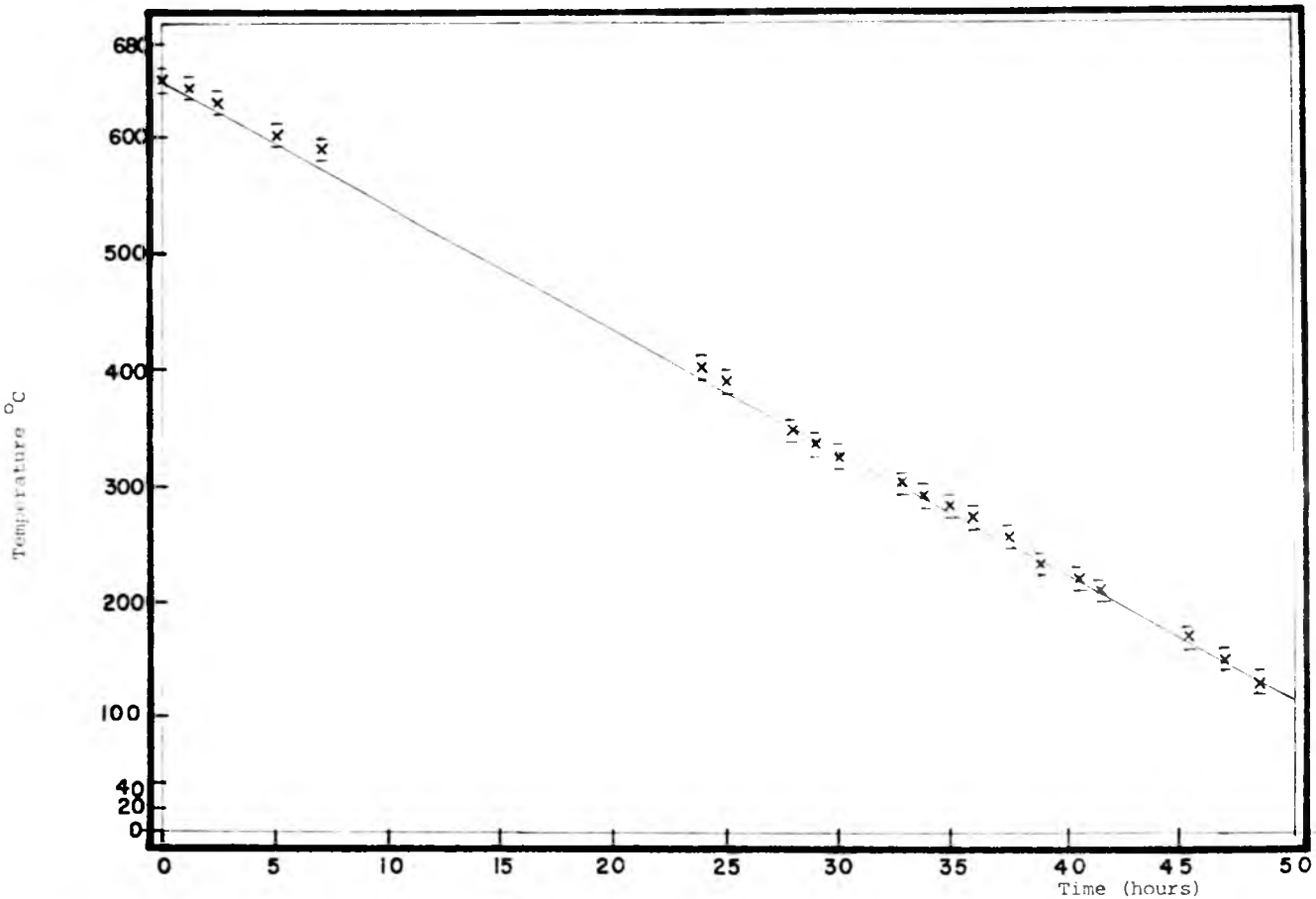
Temperature °C
680
600
500
400
300
200
100
40
20
0
0
5
10
15
20
25
30
35
40
45
50
Time (hours)

unit withour any further cleavage, so all six faces of the sample were covered with the manganese oxide layer described before. The surface to be decorated was produced by cleavage under high vacuum conditions (10^{-5} torr or less), and this was achieved by means of the cleaving device shown in figure 2-4. It is basically a pendulum on whose end a razor blade was mounted and which was released on interrupting the current of an electromagnet.

It was considered that cleavage in vacuum was necessary since there is evidence that cleavage in air results in anomalous decoration features associated with water dissolution of the surfaces (43 to 45).

After cleavage and gold deposition a carbon film was laid down in the usual way (24). In some instances it was deposited in such a way that a film was formed not only on the crystal face with gold, but also on another face (which it must be remembered, contains the manganese oxide film formed during the heat treatment). Thus after dissolving the crystal in distilled water and mounting the films onto electron microscope grids (in the manner described in the literature (24)) three kinds of samples were obtained, which for simplicity will be called samples I, II and III.

Samples I were those in which the grid supported the carbon film with the decorating gold, they corresponded to the usual decoration samples. Most of the present research is based on this kind of sample.

Samples II were those in which the grid supported the carbon film with the manganese oxide layers, they were obtained in a way similar to that of samples I but the carbon film picked was that on a face that was not decorated but was instead covered with the

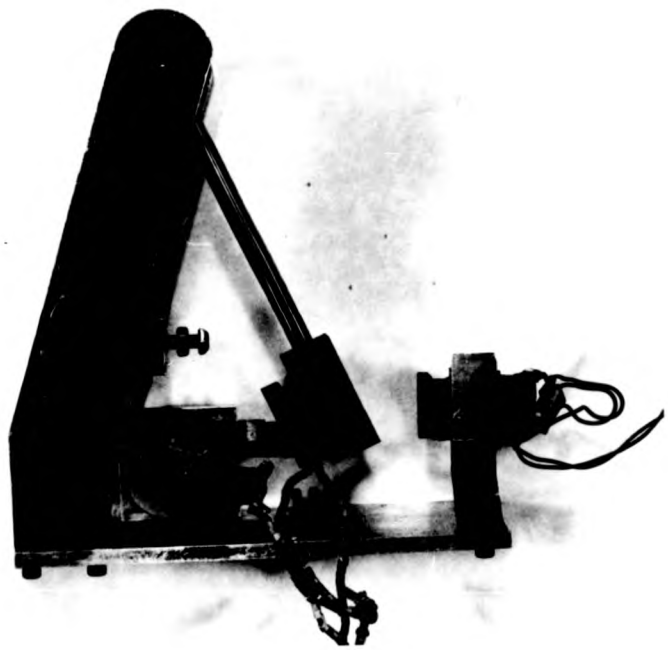

2-4 Device to cleave in high vacuum, with a heating stage.

surface Mn oxide material. That in this way the MnO and Mn_2O_3 films can be observed later at the electron microscope is well documented (42). These samples were required to confirm the fact that surface oxidation had actually taken place.

Samples III were those in which the piece of carbon was selected to contain a region with gold decoration and a region of oxide film with the boundary between them. These samples were used to produce further evidence concerning the orientation of the precipitates, taking advantage of the fact that the boundary between both regions corresponds to an edge of the crystal and consequently marks a 100 direction.

2.5 Impurity Contents Determination

The amount of Mn in each of the samples was determined by wet chemical analysis; these measurements were carried out by Dr. Evans at the University of Birmingham, his data are presented in table 2-1. For some crystals a check was made by atomic absorption spectroscopy, these measurements were performed by the Crystal Growth Group at the Instituto de Física (México); their data have also been incorporated into table 2-1.

2.6 Observation of the Samples

The observation of the samples was carried out with a Jeol 100-C transmission electron microscope operating at 100 K.V. and which was fitted with a side entry goniometer stage.

In this microscope it is possible to adjust the position of the sample not only in a plane normal to optical axis but also along the direction of this axis itself. In this way variations in the

TABLE 2-1

Sample	A	B	Average	Atomic Absorption
87	348	351	349	
93	367	369	368	380
96	456	463	459	
98	439	438	438	
99	387	393	390	
103	380	379	379	
104	471	455	463	
105	437	447	442	475
109	340	340	340	
114	377	379	378	356

Impurity contents of the crystals used (in molar parts per million), A and B represent independent measurements.

Note: Measurements A and B were made by Dr. D.M. Evans at the University of Birmingham, the atomic absorption measurements were made by E. Camarillo at the Universidad Nacional Autónoma de México. Their collaboration is kindly acknowledged.

magnification due to differences in the height of the sample can be minimized; the position of the samples under observation was always adjusted to be the "Eucentric" one, that is the height at which tilting the specimen by a few degrees does not produce a uniform translation of the field of view. The magnification and camera lenghts displayed on the microscope are referred to this eucentric position.

The magnifications (as measured from the lens currents) at the eucentric position were compared with those obtained from a carbon replica diffraction grating of known fringe spacing, the results of this comparison are presented in table 2-2 from which it can be seen that the agreement is within 4%. It must be recognised that inaccuracies in magnification can arise due to other factors (46) such as hysteresis effects and instabilities in lens currents or accelerating voltage, and the figure quoted above will be considered as a lower limit on the error.

The observation of the samples was made under bright field conditions and in a few instances selected area diffraction patterns were photographed, all this in the standard way reported in the literature (46).

A typical decoration picture is shown in figure 2-5.

For each sample at least 100 precipitates were randomly selected and photographed. Pictures were also taken of the overall decoration pattern with considerable emphasis on the decoration features associated with the precipitates, such as grain boundaries and cleavage and slip steps. Low magnification (5000X) pictures were taken to study the spatial distribution of the precipitates.

Nominally pure crystals were also observed to establish the

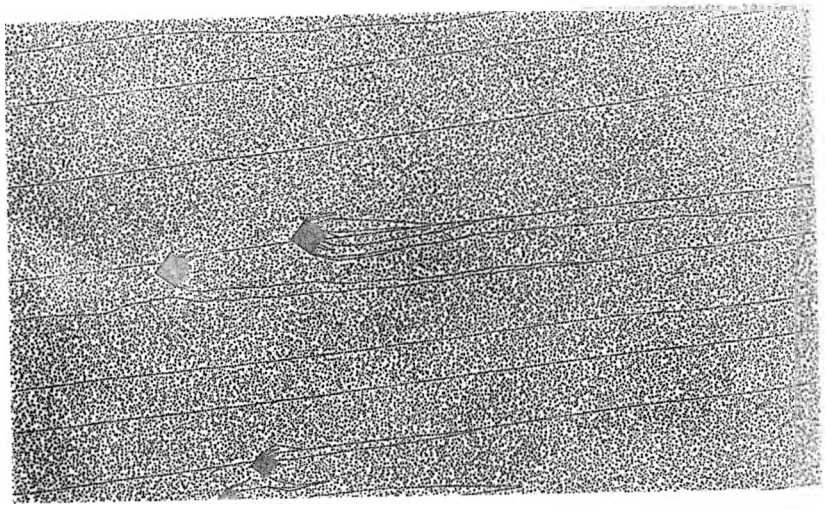

2-5 A typical decoration pattern in a NaCl:$MnCl_2$ crystal slowly cooled from 650°C

TABLE 2 - 2

Magnification (displayed)	Magnification (measured)
1.6×10^3	$1.67 (\pm 0.008) \times 10^3$
5×10^3	$5.24 (\pm 0.03) \times 10^3$
10×10^3	$11.2 (\pm 0.09) \times 10^3$
20×10^3	$21.1 (\pm 0.2) \times 10^3$
33×10^3	$36.3 (\pm 0.3) \times 10^3$
50×10^3	$48.8 (\pm 0.5) \times 10^3$

Comparison of the image magnification as displayed by the microscope (with the sample at eucentric position) and the magnification as measured from a carbon replica grating of 28800 lines per inch.

comparison between the gold decoration features in pure and Mn doped specimens.

2.7 Analysis of Pictures

2.7.1 Determination of the Orientation of Precipitates.

The orientation of the precipitates with respect to the NaCl matrix has been studied by means of three different techniques. The first of these consists on comparing the direction of the boundaries of the precipitates with the direction of the steps on the surface due to slip or cross slip; this method is based on the fact that such steps can be observed and identified by decoration (24).

The second technique is based on observation of the type III samples, in this case the orientation of the precipitates is compared with the 100 direction of the boundary between the two kinds of films that formed. This method has the disadvantage that during the stripping of the carbon film and mounting onto the grid, the boundary breaks easily so this method was used only to confirm the determination of orientation.

The third technique used was that of Yacaman and Gómez (47). This is based on the fact that, for the gold deposition conditions used, the gold nuclei appear with several specific orientations among which the $(100)_{NaCl} // (100)_{Au}$ $[100]_{NaCl} // [100]_{Au}$ is prominent; in this way the rotation angle between the diffraction pattern and the image permits the identification of the [100] direction on the image.

2.7.2 Measurements from the Micrographs.

The projected length of the sides of the precipitates were

measured directly from the plates. The average values for the cross sectional area and precipitate side were calculated and from these size distribution histograms were constructed. The "shape" of the precipitates was quantified in terms of the parameter S defined as

$$S = b/a$$

where b and a represent the projected lenghts of the sides of the precipitates along two orthogonal directions and chosen so that $b/a \geq 1$ (i.e. b represents the largest side). From this the distribution in shape was obtained.

The spatial distribution of the precipitates was analyzed paying particular attention to the presence of clusters of precipitates. This was done in order to get some clues concerning the preferred sites (if any) for the nucleation of the precipitates.

In a few samples the gold nuclei sizes and densities have been measured for different regions of the crystal, e.g. regions outside the precipitates and free from steps, on steps, on the boundary NaCl-Suzuki phases and inside the precipitate regions. This was done in order to establish and quantify the differences in the nucleation of gold in precipitate areas and outside them. Samples III (described in section 2.3) were examined in order to confirm the presence of the manganese oxide film. This was achieved by comparing the images and diffraction patterns with those already available in the literature, paying particular attention to the nuclei habits, extinction fringes and preferred orientations.

Wherever statistical procedures were used, such as averaging; standard deviation calculation on curve fitting; the methods employed are those standard in the literature (c.f. 49).

2.7.3 Analysis of Decoration Patterns.

In order to find out what decoration features are characteristic

of the Mn doped crystals, the decoration patterns of nominally pure crystals and Mn-doped ones were compared. The decoration patterns of pure NaCl crystals have been reported by many authors (c.f. 24, 39) and the observations of the present study have been compared with theirs.

Since it is known (43, 40) that lack of control over the surface cleanness (for instance when cleavage is in air) can result in anomalous decoration features, care has been taken to ensure that the samples selected corresponded to "clean" surfaces. Here by "cleanness" one means that there are no spurious effect due to the dissolution of a few layers of the crystal by water (and the subsequent recrystallization produced by exposure to a low pressure) or due to the presence of Mn oxides produced during the heating for decoration; the present usage of the word "clean" must be distinguished from that used by surface physicists for whom a clean surface is one produced under ultrahigh vacuum conditions (52).

In chapter three this point is discussed further in the context of the experimental results. Although the decoration was carried out at substrate temperatures ($\sim$ 100°C) at which Mn oxide film formation and evaporation are not expected to be present, in the analysis of the micrographs attention was paid to any possible clues concerning either phenomena, for it has been shown (42, 47) that they affect the resulting gold decoration.

Concerning the precipitates themselves the attention has been focused on the following aspects.

1) The presence (or absence) of precipitates: the general criteria used for the identification of the structures corresponding to precipitates are those described in previous studies (c.f. 21); briefly it can be said that the precipitates are revealed as

square or rectangular regions inside of which the gold has been nucleated with samller mean diameter and greater density than elsewhere on the crystal surface.

2) The interaction of cleavage steps with precipitates. This analysis has been carried out with a twofold purpose; firstly the fact that cleavage steps interact with the precipitates is direct evidence that the structures revealed correspond indeed to the precipitates themselves and not to any sort of phenomenon that has taken place after cleavage (14). Secondly, it yields information concerning the effect of precipitates on the propagation of the cleavage crack (40, 50).

3) All the step structures associated with the precipitates. Examples of this are: steps running across the precipitate area, steps completely inside the precipitate and steps and step structures (such as V-shaped patterns) emerging from the precipitates. The purpose of this analysis has been again twofold, firstly it is important in view of the fact that these step structures can yield information concerning the nature of the interface Suzuki-precipitate-NaCl (23); secondly these structures can give extra information concerning the mechanism whereby step-structures are generated in ionic crystals. This analysis has been carried out within the experimental and theoretical frameworks provided by earlier studies (39, 40, 50, 38, 51). In the following chapters the details of such an analysis will be presented.

4) The presence and location of grain boundaries with respect to the precipitate structures. This was done in order to seek evidence in the sense that the precipitates form (or do not form) preferentialy at boundaries; use was made of the capabilities of

the gold decoration technique to reveal different kinds of boundaries (39, 40).

The results obtained using the techniques and methods described in this chapter are presented in chapter 3, where they will be discussed in detail.

CHAPTER 3

EXPERIMENTAL RESULTS

3.1 Introduction

In this chapter the observations carried out on gold decorated NaCl-$MnCl_2$ crystals with the Suzuki precipitates are presented. The procedure followed for the preparation and observation of the samples is the one already described in chapter 2. The discussion of the results is the subject matter of chapter 4, and this chapter is restricted to a presentation of data.

The basic facts underlying the work in this chapter can be listed as follows:

a) The fact that in crystals of NaCl-$MnCl_2$, with Mn contents in the range studied, and subjected to the thermal treatments described in chapter 2, Suzuki phase precipitates form (21, 20).

b) The fact that the gold decoration technique permits the study of the precipitates (21, 20).

c) The fact that the gold decoration technique permits the study of dislocation and step structures (39, 40).

3.2 General Characteristics of the Decoration Patterns.

The gold decoration features observed in the doped crystals can be divided in two broad categories. The first of these includes all the structures normally found in pure NaCl crystals as reported by the numerous authors in this field (24, 39) such as cleavage steps, slip steps, V-shaped and zig zag steps. The second category comprises all the decoration structures found exclusively in the NaCl:$MnCl_2$ crystals. Figure 3-1 shows the decoration obtained with

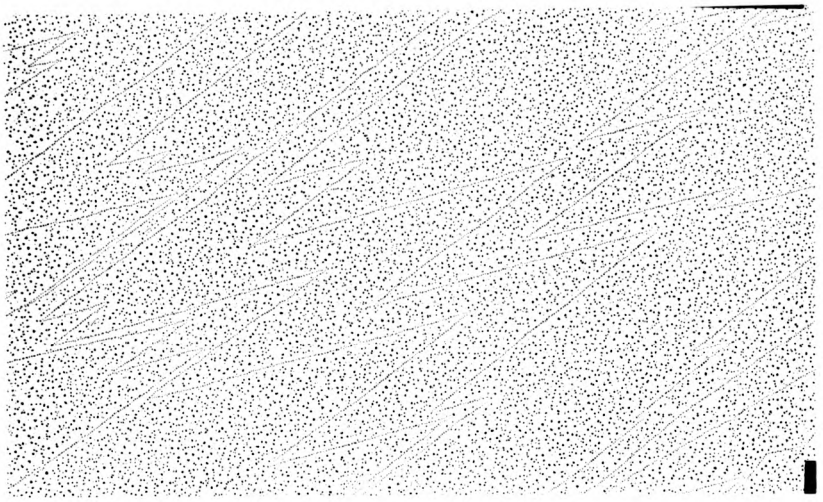

3-1 Gold decoration of a nominally pure Harshow Crystal, cleavage in 10^{-5} torr vacuum (22000x)

nominally pure NaCl crystals.

The analysis of the decoration features in the first category (i.e. those features common to pure and doped samples) revealed that none of the structures normally associated with water, atmospheric or diffusion pump oil contamination were present (43). Figure 3-2 shows a typical decoration pattern of a crystal in a region where the decoration structures are similar to those in pure NaCl. Hence it can be concluded that the surfaces studied were "clean", the word being used in the sense defined in chapter 2. Figure 3-3 shows the effect of air cleavage upon samples (this sample was deliberately exposed to air for about ten minutes).

No evaporation structures were found, as expected from the fact that the decorated surface was never at temperatures higher than 100°C. At the same time no evidence whatsoever was found indicating the presence of a Mn oxide film (42) on the vacuum cleaved faces (samples I described in chapter 2).

An examination of samples of types II and III (chapter 2) revealed that in the crystal faces exposed to the air during the heat treatments a thin film of manganese oxide had formed. Figure 3-4 shows the appearance of the nuclei of this film in a sample of type II, and comparison with the reported data on surface oxidation (42) indicates that the observed nuclei correspond to the diffusion to the surface effect indeed. Figure 3-5 shows the same effect on a surface exposed to air during the heat treatment (400°C for 10 minutes) and decorated.

The (decoration) structures found exclusively in the Mn doped crystals have been divided, for convenience, into three groups: 1) square or rectangular structures, 2) step structures associated with those in group 1 and 3) localized but irregular structures.

Figures 3-6 and 3-7 show typical examples of these groups. The

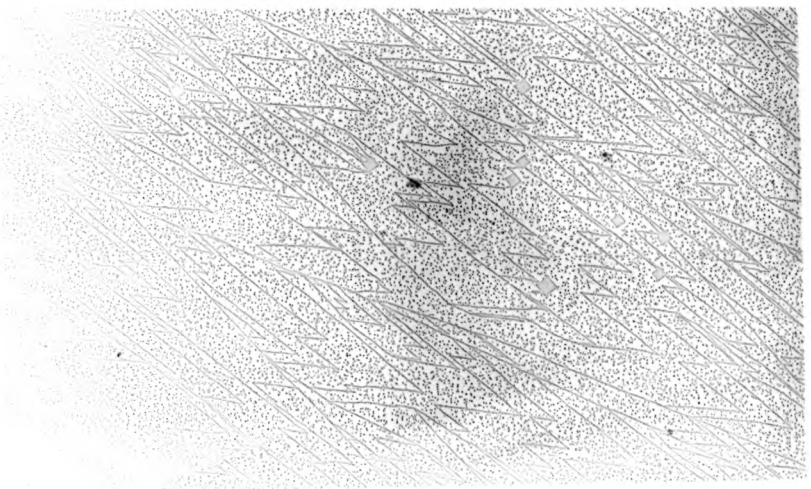

3-2 Sample 104; view of a region containing features also present in pure crystals and also Suzuki phase precipitates (17000X)

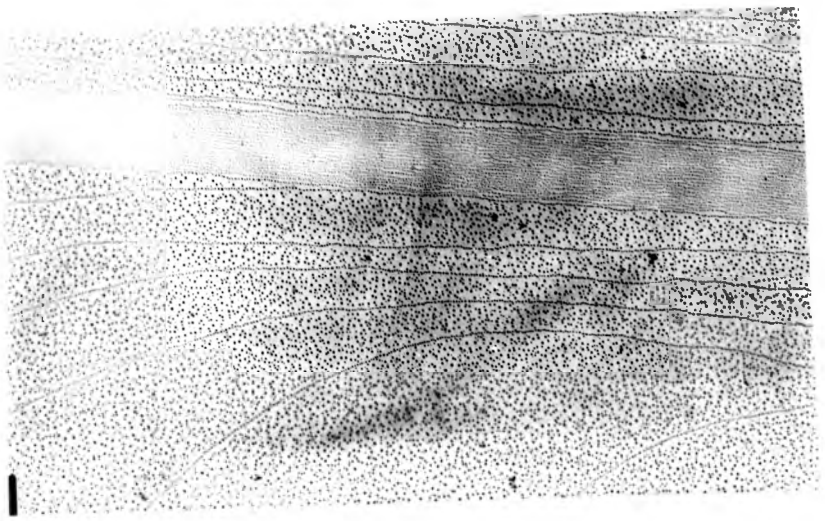

3-3 Effect of air cleavage on decoration. The sample is a pure Harshaw crystal, cleaved in air and exposed to it for about 10 minutes before chamber evacuation (44000X)

3-4 The non decorated surface of a NaCl: $MnCl_2$ crystal. The Mn contents was about 550 parts per million; This surface was exposed to air during an anneal at 400°C for 1 hour. The nuclei of the manganese oxide formed by diffusion to the surface are apparent. It is a sample of type II, as described in chapter 2. (22000X).

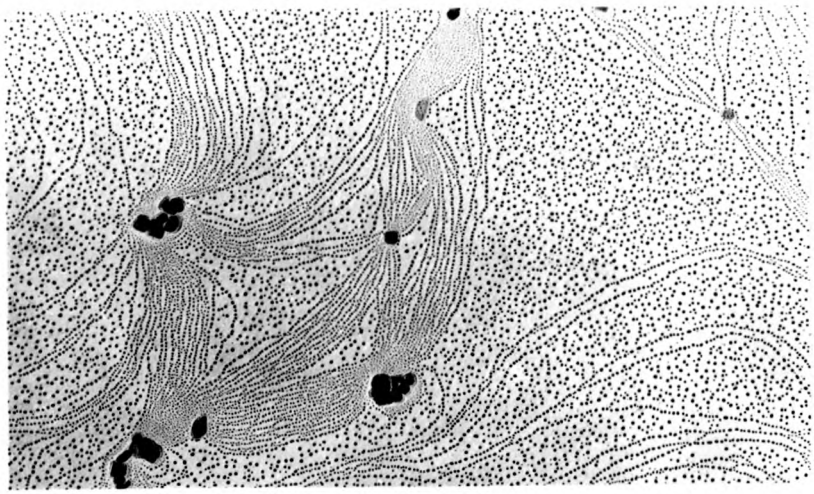

3-5 A sample similar to that shown in figure 3-4, but the treatment was for 10 minutes and the sample was decorated. The interaction of the evaporation ledges with the impurities is apparent (55000K)

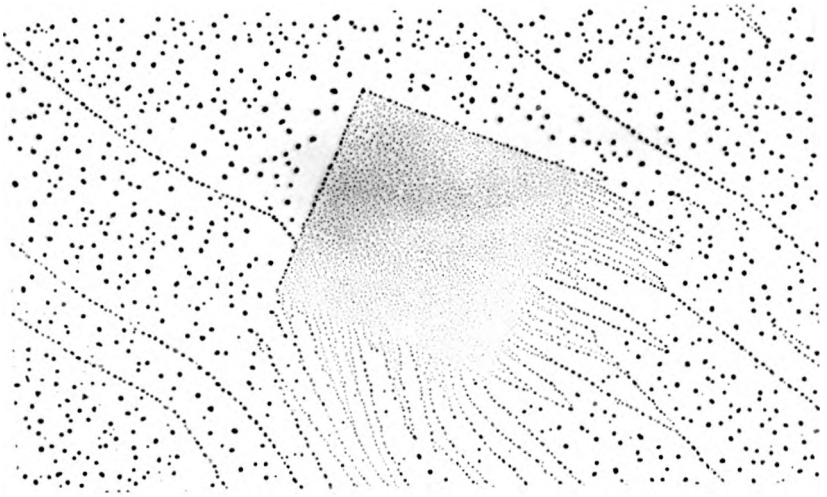

3-6 Sample 109, showing the appearance of Suzuki precipitates as revealed by the gold decoration (84000X).

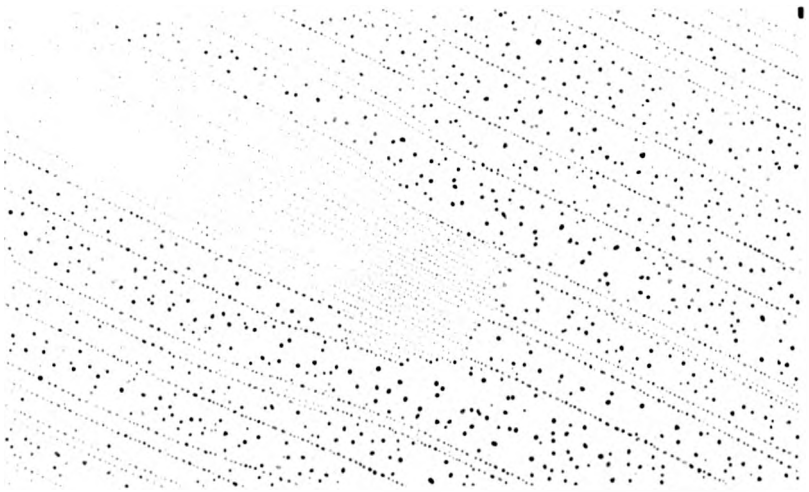

3-7 Same sample as in figure 3-6, showing an example of the structures described in the text as "irregular structures".

observations concerning group 1 will be presented in sections 3.4 and 3.5, sections 3.6 and 3.7 are devoted to groups 2 and 3 respectively.

3.3 Characteristics of Precipitates.

Previous studies (20, 21) have established that the square or rectangular structures correspond to the Suzuki phase precipitates. The reasons for accepting this conclusion can be briefly summarized as follows:

a) That the square (or rectangular) structures appear only in the doped crystals.

b) That both the shape (square or rectangular) and the orientations (the sides of the rectangles are parallel to [100] directions in NaCl) are fully consistent with the structure of the Suzuki phases.

c) That the volume fraction of the revealed structures depends linearly on the concentration of Mn. The slope of the volume fraction versus concentration line is about "2" as required by the structure of the Suzuki phase.

d) That the thermal resolution of the observed structures proceeds as expected for second phase particles.

e) The temperature limits of the thermal resolution obtained by decoration match those obtained by ionic conductivity.

For these reasons, in what follows, all the square or rectangular structures of the sort shown in figure 3.6 will be referred to as precipitates.

As illustrated in figure 3-6, the precipitates are revealed as square or rectangular regions inside of which the gold nuclei are smaller in size but appear with a higher density than those elsewhere on the crystal. In table 3-1 some typical data for nuclei sizes and densities

TABLE 3 - 1

Region	Size (diameter)	density
free of steps and outside precipitate area	140 A	1.34×10^{11} cm^{-2}
on steps outside precipitate area	140 A	7.34×10^{6} cm^{-1}
inside precipitate area	56 A	1.23×10^{12} cm^{-2}
on precipitate boundary	140 A	7×10^{6} cm^{-1}

Gold nuclei sizes and densities in different regions of the crystal

are presented for the gold on different regions of the sample. It is to be noticed that the boundary of the precipitates is composed of step-like lines along which the mean nucleus size is larger than inside the precipitate region.

The orientation of the precipitates was studied by means of the three techniques described in chapter 2, namely: by comparing the sides of the precipitates with the directions of surface features of known orientation (such as slip and cross slip steps); by comparing the sides of the precipitates with the boundary of the carbon film (samples II of chapter 2) and by photographing the diffraction pattern and comparing it with the bright field image. Figures 3-8, 3-9 and 3-10 show the results obtained, it can be concluded that the squares and rectangles have their sides parallel to 100 directions; this result is regarded as accurate within $\pm$ 1°, the possible experimental errors in this determination arise primarily from the fact that the sides of the precipitates are composed of discrete nuclei and several different straight line fittings can be made. These observations agree with those previously reported (21).

The precipitates exhibit rectangular habits, (by this it is meant that the projections of the precipitates onto (100) planes are rectangles), which in most of the cases correspond to perfect squares. Figure 3-11 shows their "shape" distribution, the vertical axis represents the number of precipitates (from a sample of 1000) and the horizontal one indicates the ratio $s = b/a$ of the larger side to the smaller (s has been defined in chapter 2). It was found that there are no significant differences in shape for different Mn concentrations nor for various cooling rates.

The accuracy in the determination of the values of s was estimated as

$$|\delta s| = \left|\frac{a.\delta l}{a^2}\right| \leq \left|\frac{a\delta l + b\delta a}{a^2}\right| = \Delta\left(\frac{a+b}{a^2}\right) \approx \frac{2\Delta}{a}$$

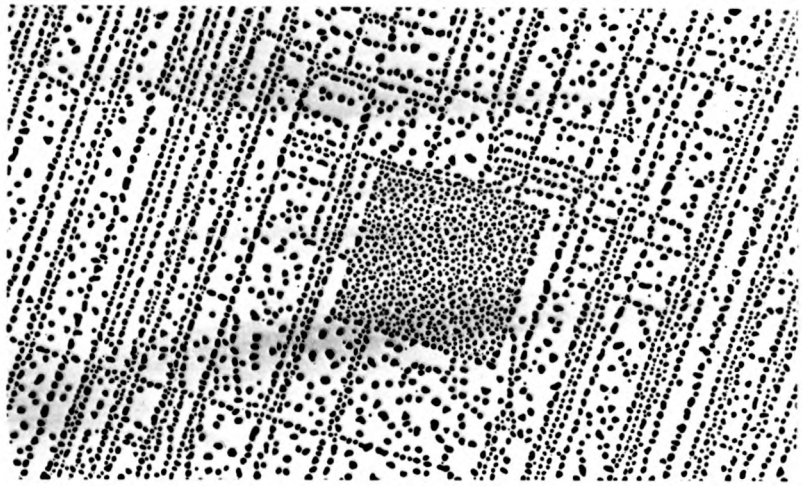

3-8 Sample 105; region of the crystal surface close to the point where cleavage was started. The slip steps present confirm the fact that the square structures (Suzuki precipitates) are aligned along <100> (84000X)

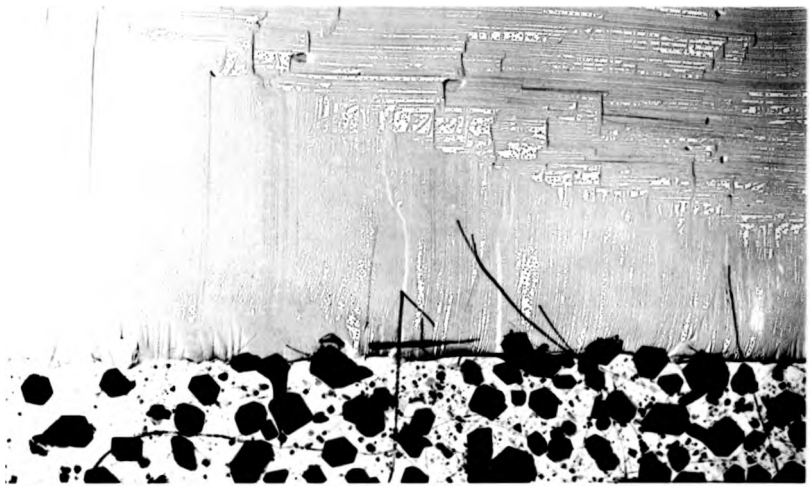

3-9 A sample of type II (chapter 2). The nuclei of manganese oxide can be appreciated in the lower part of this picture, they correspond to the surface exposed to air during the heating (linear cooling at 11/°C/h from 650°). The upper part shows the vacuum cleaved and decorated surface. The boundary between the two surfaces is also shown. The precipitates (not shown in this figure) are aligned with their sides parallel to this boundary (14000X).

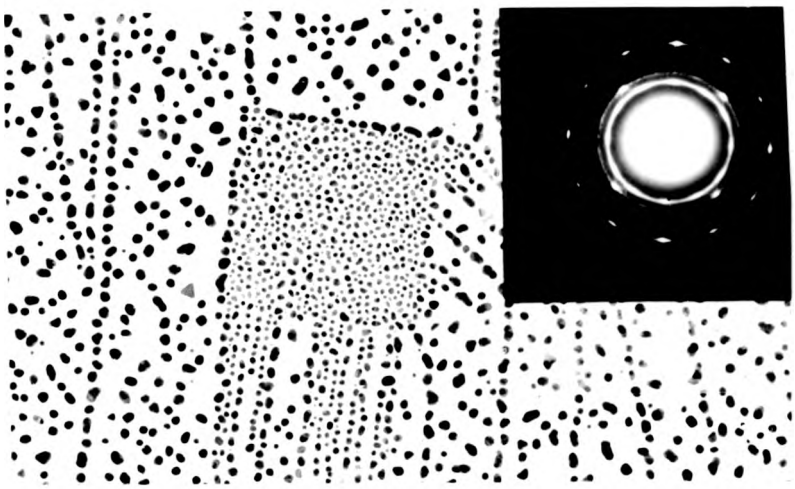

3-10 The diffraction pattern of sample 98, showing the preferential orientation for Gold onto NaCl. The central figure is the image of the same region from which the diffraction pattern was taken. Camera length= 76 cm magnification on plate 66000X, on print 110 000X. The diffraction pattern image angle at this setting is 129°. From plates the angle between the side of the precipitate and a (200) spot is 35° which compares favourably with expected 39 = T29 (mod 90°).

3-11 Shape distribution for 1000 precipitates.

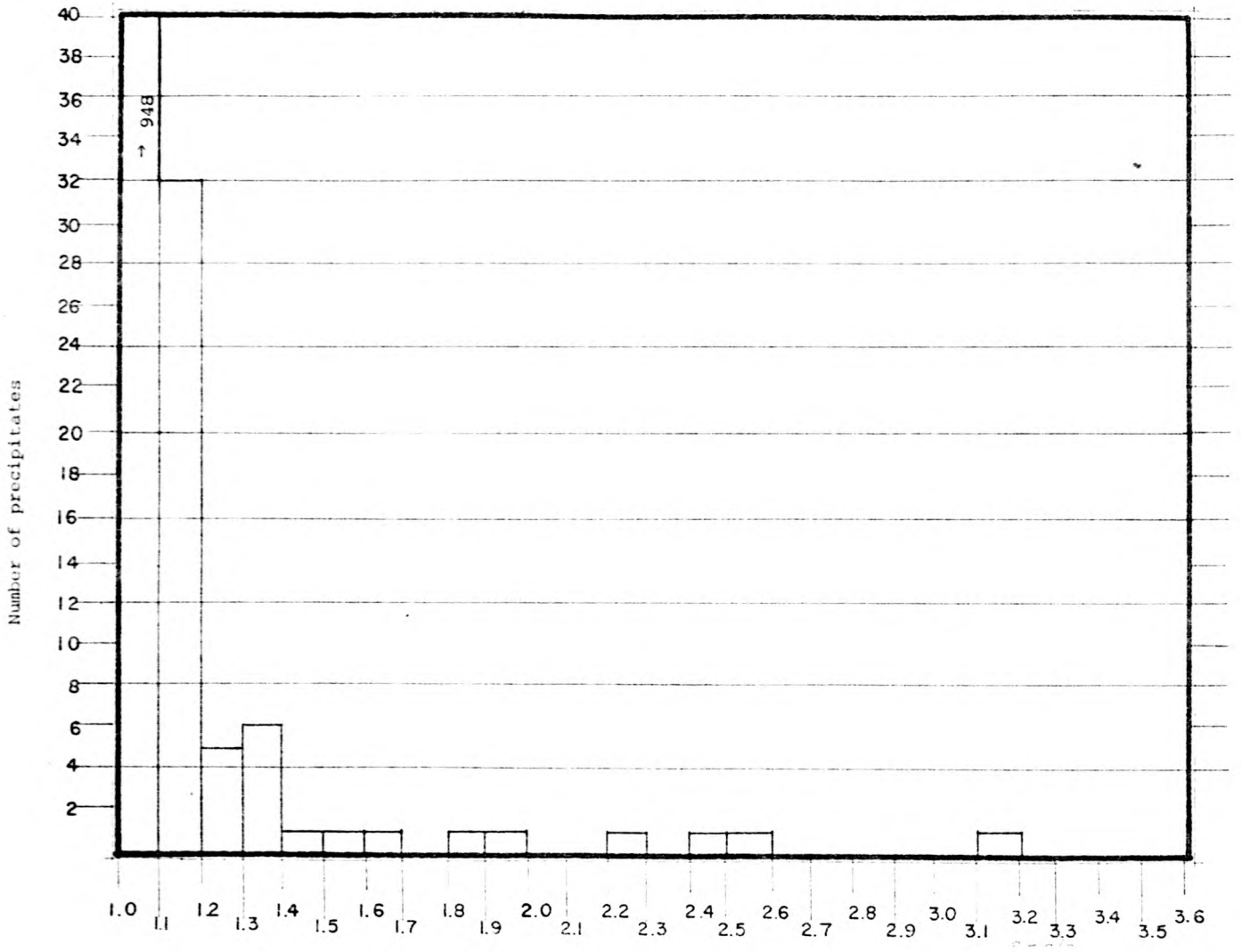
Number of precipitates
40
38
36
34
32
30
28
26
24
22
20
18
16
14
12
10
8
6
4
2
→ 948
1.0
1.1
1.2
1.3
1.4
1.5
1.6
1.7
1.8
1.9
2.0
2.1
2.2
2.3
2.4
2.5
2.6
2.7
2.8
2.9
3.0
3.1
3.2
3.3
3.4
3.5
3.6

where δ stands for "error in", "b" and "a" have the meanings previously described, and $\Delta = \delta b = \delta a$. All plates for these measurements were taken at 50000 X and b and a were measured within $\pm$ 0.5 mm (on the plate); for the sample with samllest precipitates (on the average) $\langle a \rangle$ = 8.9 mm (on the plate) so $\delta(b/a) \gtrsim 0.1$. In figure 3-11 the width of the bars corresponds to the error estimated in this way.

From figure 3-11 it can be seen that, within the accuracy of these measurements, 94% of the precipitates show square sections.

Given the frequency α (0.94 in this case) with which square sections are obtained, it is possible to calculate what the "true" shapes are (in 3 dimensions). In order to do that define

P_1 = the frequency with which the precipitates are cubes.

P_2 = the frequency with which the precipitates are prisms of sides $X = Y \neq Z$

P_3 = the frequency with which the precipitates are prisms of unequal sides $X \neq Y \neq Z$

In order for a precipitate to be cubic it is necessary and sufficient that it has square sections on two perpendicular planes, hence $P_1 = \alpha^2$. If the precipitate is a prism with two equal sides then $P_2 = 2\alpha(1 - \alpha)$; the factor "2" comes from the fact that there are two possibilities: $X = Y \neq Z$ and $X \neq Y = Z$ (the third one $X = Z \neq Y$ does not enter, since the shape is determined by the sections on just two orthogonal planes). Finally if the precipitate is a prism with unequal sides then $P_3 = (1 - \alpha)^2$. In all these calculations use has been made of the results from probability theory $P(A \text{ and } B) = P(A)P(B)$

where P stands for "probability" and A, B refer to (independent) events.

Inserting the measured value of $\alpha = 0.94$ one gets $P_1 = 0.884$ $P_2 = 0.113$ $P_3 = 0.004$ from which it can be concluded that 88% of the precipitates are cubes, it can also be seen that of the remaining 12% most of them are prisms with two equal sides (11.3% of the total) and just a few are prisms of three unequal sides (0.4%).

It is interesting to notice that one of the most obvious differences between a cube and a rectangular prism lies in the fact that, given the volume, the former has the least area; this in turn suggests that minimization of the total area plays a role in the determination of the growth habits of the Suzuki precipitates.

The precipitates appear distributed on the surface in a random manner, but in a small fraction of the cases (3%) they appeared in groups composed of 2, 3 or 4 elements (figure 3-12). In these groups the usual configuration was found to be one in which no special correlation between the positions of the different precipitates was present; however a few instances (5 in 1000 precipitates analyzed) were observed in which the precipitates were aligned over distances of the order of 1 μm (figure 3-13). This suggests that in this case the precipitates were nucleated along an extended defect, such as a grain boundary, but no decoration clues towards the presence of such a boundary were found; and it must be emphasized that the alignment of the precipitates is the exception rather than the rule.

"Collisions" between the precipitates were occasionally observed (figure 3-14); the boundary of each precipitate in the area of intersection can not be seen but otherwise the resulting structure is the overlapping of two precipitates.

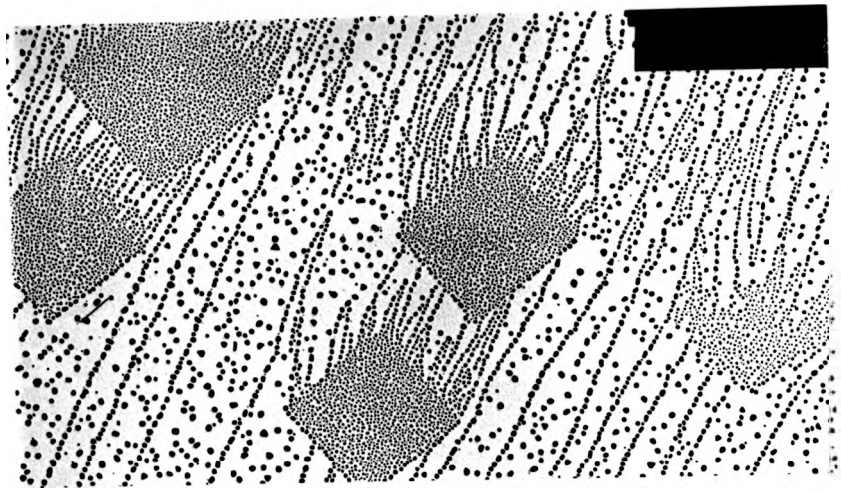

3-12 Sample 98, showing a group of precipitates (84000X).

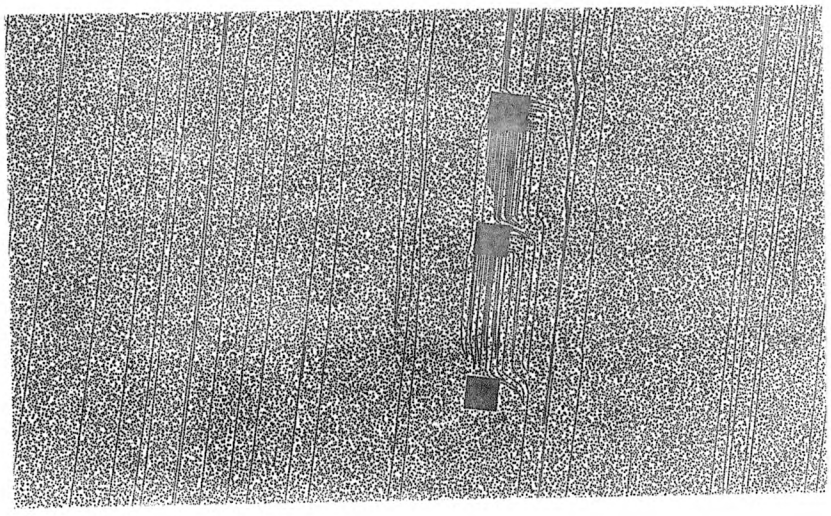

3-13 Sample 114 showing precipitates aligned along a 100 direction (17000X)

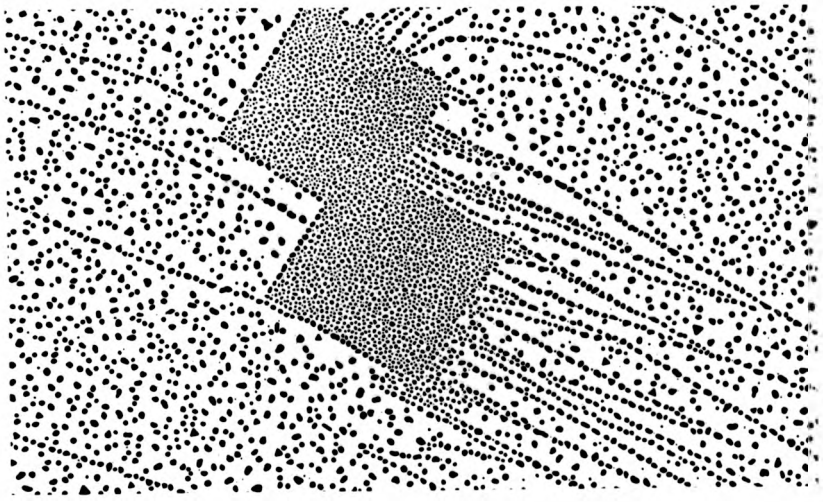

3-14 Sample 96 showing the "collision" of two precipitates (84000).

3.4 Size Distribution of the Precipitates.

In figures 3-15-1 to 3-15-10 the size distribution histograms for the square precipitates are presented. On the vertical axis the number of precipitates is shown and on the horizontal one the corresponding size; the units for the sizes of the precipitates are in mm and correspond to the measured sides on the plates taken at 50000 X (hence 1 unit = 200 A). The sides, on the plate, can be measured within ± 0.5 mm; and the width of the bars on the histogram has been chosen to be twice the estimated error so the bars can be considered as representative of the size interval to which they refer.

In figure 3-16 the mean precipitate size is plotted against impurity concentration for the three cooling rates used (full line) and these results are compared with those by Kirk et.al. (21) (dotted line), the later were calculated directly from their histograms. From the graph it can be seen that the precipitate mean side is an increasing function of impurity contents and a decreasing function of cooling rate. This is in agreement with the facts that the larger the impurity content the larger amount of material that can be precipitated; and the slower the cooling rate the larger the time spent at the temperature at which precipitation takes place.Similar results have been reported previously by Kirk et.al. (21); however, as shown in figure 3-16, given an impurity contents the mean size obtained in the present research is smaller than that obtained by these authors.

In table 3-2 the "spread" in size for the precipitates is presented against impurity concentration for different cooling rates. Here the root mean square deviation from the mean has been used as a measure of the spread; the dotted line represents the results by Kirk et.al. (21) as obtained from their size distribution histograms. It can be seen that the

3-15 1 to 3-15-10. Size distribution for ten samples.

Figure 3-15-1 Sample 87

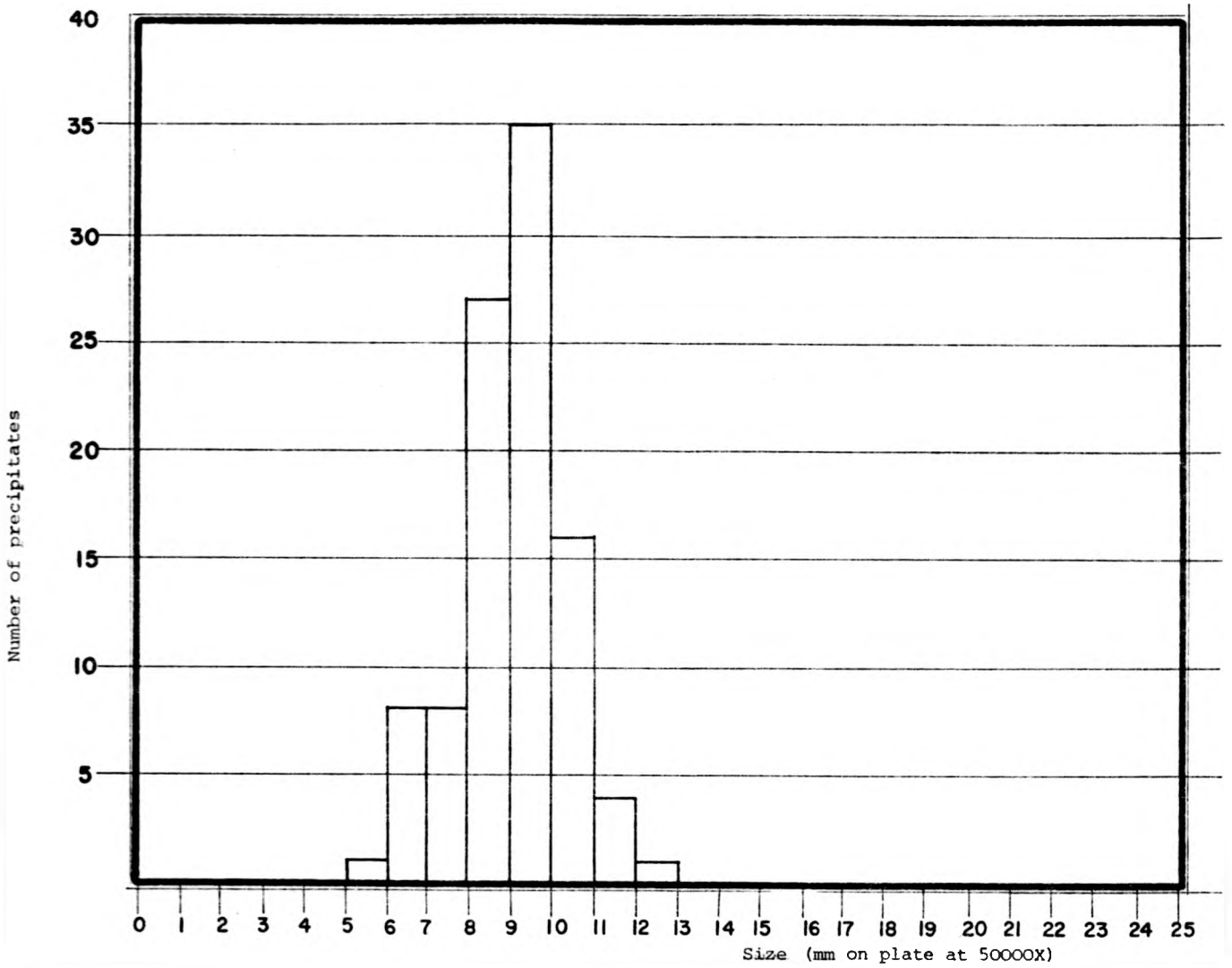

Figure 3-15-2 Sample 104

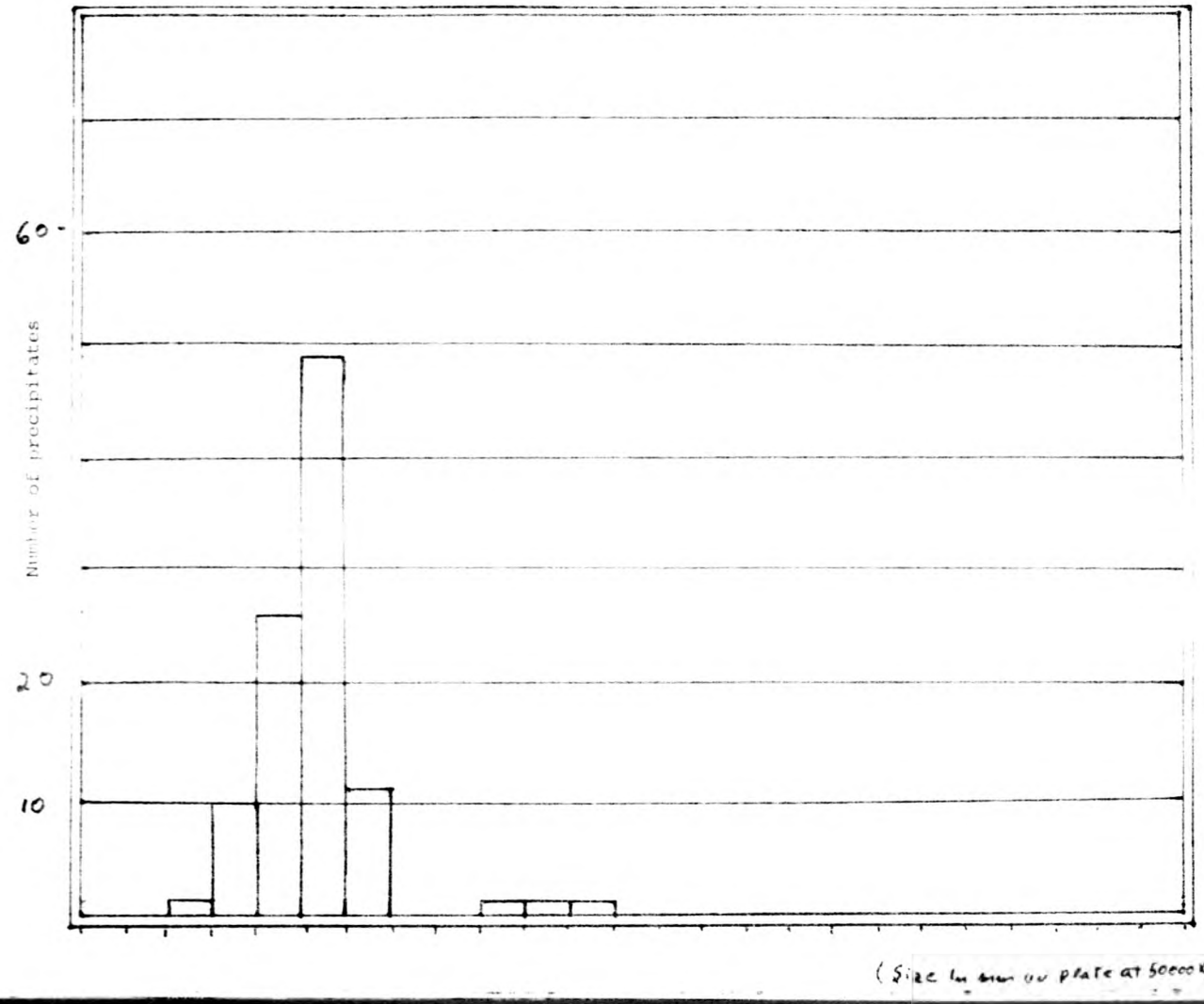

Figure 3-15-3 Sample 96

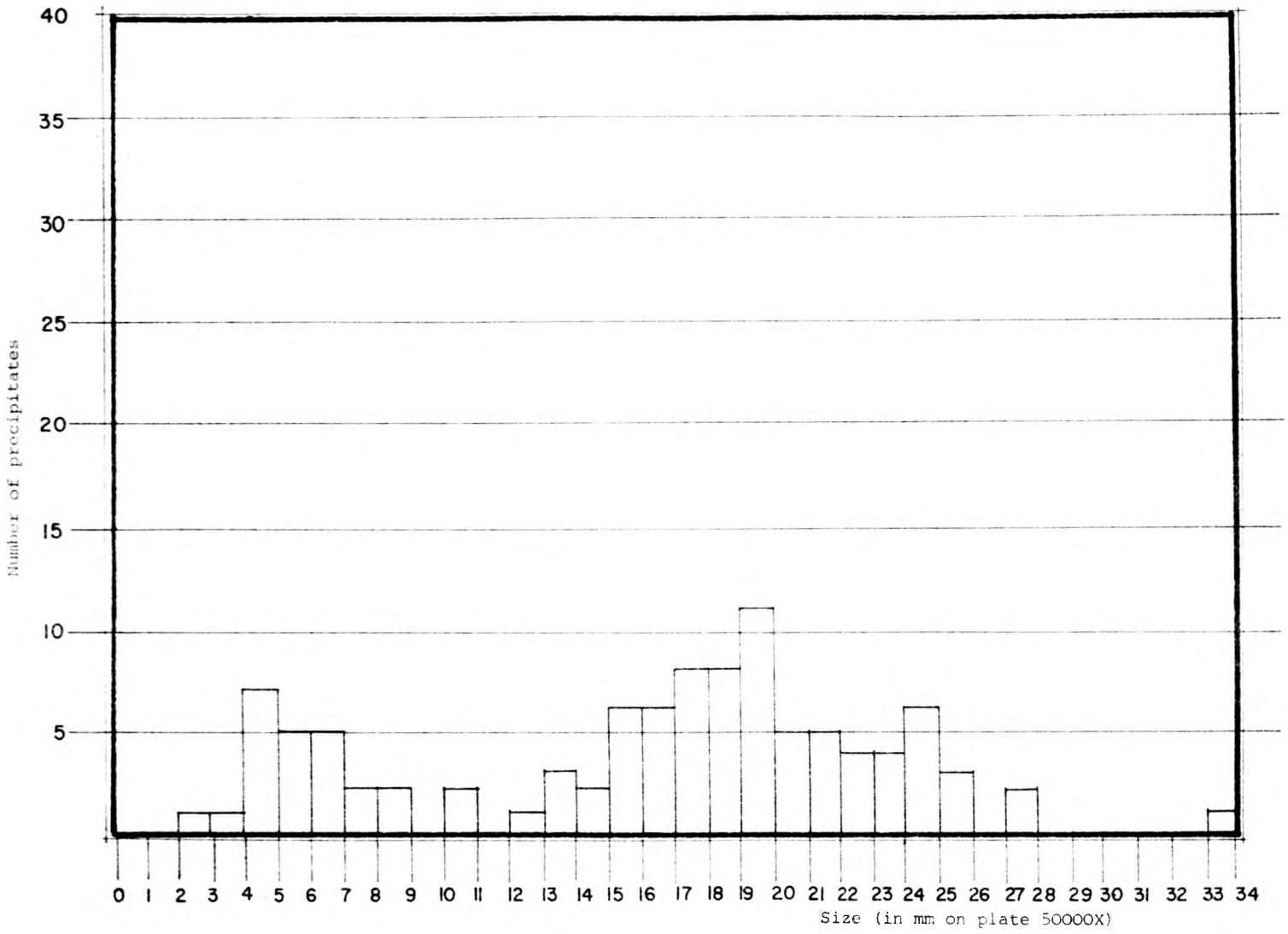

Figure 3-15-4 Sample 103

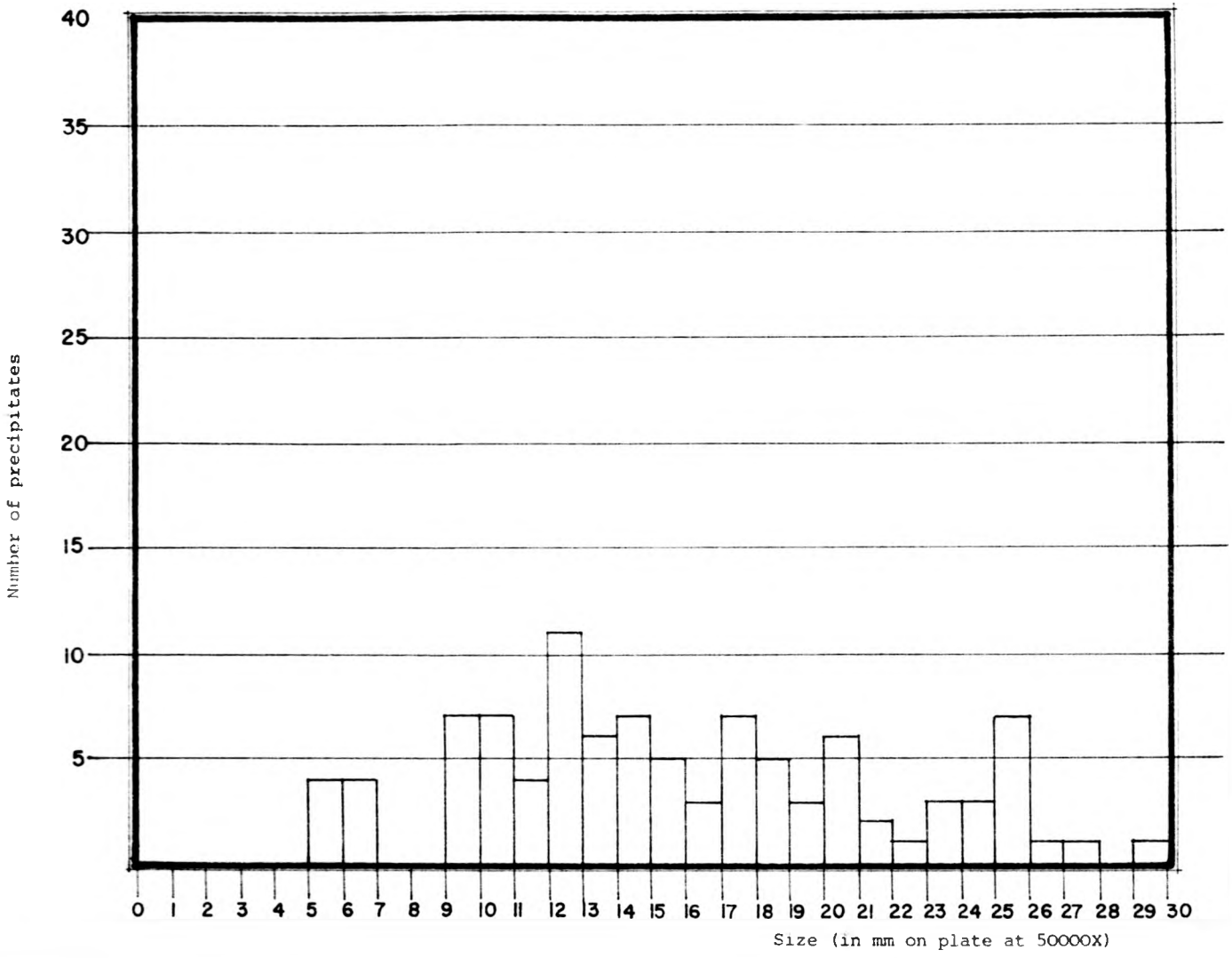

Figure 3-15-5

Sample 105

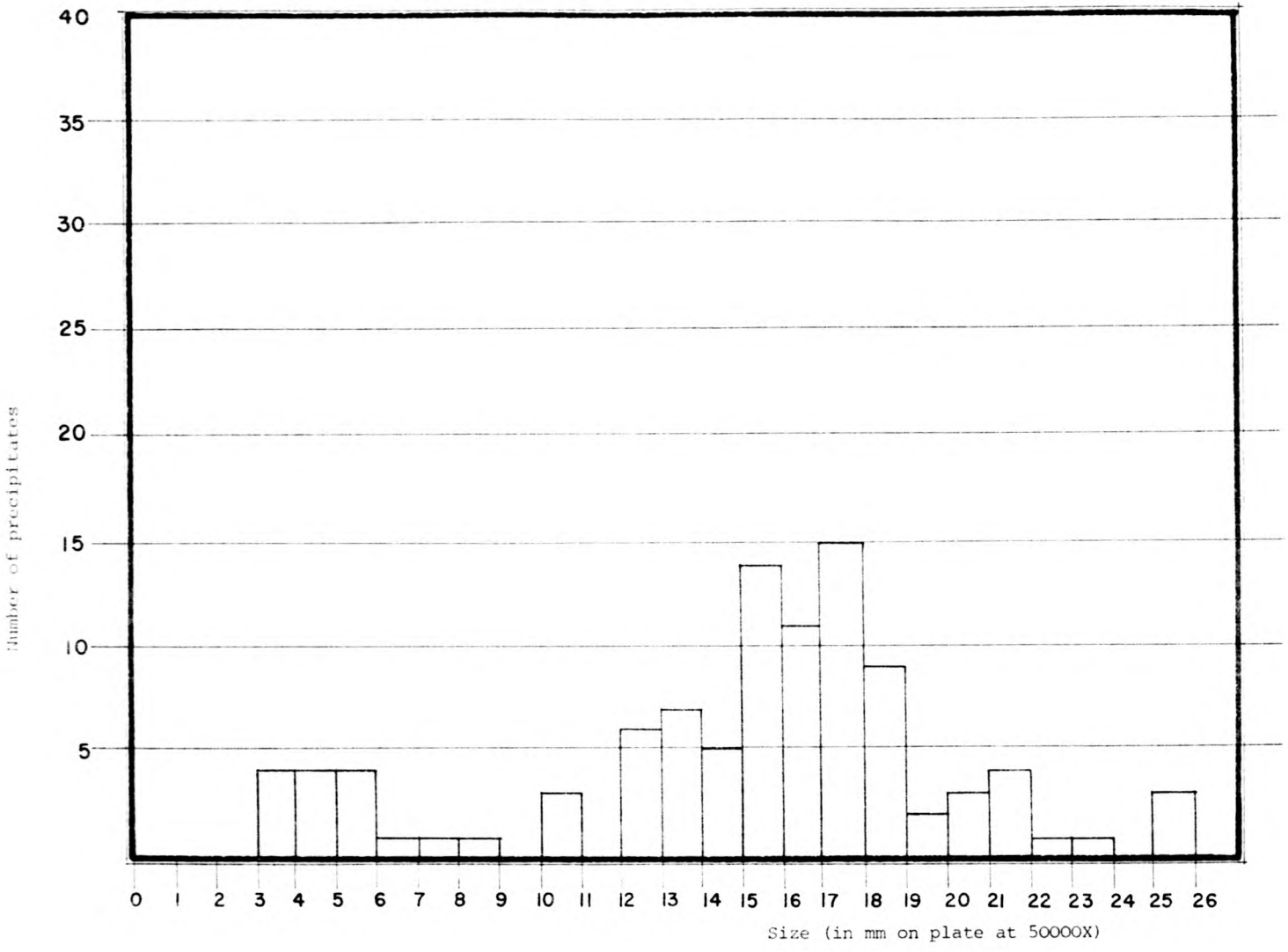

Figure 3-15-5

Sample 105

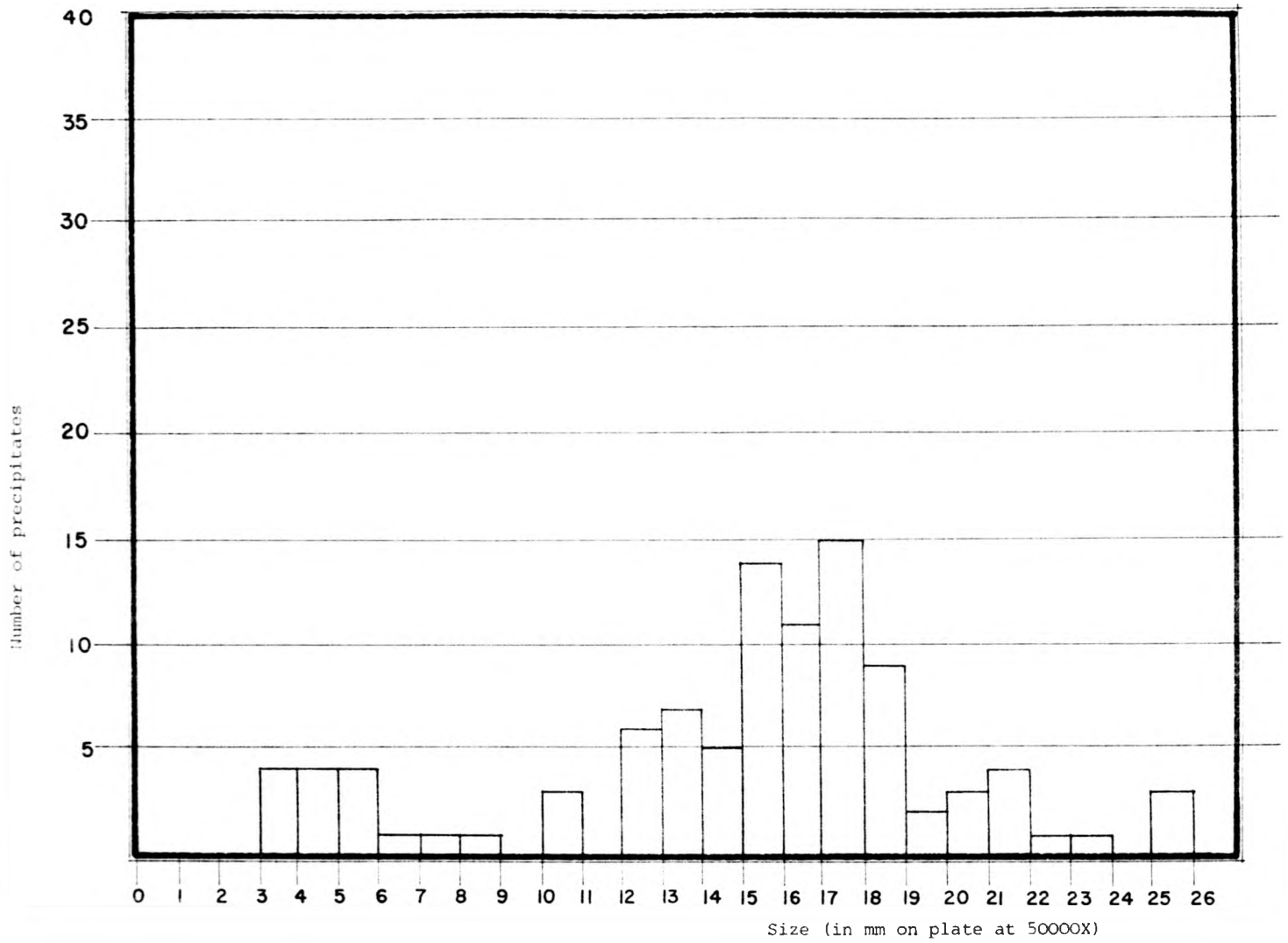

Figure 3-15-6 Sample 99

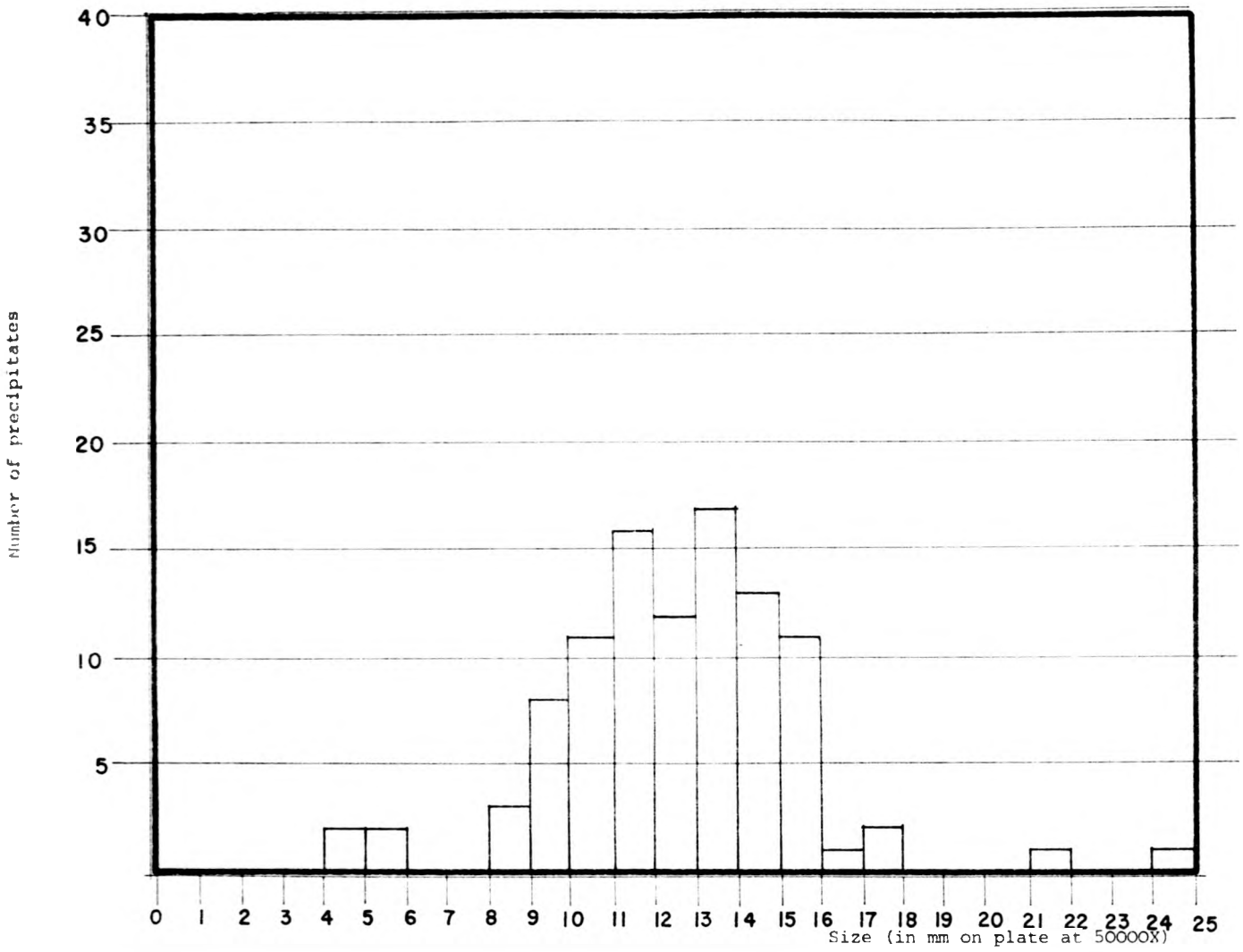

Figure 3-15-7 Sample 109

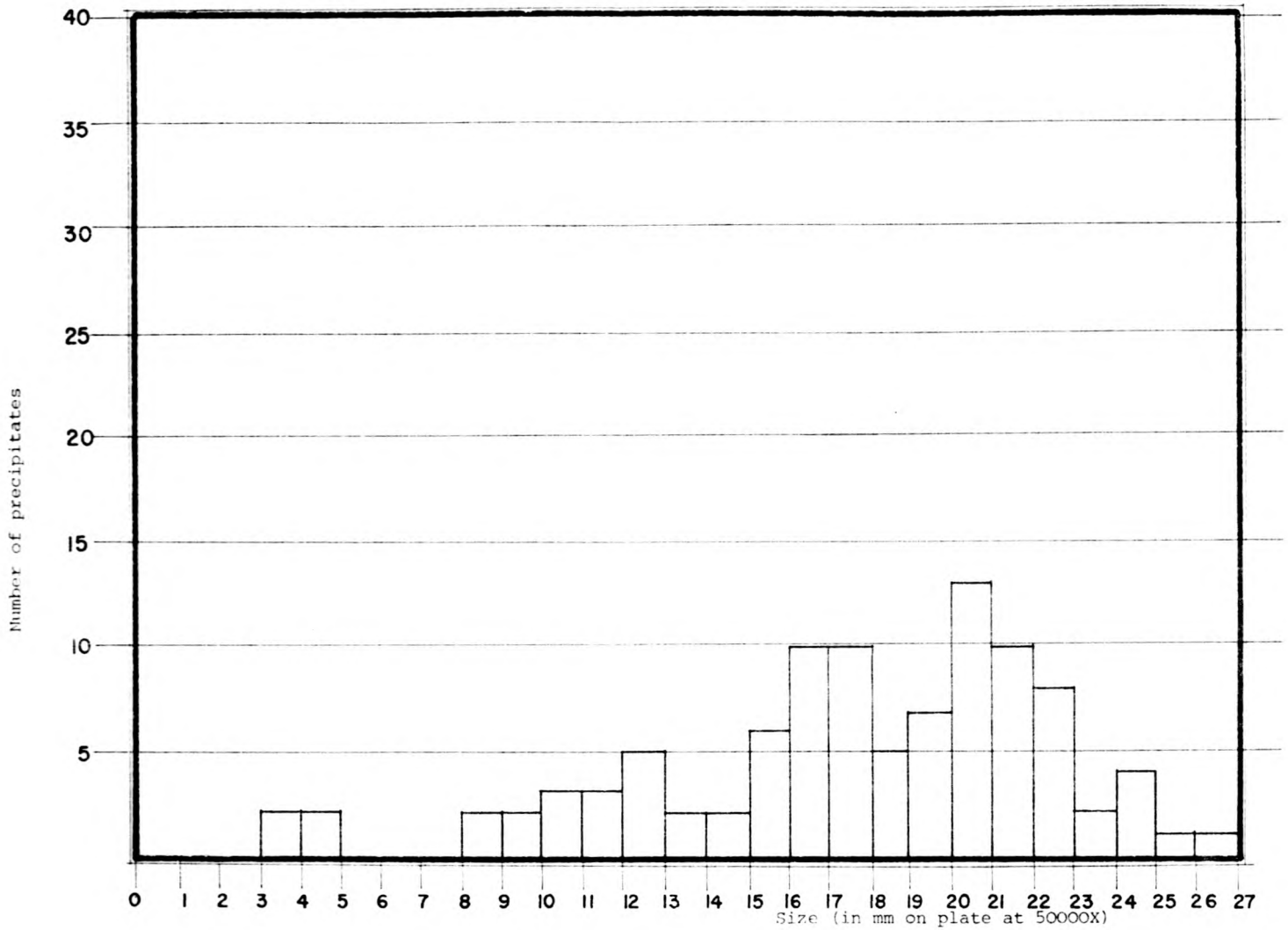

Figure 3-15-8 Sample 98

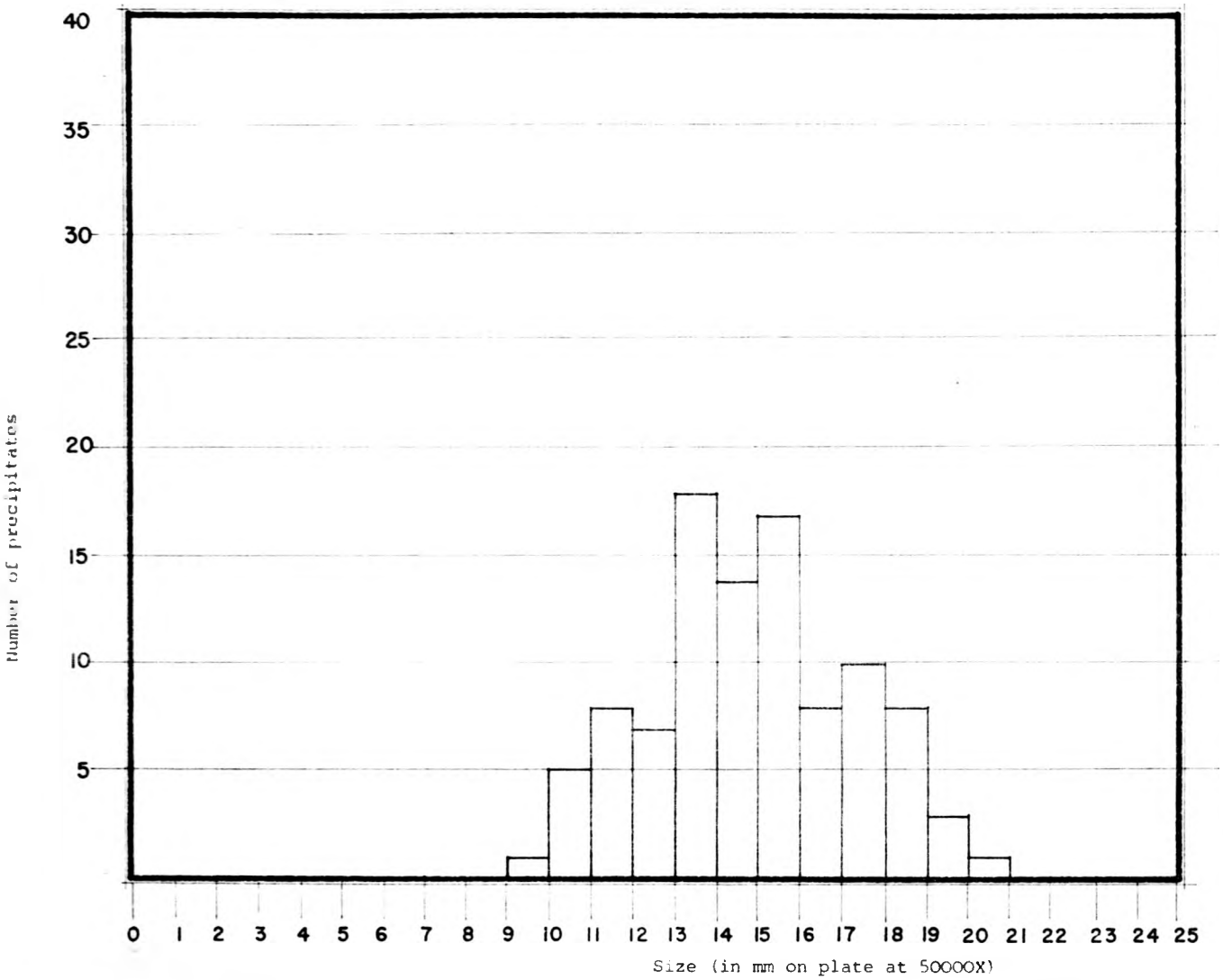

Figure 3-15-9 Sample 93

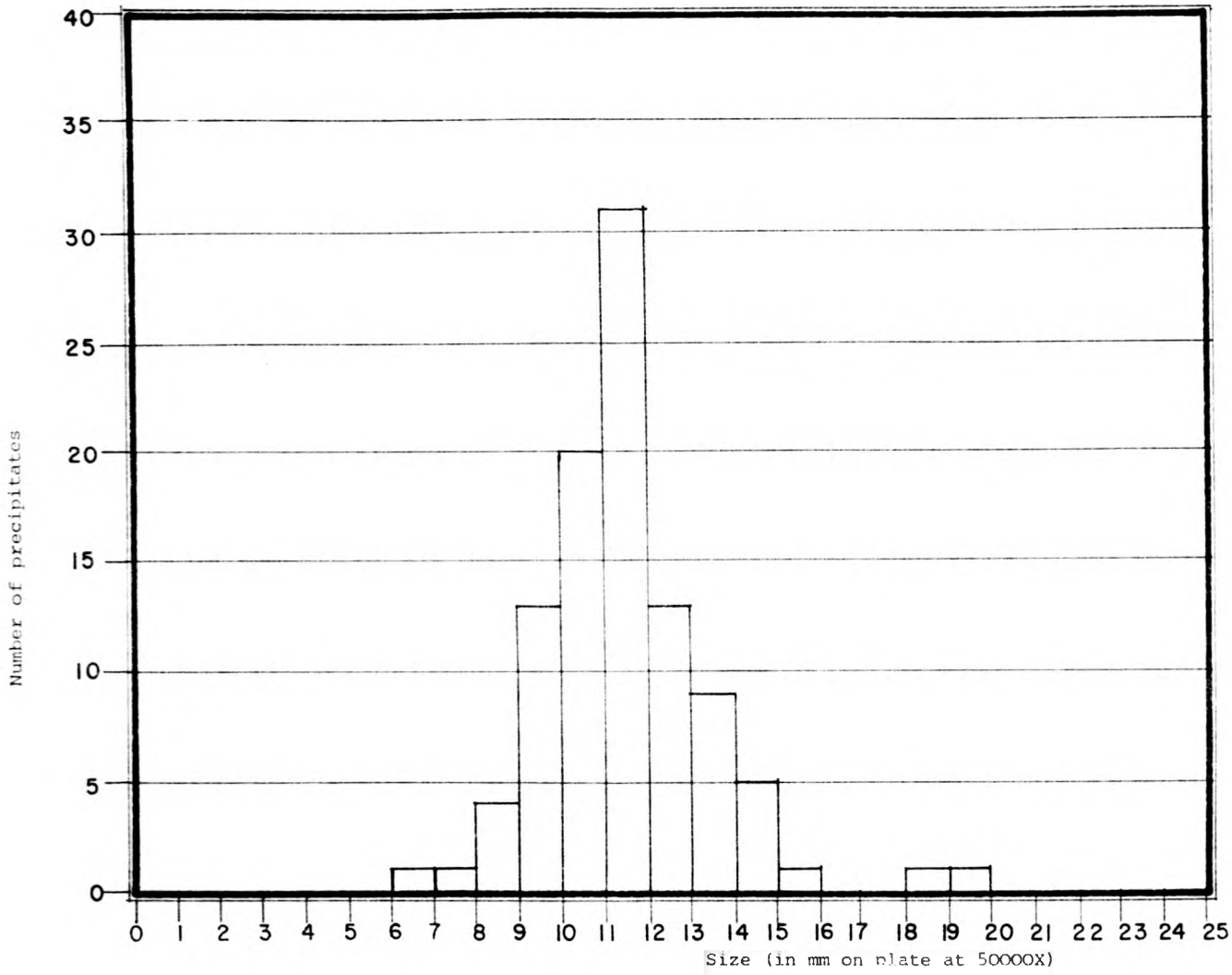

Figure 3-15-10 Sample 114

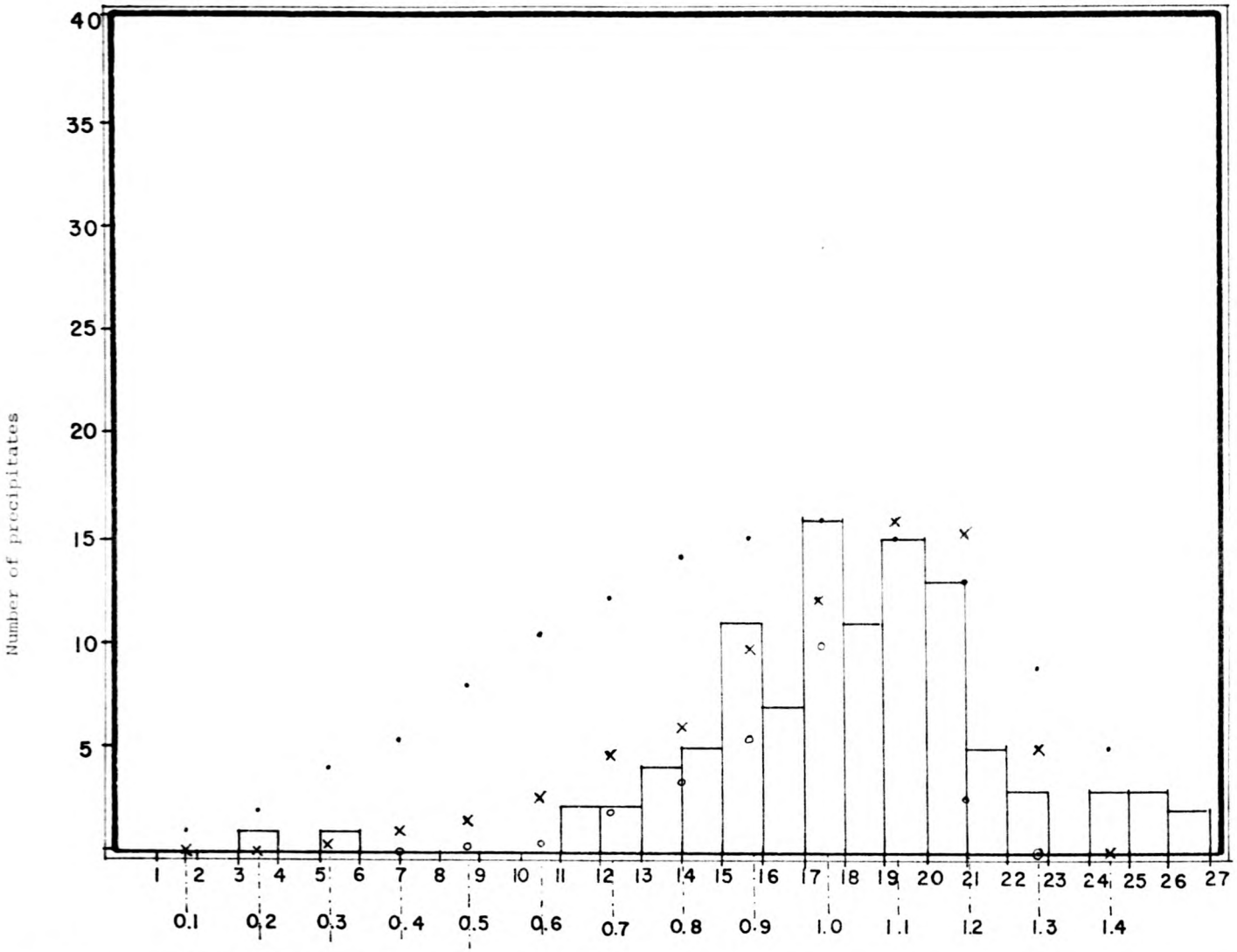

TABLE 3 - 2

Sample	Concentration ppm	Cooling Rate (C°/hr)	Spread (Å)
87	349	11	250
93	368	11	380
96	459	11	1380
98	438	11	480
99	390	6.9	600
105	442	6.9	1000
109	340	4.1	1000
114	378	4.1	740
104	463	as grown	1000

Concentration of Mn, cooling rates (linear cooling from 650°C) and spread in size of the Suzuki Precipitates (root mean square deviation from the mean for 100 precipitates) for the samples used in this work.

3-16 Dependence of mean precipitate size with concentration for various cooling rates. The results by Kirk et al. (21) are also shown.

Key: ○ Kirk et. al. (21)

× Present research (11°C/h cooling)

□ Present research (4.1°C/h cooling)

• Present research (6.9°C/h cooling)

tration
et al.

spread increases with the Mn concentration and decreases with the cooling rate; again the present results are qualitatively in agreement with those by Kirk et.al (21) but in quantitative disagreement.

As it has been mentioned in chapter 1; Jain and Hughes (25) studied the Ostwald ripening in the NaCl:$MnCl_2$ system. Following the Lifschitz-Slezov-Wagner (LSW) theory for Ostwald ripening and extending it to the case when diffusion through dislocation is the main transport mechanism; these authors considered three cases for the ripening:

1) When the predominant mechanism is a surface controlled aggregation.
2) When the predominant mechanism is the bulk diffusion.
3) When the predominant mechanism is diffusion through dislocations.

In these cases it is possible (within the LSW theory) to derive expressions for the size distribution of the particles, the distribution functions being for the three cases described above $F_1(u)$, $F_2(u)$, and $F_3(u)$ respectively and given by equations 3-1, 3-2 and 3-3.

$$(3\text{-}1)\quad F_1(u) = \begin{cases} \dfrac{u\,\exp\left(\dfrac{-3u}{2-u}\right)}{(2-u)^5} & \text{if } u \in [0,\ 2] \\ 0 & \text{if } u \in [2,\ \infty] \end{cases}$$

$$(3\text{-}2)\quad F_2(u) = \begin{cases} \dfrac{u^2\,\exp\left(\dfrac{-2u}{3-2u}\right)}{(3+u)^{7/3}\,(3-2u)^{11/3}} & \text{if } u \in [0,1.5] \\ 0 & \text{if } u \in [1.5,\infty] \end{cases}$$

$$(3\text{-}3)\quad F_3(u) = \begin{cases} \dfrac{u^3\,\exp\left(\dfrac{-2}{3(uo-u)}\right)\,\exp\left(\dfrac{-1}{6\sqrt{2}}\right)\tan^{-1}\left(\dfrac{u+uo}{uo\sqrt{2}}\right)}{(uo-u)^{17/6}\,(u^2+2\,uuo+4\,uo)^{23/2}} & \text{if } u \in [0,\ uo = \tfrac{4}{3}\,] \\ 0 & \text{if } u \in [uo = 4/3,\ \infty] \end{cases}$$

where F represents the distribution function and u is the reduced variable $u = R/\bar{R}$ (R is the precipitate size, $\bar{R}$ is the mean value for R in the sample). These expressions are not expected to hold for very small particles, if by small one means particles for which α^* is not small compared with the unity, α^* being defined as

$$\alpha^* = \frac{2\Omega\sigma}{KT} \tag{3-4}$$

Ω = atomic volume
σ = surface energy
K = Boltzman's constant
T = the absolute temperature

In the region of small u (or R) the expressions for the distribution curves become $F \propto R^n/(\exp(\alpha^*/R)-1)$

(n = 1, 2, 3 depending on the case, as described before). In their study, Jain and Hughes explored the agreement between these theoretical distribution curves and the experimental data by Kirk et al. (21). It was found that for the sharpest distribution obtained by Kirk et al., there is a good fit if one uses the surface controlled F_1 (u) expression (eq. 3-1).

The experimental distribution curves obtained in the present research (figures 3-15-1 to 3-15-10) have been compared with the three distribution functions F_1, F_2 and F_3. For the samples in figures 3-15-3 to 3-15-8 and 3-16-10 the data presented can not be fitted with a single distribution curve F_i (i = 1,2,3) for they show several peaks.

TABLE 3 - 3

distribution	value of u = for which curve has a maximum	half width	case
F_1	$1.00 = u_0$	0.845	surface controlled process
F_2	$1.135 = u_0$	0.48	bulk diffusion controlled process
F_3	$1.142 = u_0$	0.25	dislocation-line controlled process

Sample	experimental u_0	u	possible distribution
104	1.135	0.40	F_2
87	1.135	0.33	F_2
99	1.2	0.49	F_2
109	1.19	0.406	F_2
114	1	0.45	F_2
93	1.026	0.35	F_2
98	1.08	0.41	F_2
• Kahn's (9) with a = 1280 A	1	0.83	F_1

Expected and observed parameters for the size distribution curves.

The symbols have the meanings adscribed in the text.

The distribution curves in figures 3-15-1, 3-15-2 and 3-15-9 were plotted in terms of the variable u and are presented again in figures 3-17, 3-18 and 3-18-a together with the appropriate F_1, F_2 and F_3. Here by appropriate it is meant that u has been calculated in terms of the experimentally measured R = a = precipitate mean side. It should be noticed that the F_i (i=1,2,3), given R contain no adjustable parameters, apart from a normalization constant.

From figure 3-17 it can be seen that none of the 3 distribution curves gives a good fit to the experimental histogram. That the fit is not good in the region $[0, u = 1]$ can be understood on the basis that one of the approximations used in deriving equations 3-1, 3-2 and 3-3 breaks down, namely that the Gibbs-Thompson equation can be written as

$$(3\text{-}5) \qquad C = C_\infty \exp\left(\frac{2\Omega G}{RKT}\right) \simeq C_\infty\left(1 + \frac{2\Omega G}{RKT}\right)$$

(here C is the solute concentration in equilibrium with a precipitate of radius R whose surface energy is G and of atomic volume Ω ; K and T are Boltzmann's constant and the absolute temperature respectively; C_∞ is the solute concentration in equilibrium as R tends to ∞). The fit is unsatisfactory also in the range $[1,2]$.

The sample used for graph 3-17 contained 349 $\pm$ 5 mppm of manganese and was cooled at a rate of 12.5° C/hour, this can be compared with figure 3-6 of Kirk et al. (21) for a crystal with 375 mppm and cooled at 15° C/hour. It can be concluded that none of the theoretical distributions fits well the experimental data, but the distributions $F_2(U)$ and $F_3(U)$ gave a reasonable fit; it is

3-17 Same size distribution as in figure 3-15-1 but in terms of $V = R/\bar{R}$. The three theoretical distribution curves are also plotted.

• F_3

⊙ F_2

X F_1

Figure 3-17 Sample 87

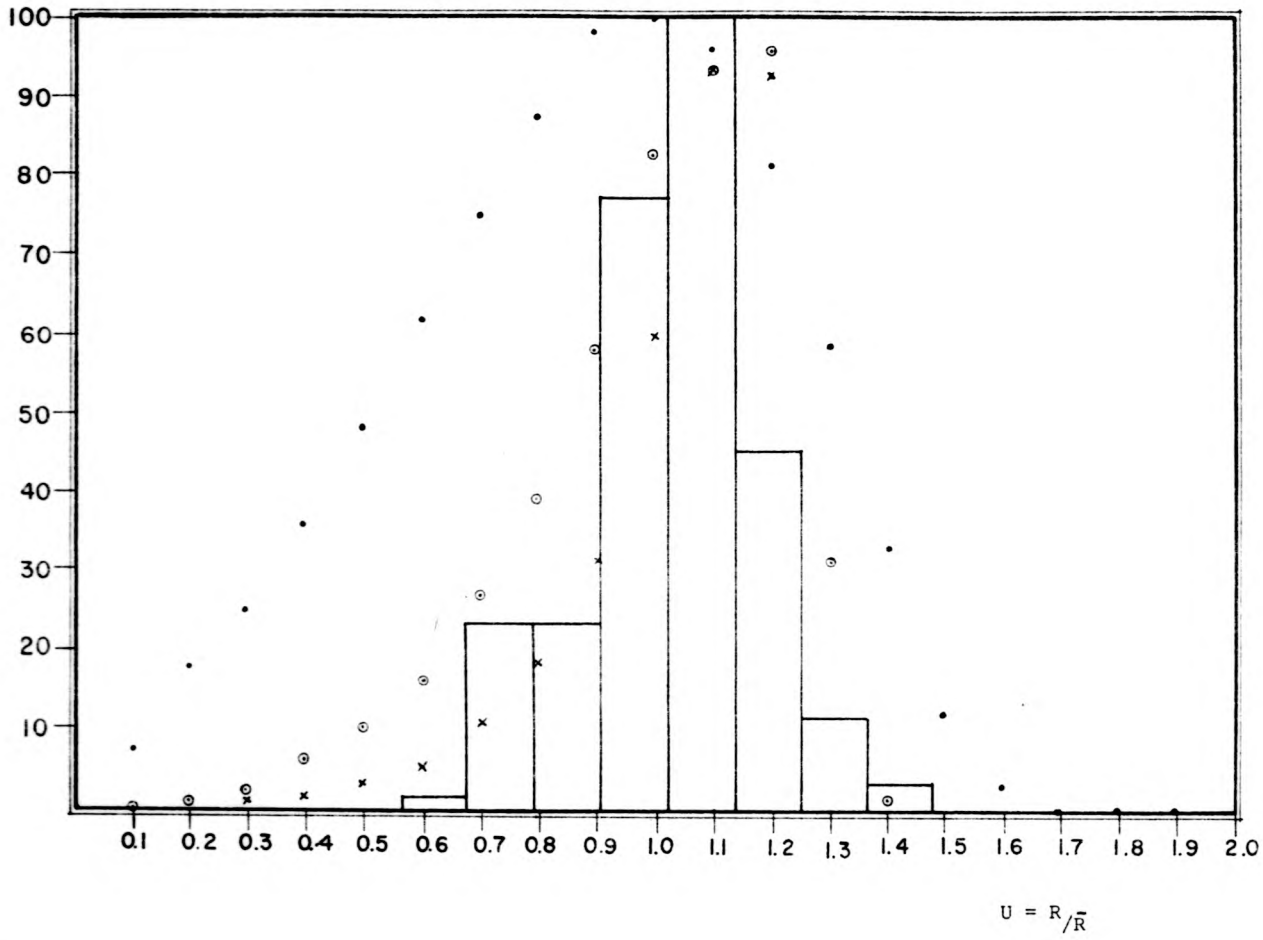

3-18 The same size distribution as in figure 3-15-2 in terms of $V = R/\bar{R}$ and comparison with theoretical curves.

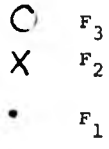

oretical

Figure 3-18 Sample 104

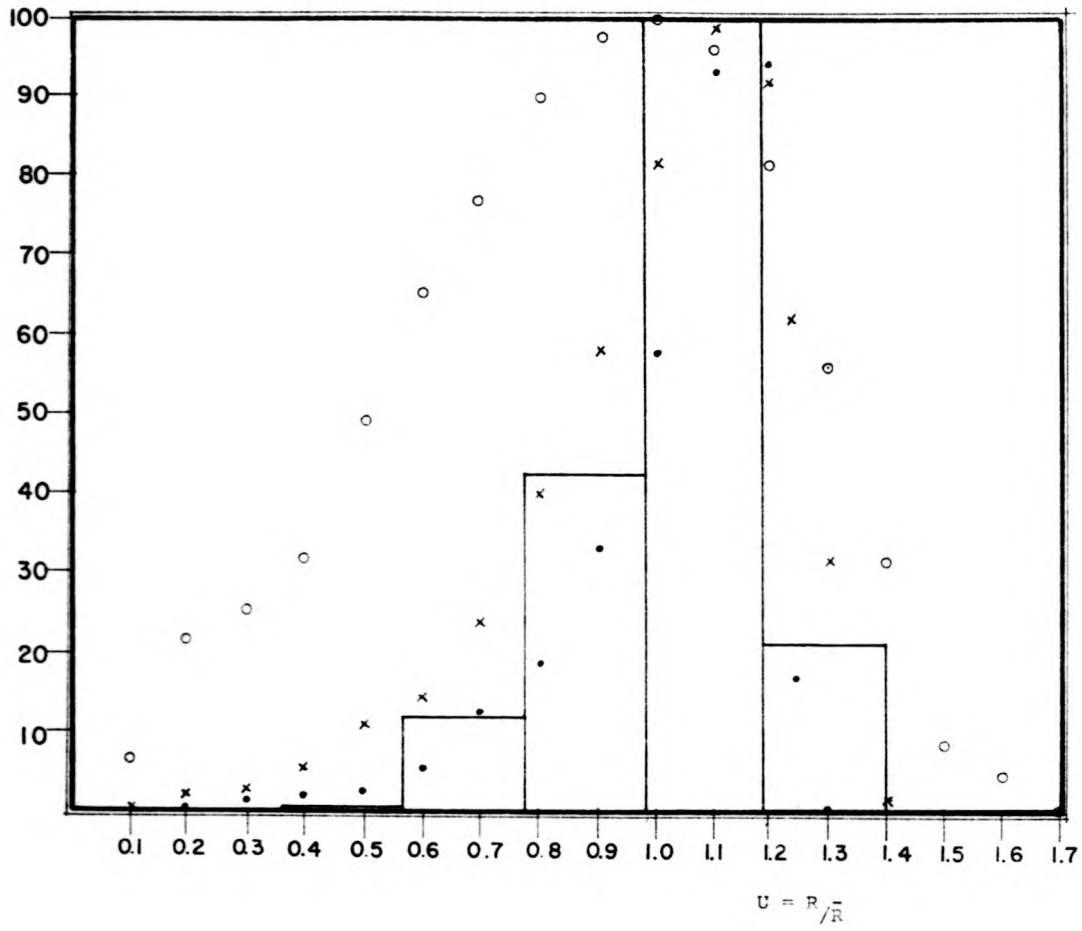

3-18- a Size distribution for sample 93 (370 ppm)

and comparison with the theoretical curves

• = F_1

0 = F_2

X = F_3

Figure 3-1 8-a Sample 93

Figure 3-1 8-a Sample 93

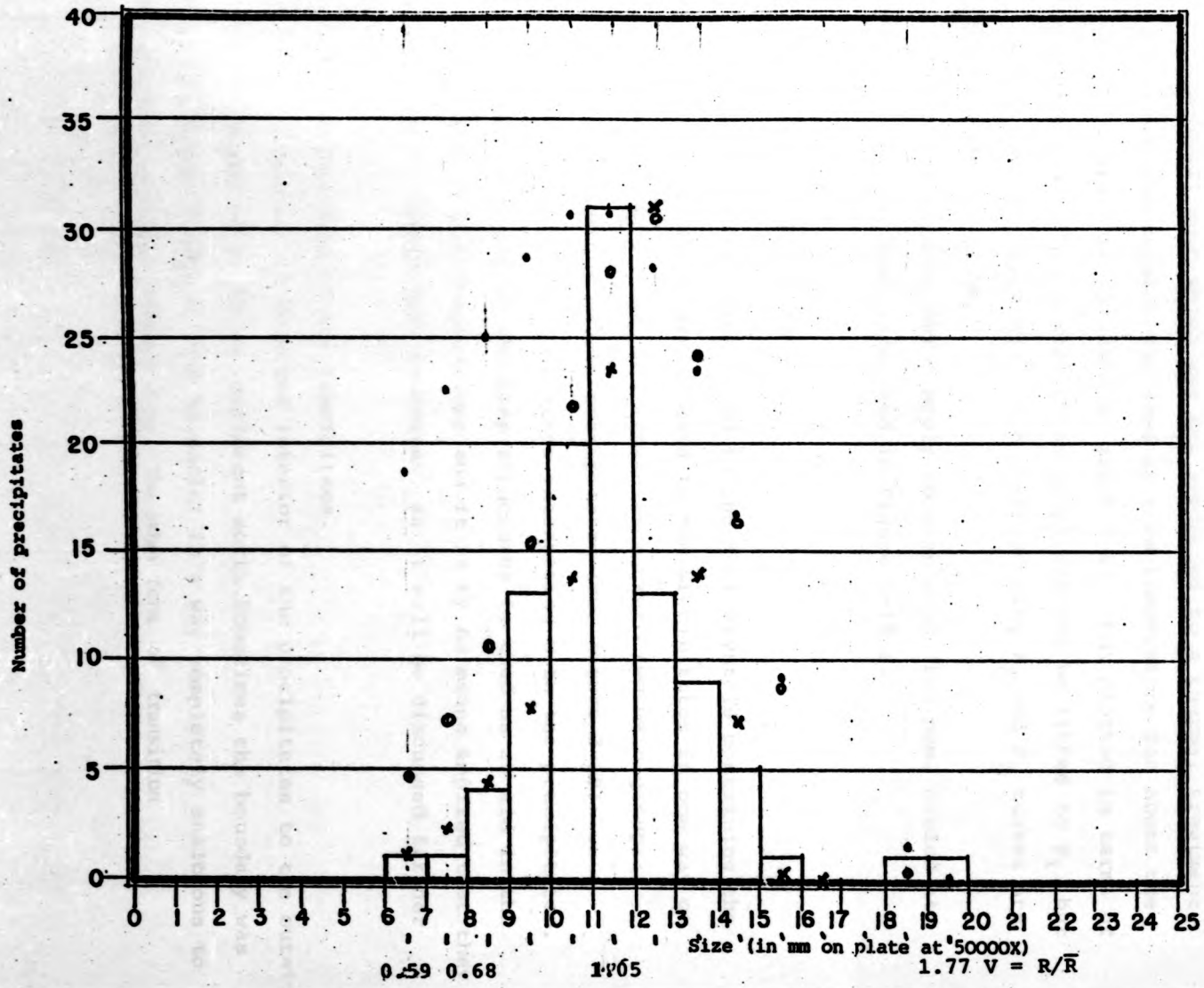

concluded, however, that of the three processes represented by equations 3-1, 3-2, 3-3; the surface controlled one cannot be the dominant in this case.

Figure 3-18 shows the experimental distribution curve for a sample with 471 mppm which was not subjected to a thermal treatment, after growth the crystal was aged at room temperature for about one year. This graph is the same as graph 3-13-1 but plotted in terms of the variable u. This distribution graph can not be fitted to F_1, but F_2 and F_3 give a closer fit. The corresponding F_2 and F_3 curves are shown also on the graph.

Similar consideration apply to sample 93 (B68 ppm, cooled at 11°C/h) which has been presented in figure 3-18-a.

3.5 The Step Structures.

The step structures found in the NaCl crystals containing the Suzuki phase and which are related to the precipitates in one way or another can be separated, for convenience, into two main groups:

a) The boundaries of the precipitates (see figure 3-19)

b) The cleavage and slip steps interacting with the precipitates.

This division of the step structures is used as an aid in the presentation of the observations and it is by no means implied that they correspond to independent processes, as it will be discussed further later.

3.5.1 The Boundary of the Precipitaes.

The transition from the interior of the precipitates to the outside was found to be of two different sorts.Sometimes the boundary was marked by"lines"formed by the Au nuclei in a way completely analogous to gold decoration of normal cleavage steps. The other form of transition

was characterized by the absence of step-like lines; the boundary was just the region in which small but more numerous nuclei (revealing the precipitate) were separated from the rest of the surface, which had a nuclei density similar to that in flat regions of undoped crystals. Figure 3-20 shows a precipitate two of whose boundaries are of one sort and two of the other.

The presence and nature of the boundaries was found to depend on the relative orientations of the precipitate and the local direction of propagation of the cleavage front (as determined by the direction of neighbouring cleavage steps) in the following ways:

1) When the direction of the cleavage was (100) or close to it, the boundary consisted generally of three lines of step-like character (figure 3-21). In a few instances all four sides were of this sort (figure 3-22). (In these figures the direction of cleavage is represented by an arrow).

2) When the direction of propagation of the cleavage crack was not parallel to the sides of the precipitate, then invariably 2 sides of the precipitate were marked by step-like lines and on two sides there was no such a step-like boundary. The two sides revealed in a step-like manner were always those met by the cleavage front first (figure 3-20).

In figure 3-23 different morphologies for the boundaries are presented and figures 3-24 to 3-26 show examples of these. In some instances the boundary of the precipitates appear to be curved towards the outside of the precipitate, as shown in figure 3-24; giving extra support to the idea that the boundaries are cleavage structures. Instances have been also found where a cleavage step meets the boundary (figure 3-27) and merges with it so it is concluded that the step-like boundaries

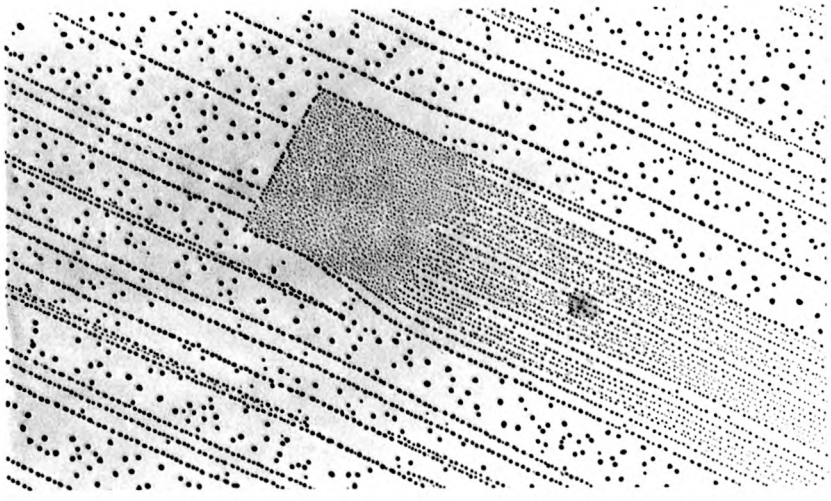

3-19 Sample 109, to illustrate the boundary (step) of the precipitates (84000X).

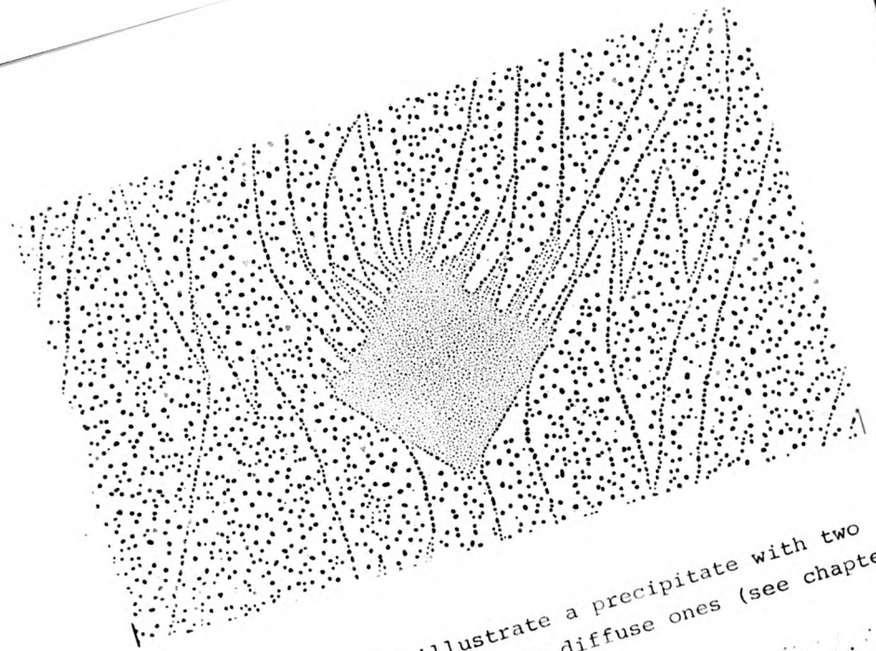

3-20 Sample 98, to illustrate a precipitate with two step-like sides and two diffuse ones (see chapter 3). (84000X).

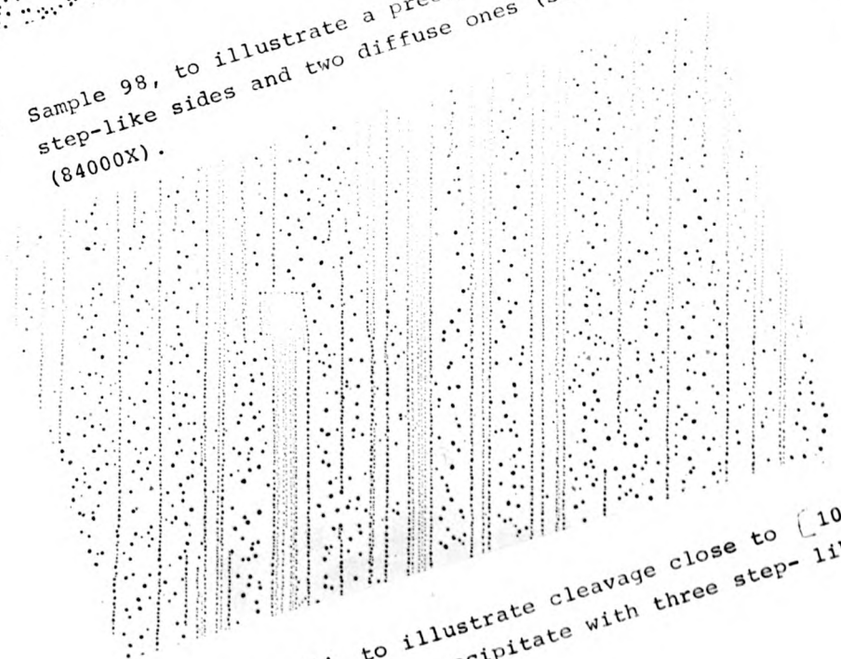

3-21 Sample 104, to illustrate cleavage close to {100} direction and a precipitate with three step- like sides (84000X).

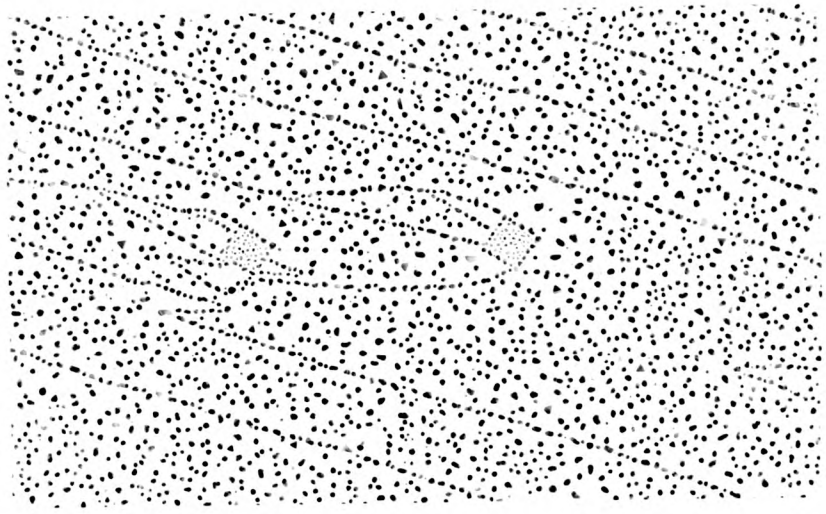

3-22 Sample 96, illustrating precipitates with four step-like sides (84000X).

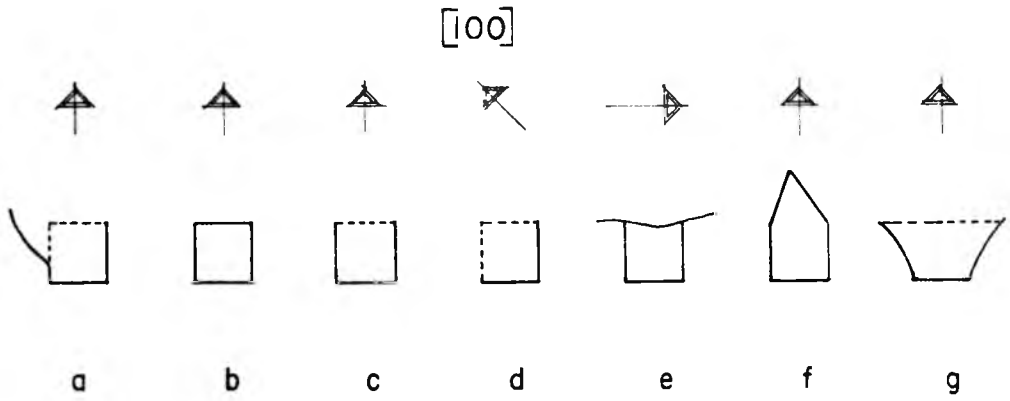

Arrow indicates cleavage direction

Figure 3-23: Schematic representation of the various morphologies found for the boundary of the precipitates.

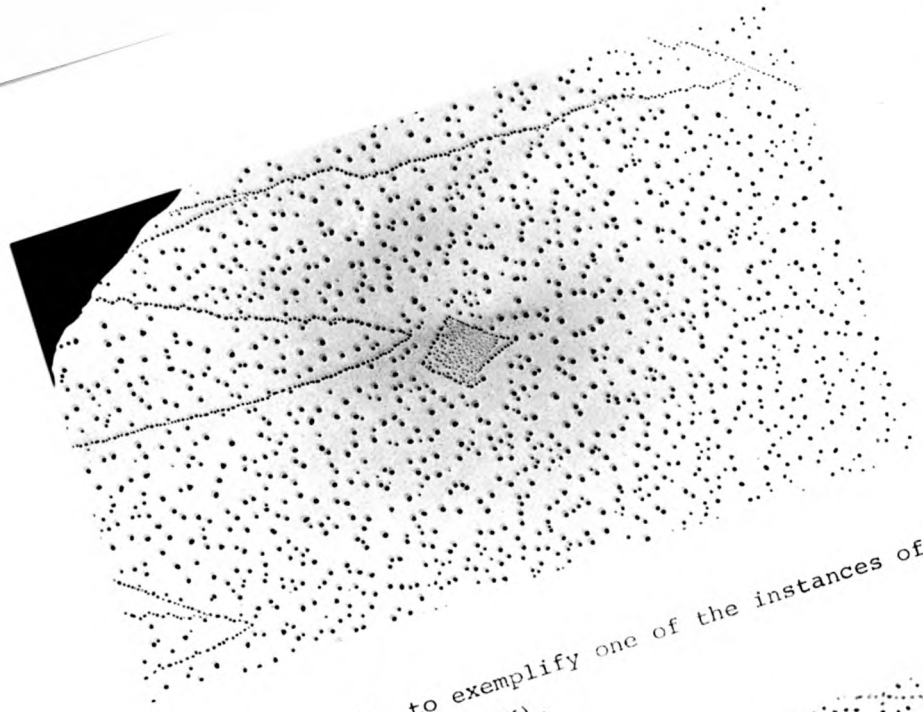

3-24 Sample 104, to exemplify one of the instances of figure 3-23 (84000X).

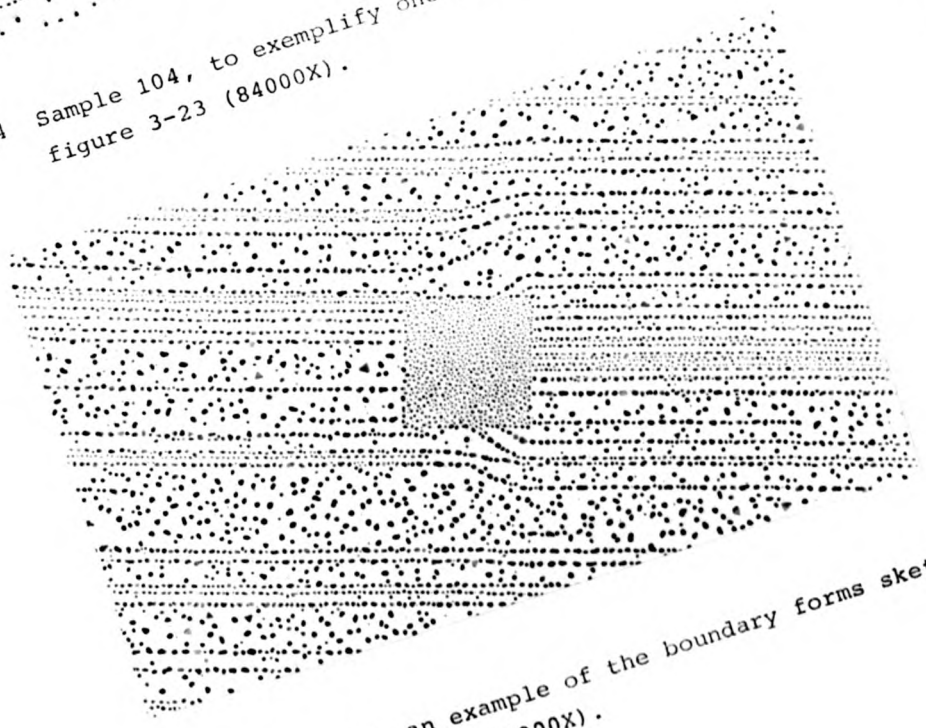

3-25 Sample 99, an example of the boundary forms sketched in figure 3-23 (84000X).

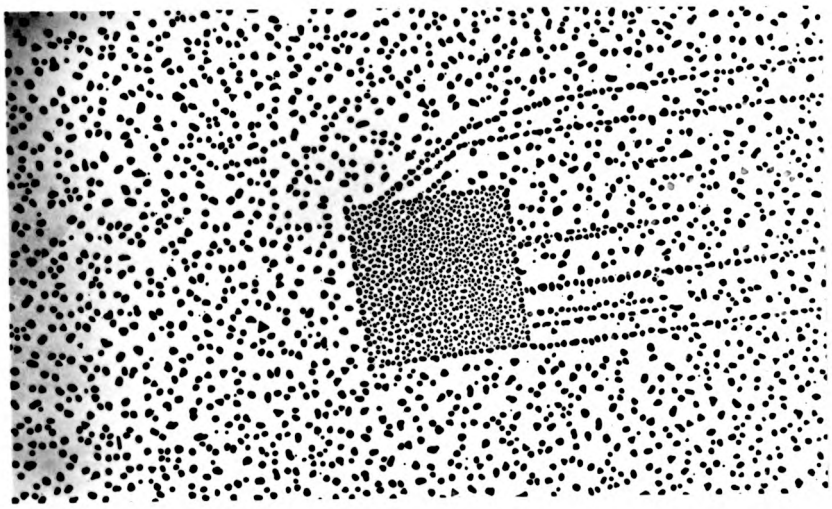

3-26 Sample 105, to exemplify figure 3-23 (84000X)

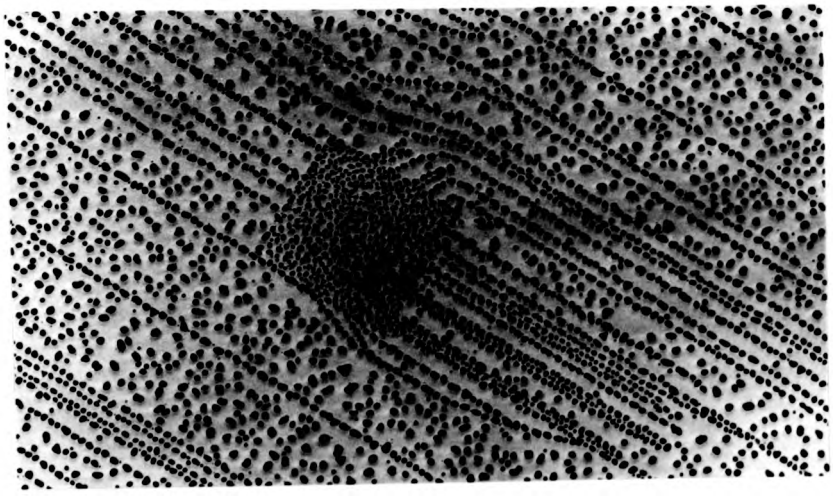

3-27 Sample 96, example of cleavage steps meeting and joining the precipitate boundary (84000X)

are steps indeed.

3.5.2 Interaction of Steps with Precipitates.

For convenience the observed interactions between the precipitates and the various step structures present on the surface of the crystals will be divided in three categories (again it is not implied that the phenomena responsible for these structures are different or independent):

1) The interaction of cleavage steps with precipitates.
2) The step structures inside the precipitate.
3) Steps and V shaped structures arising from the precipitates.

3.5.2.1. Interaction of Cleavage Steps with Precipitates.

The cleavage steps on the surface are affected by the presence of the precipitates. Figure 3-28 shows schematically the different morphologies observed, in this figure the arrow represents the direction of the incoming cleavage front and the full lines refer to the cleavage steps. All the cases shown in this figure are really variations of the same phenomenon: the cleavage steps curve in the neighbourhood of the precipitates.

When the cleavage proceeds on a $\{100\}$ direction (or very close to it) the steps behave in the neighbourhood of the precipitates in the ways a, b, c shown in figure 3-28, the cases a and b being the least frequent. The general trends observed have the following characteristics:

1) The bending is always such that the step tends to avoid the precipitate (figure 3-29).
2) Those steps that meet the precipitate despite of the bending, bend all in the same direction for a given precipitate. The direction in which the cleavage steps bend is always the direction in which the direction of propagation of the crack (close to $\{100\}$)

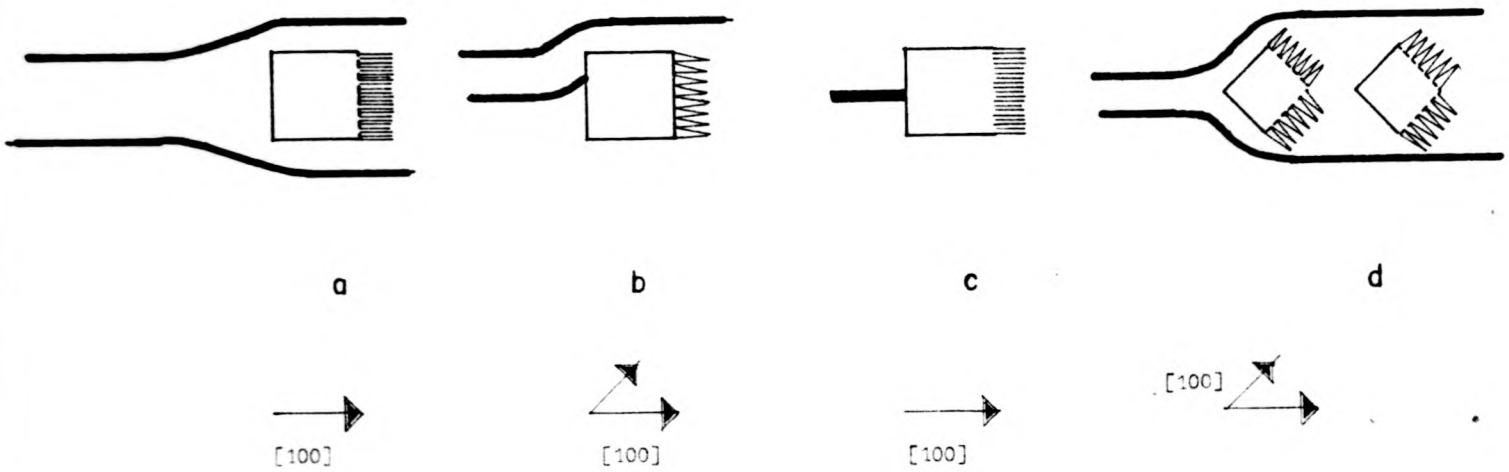

Figure 3-28: Schematic representation of the observed interactions between steps and precipitates.

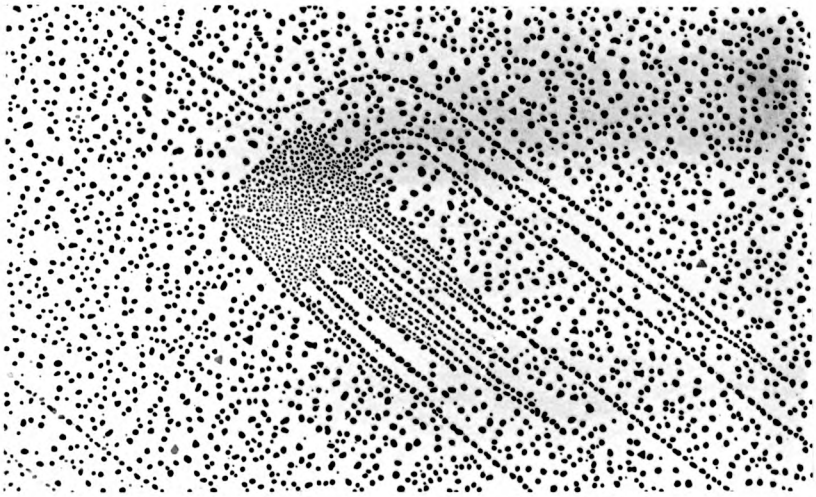

3-29 Sample 99, showing the deflection of steps in the neighbourhood of the precipitate (84000X).

departs from the ⌊100⌉ direction, see figure 3-29.

3) Away from the precipitates (≈ 2000 Å) the cleavage steps recover their original direction (i.e. that direction they had some 2000 A before meeting the precipitate). See figure 3-29.

When the cleavage proceeds at directions noticeably different from ⌊100⌉ directions, the steps behave in the ways illustrated in figure 3-28. The general trends observed are:

1) In this case the steps also bend avoiding the precipitate. When the steps meet the precipitate they do so approaching the direction of the side of the precipitate, that is a ⌊100⌉ direction (figure 3-30).

2) In all other respects they behave as the steps in the case where the cleavage was along ⌊100⌉ directions, in particular the steps recover their original directions after the precipitate.

All these data indicate that a strong interaction exists between the precipitates on the surface and the advancing cleavage crack. Similar observations have been described by Forwood and Forty (50), who found that in NaCl with gold precipitates the cleavage front is impeded in its motion by the Au inhomogeneities (and the voids associated with them); it was also found that at the precipitates V shaped patterns arise having one arm in a ⌊100⌉ direction and the other in the direction of motion of the incoming cleavage crack. This was interpreted in terms of dislocation loops produced when the crack is impeded by the obstacle; upon cutting one side of the loop (provided it has a screw component) the crack generates a cleavage step whereas pushing the other side of the loop ahead; the loop then proceeds to emerge at the surface producing a slip step. Bethge (40) has also studied the effect of inhomogeneities on the cleavage step structures.

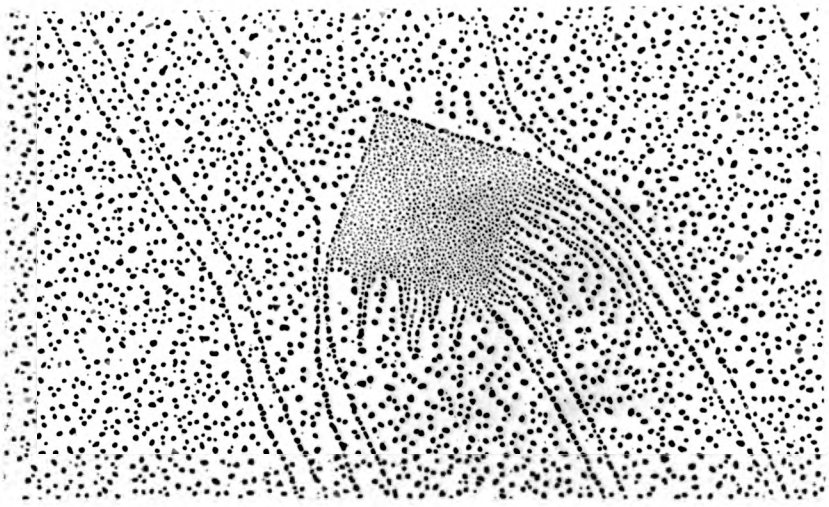

3-30 Sample 99, showing the deflection of steps around a precipitate when the cleavage direction is close to 110 . (84000X)

3.5.2.2 Steps Inside the Precipitate Area.

In general the enhanced nucleation inside the precipitate region tends to mask the steps present there. However instances have been found of steps running inside the precipitate area (figure 3-31). They proceed in a radial way starting at the corner of the precipitate met first by the cleavage front when the sides of the precipitate are not exactly parallel to the cleavage direction (figure 3-32); these steps follow curved trajectories (figure 3-33). The steps inside the precipitate are continued before and after the precipitate; in some cases multiple height steps (as evidenced by the many cleavage steps annhilated by them) cross the precipitate completely (figure 3-34).

In some samples the gold nuclei showed some coalescence, tending to mask the steps inside the precipitate areas; the conclusions regarding such steps have been drawn from samples in which the steps have been revealed unmistakably.

3.5.2.3 Steps and V shaped Patterns Emerging from the Precipitates.

Another feature of the gold decoration around the precipitates is the presence of a large number of closely spaced steps emerging from the precipitate (figures 3-35 and 3-36). These structures have several characteristics:

1) Are formed by nuclei whose size is similar to that found inside the precipitate.
2) If the cleavage front is running along they only appear on the side of the precipitate on which the cleavage front leaves the precipitate. This side is

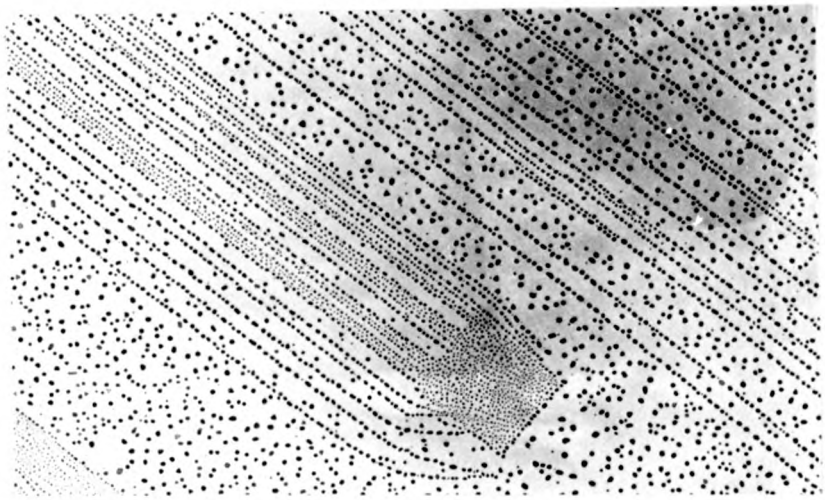

3-31 Sample 98, an example of steps running inside the precipitate area (84000X)

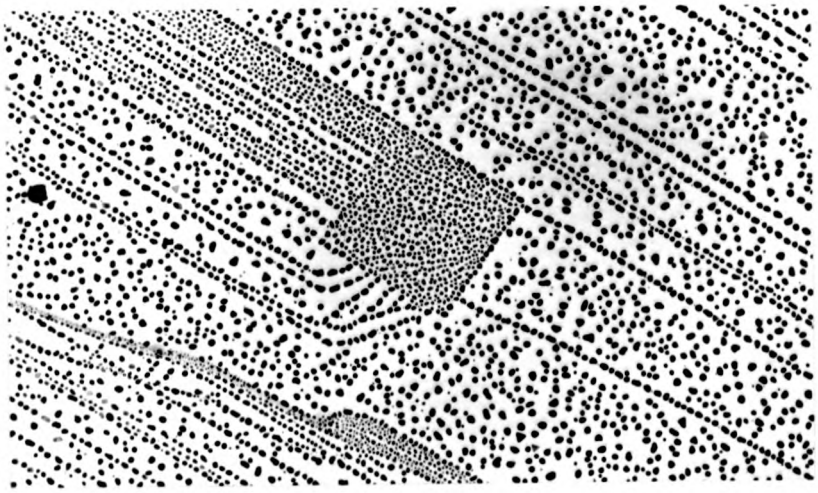

3-32 Sample 96, showing the radial nature of steps inside precipitate areas (84000X)

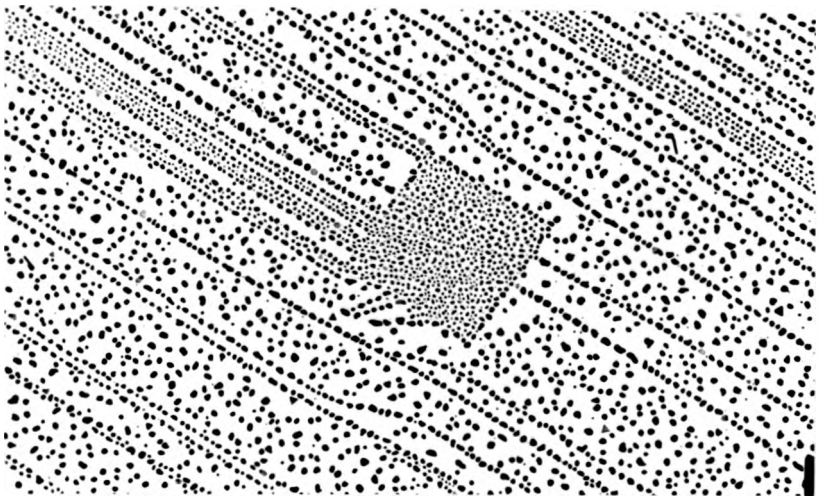

3-33 Sample 96, an example of curved step trayectories inside the precipitate area (84000X).

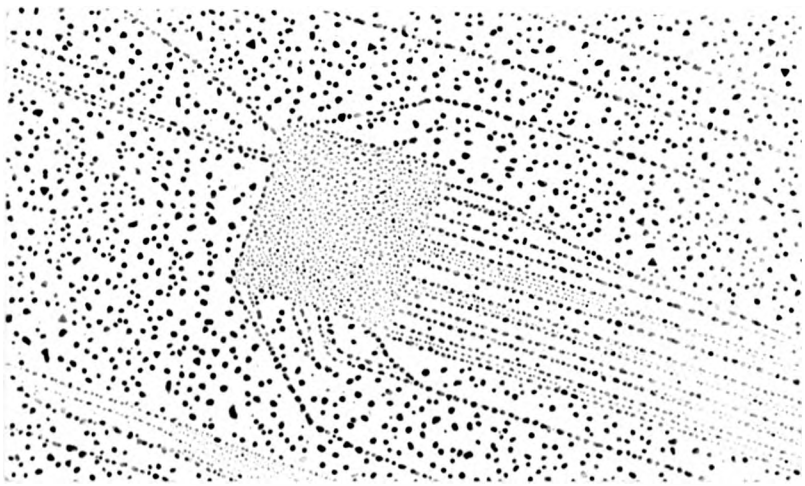

3-34 Sample 99, showing clevage steps crossing the precipitate area (81000X).

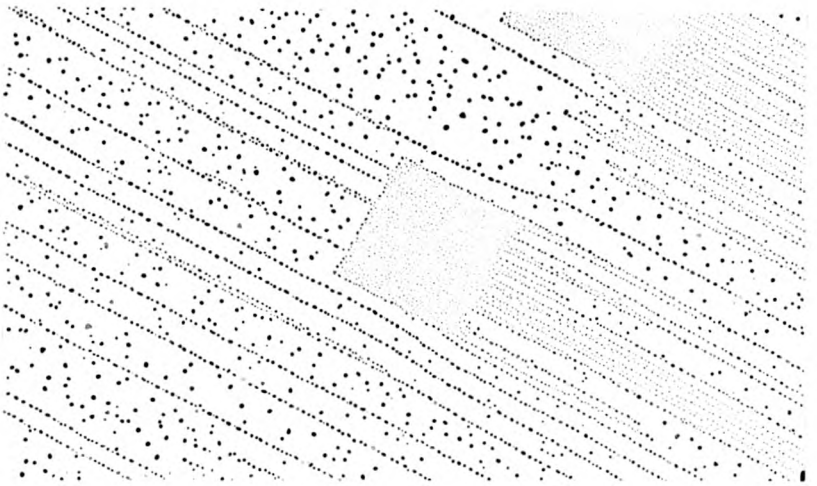

3-35 Sample 109, to illustrate the steps generated at the precipitate (84000X)

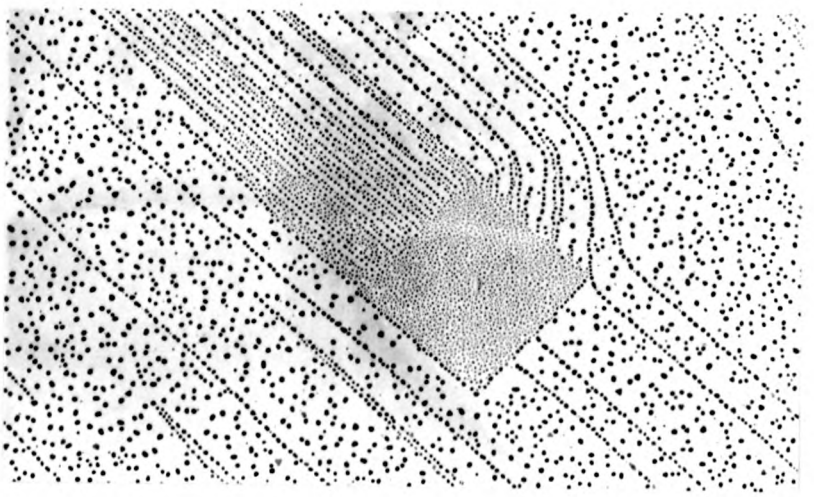

3-36 Sample 98 to illustrate steps emerging from a precipitate (84000X)

also characterized by the absence of a step-like boundary (refer to section 3.5.1 for a presentation of the boundaries). (Figure 3-35).

3) If the cleavage is running along directions close to $\langle 110 \rangle$ then these steps appear on the two sides of the precipitate that are met by the cleavage front later (figure 3-36); these sides also lack a step like boundary.

4) If the cleavage is running along an arbitrary direction, then steps will also appear on 2 sides of the precipitate, these 2 sides are those farthest from the incoming crack and they lack a boundary. In this case the density of steps tends to be larger on the side of the precipitate whose normal is closer to the direction of the crack (figure 3-36).

5) Ordinarily these steps consist of an array of V shaped steps similar in appearance to those found elsewhere outside the immediate neighbourhood of the precipitate; but when the cleavage is proceeding along $\langle 100 \rangle$ directions the steps frequently do not annihilate each other but run parallel over long distances ($\simeq$ microns) (figure 3-37).

6) The steps emerging from the precipitate have, close to it, a direction nearly normal to the precipitate side; but farther from it they bend and approach the original direction of the cleavage crack. The steps composing this V shaped pattern have different curvatures but such that they approach each other till they annihilate.
This implies that they are of opposite sign (figure 3-38).

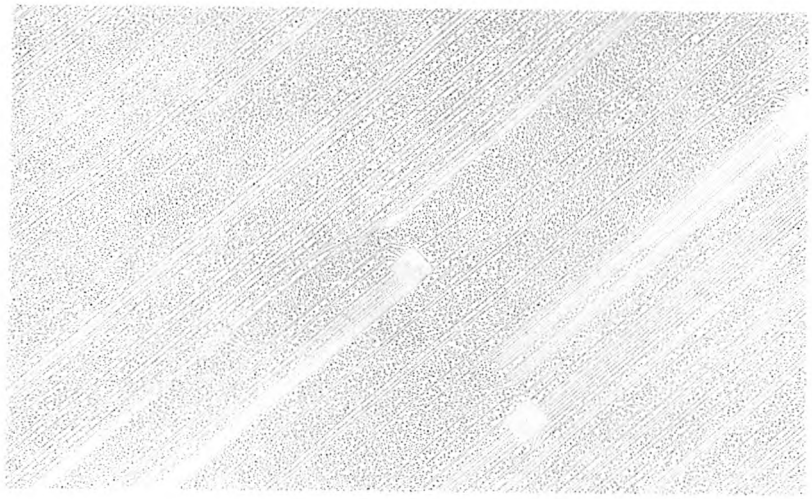

3-37 Sample 96 showing how when cleavage is proceeding along 100 the steps after the precipitate do not anihilate each other (17000X)

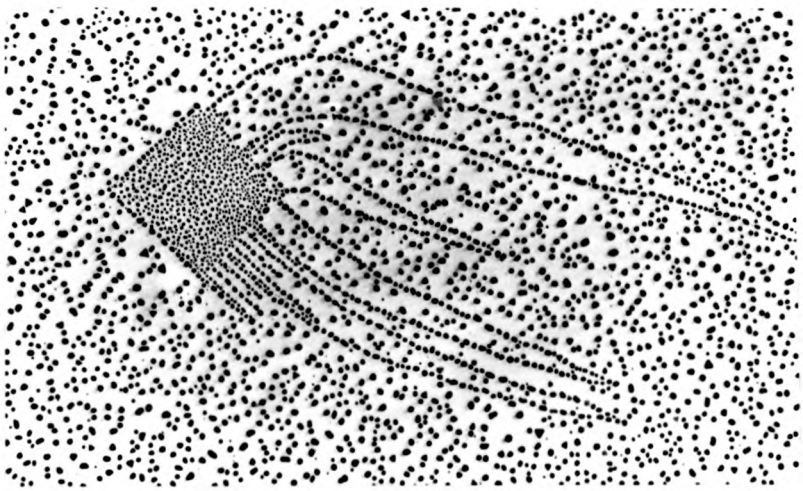

3-38 Sample 99, showing anihilation of steps of opposite sign after a precipitate (84000X)

No correlation was found between the density of these steps and the size of the precipitates. Frequently precipitates analogous in all respects had different number of steps emerging from them, however it was found that only the smallest precipitates were, sometimes, without steps emerging from them, and the only connections noticed between the orientation of the precipitate (relative to the cleavage direction) and the step structures are those presented in points 2 to 5 above.

3.6 Irregular but localized Structures.

Figure 3-39 shows a decoration feature observed in the Mn doped crystals. These structures were found only in the NaCl: $MnCl_2$ crystals treated in the way described in chapter 2 and also in crystals observed "as grown" (i.e. without specific thermal treatment, but aged for an appreciable time(1 year) at room temperature. They were not observed in nominally pure crystals. They have an overall rectangular appearance but they are in many respects different from the precipitates. Firstly these structures show no boundary (figure 3-39). Secondly it is noticed that these structures are composed of steps exclusively.

The steps forming these structures are similar to the zig-zag patterns reported by other authors on pure NaCl, but are different in that they are highly localized. That they are somehow related to the impurity (Mn) follows from the fact that they are never observed in pure specimens. Their possible nature will be discussed in chapter 4; other observed characteristics of them are:

1) These structures have, on the average, the same size as the precipitates.

2) As mentioned before, they have a quasi-rectangular shape and they are oriented as the precipitates.

3) They are much less frequent than the precipitates; approximately there is one for every 15 precipitates.

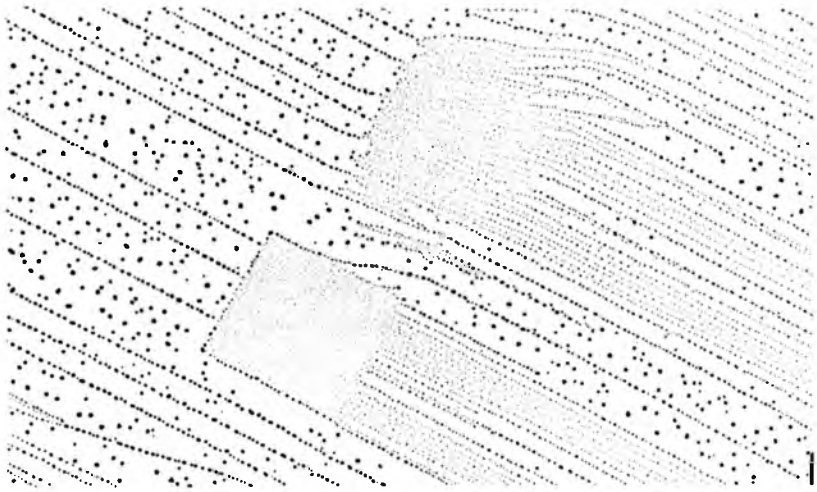

3-39 Sample 109 showing a structure of the sort called "irregular structure" (84000X)

CHAPTER 4

DISCUSSION OF RESULTS

4.1 Introduction

In this chapter the results presented in chapter 3 are discussed together with their implications.

4.2. General Characteristics of Precipitates

As shown in chapter 3, the sections of the precipitates revealed by gold decoration are always in the form of squares and rectangles which have their sides parallel to [100] directions of the NaCl. The proportion of squares and rectangles is such that it can be concluded that 88% of the precipitates are cubes, 11% are parallelepipeds with two equal sides and 1% are parallelepipeds with three unequal sides.

This growth habit of the precipitates is consistent with the fact that both the NaCl and the $6NaClMnCl_2$ are cubic; thus preserving the overall cubic symmetry. Of course symmetry considerations can not explain completely the habits of a precipitate and other factors (c.f. 54) such as the nature of the elastic distortions between nucleus and matrix, the various lattice defects and the surface energies play a part in determining the habit.

Those precipitates that are not cubes have formed, presumably, due to the influence of factors which have broken the symmetry locally. An example of such a process is the fact that in crystals of the sort used in this research (55) there occur inhomogeneities in the distribution of impurities, and it is conceivable that such inhomogeneities can cause preferential growth in one direction. Other possibilities include the growth in the prescence of dislocations or boundaries, both defects are capable of affecting nucleation and growth (34).

When crystals containing $MnCl_2$ or $FeCl_2$ are quenched from some 600°C to room temperatures and then annealed at 200°C the resulting precipitates have sections that are predominantly rectangular (26). This has been explained assuming that under these circumstances nucleation takes place preferentially on dislocation loops generated by the quenching, if the loop surrounds the precipitate it can provide a constriction to growth in two directions giving elongated precipitates. In the present research the thermal treatment consisted of a linear cooling and, thus, this mechanism is not expected to operate; the fact that most precipitates are cubes supports this assertion.

Among those precipitates that are not cubic, those with two equal sides form the majority (97%). This suggests that if the departure from the cubic habit is due to the presence of a defect constraining growth, it is a planar defect such as a low angle or tilt boundary. One possible mechanism is as follows: close to a boundary there is liable to be a local depletion of impurities, due to the fact that boundaries can act as impurity sinks. Then the growth will be constrained in the direction of the normal to the boundary and the precipitate can grow larger in the other two directions.

Having in mind the suggestion sketched above, and using the fact that the gold decoration technique reveals (at least some of) the boundaries (56), (57) any possible correlations between precipitates and boundaries have sought. The results is that in practically no case the precipitates were found at, or very close to, boundaries although the technique proved to be capable of revealing boundaries on the surface of the samples. In particular, no correlation was found between departures from the cubic shape and the presence of boundaries.

Another possible clue concerning nucleation along boundaries would be the presence of clusters of precipitates, the elements of

the cluster being "aligned". A few examples of such clusters have been found, but they are the exception rather than the rule. In general the direction along which the precipitates are aligned did not coincide with any simple low-index direction, so with the cooling rates used the alignements found by Yacaman and Vook (26) and Kahn (9) along $[110]$ were not obtained.

Within a given sample the density of nuclei was found to be very nearly the same from one region of the crystal to another. Typically the density of precipitates was found to be of the order of 2×10^6 cm^{-2} and in Kahn's work (9) it was found to be of the order of 10^7 cm^2; these figures are comparable with the expected density of dislocations present in the crystal ($10^6 - 10^7$ cm^{-2}) and thus it is perfectly valid to inquire if in the system NaCl:$MnCl_2$ nucleation is taking place preferentially at dislocations. However it is not possible to answer such a question in the context of the present results and it seems advisable to propose experiments of the sort considered in this research but with crystals in which the density of dislocations is known and can be varied.

It is interesting to notice that, under the assumption that the volume change during nucleation is small, the types of nucleation expected are (54): Bn, DS, Vc and HC; where Bn means noncoherent at a boundary, DS means semicoherent at dislocations, VC means coherent nucleation at vacancies or vacancy clusters and HC means coherent and homogeneous. If this scheme, proposed by Hornbogen (34) is right, then based on the previous discussion and on the fact mentioned in chapter 1 that there is a difference (16) between the lattice parameter of NaCl and 6NaCl$MnCl_2$ one can conclude that in the system under study, the nucleation should be semicoherent at dislocations.

Concerning the fact that most precipitates are cubes it should be added that.

1) Among all parallelepipeds the cube is the one with least surface. This suggests that the energy of the interface might be the shape controlling factor. This energy may come from misfit dislocations or elastic strain energy or both. It is interesting to notice that in the published calculations of the lattice and solution energies for the $6NaClMnCl_2$ phase no surface terms have been included, although the interface energies (elastic or otherwise) will certainly affect the thermodynamics of the solution process (for instance in the way expressed by the Gibbs Thompson relation).

2) If the unit cell of the Suzuki phase is (approximately) twice as big as that of the NaCl (or a rational multiple of it) then the coincidence lattice is also f.c.c. and parallel to the lattices of both NaCl and $6NaClMnCl_2$. Thus one would expect the boundary between the phases to be a low index plane of the f.c.c. coincidence lattice, in agreement with the observed parallel orientation. (See appendix IV).

4.3 The Measurement of Impurity Contents.

Kahn (9) and Yacamán and Vook (26) measured the impurity contents in the following way: from a piece of $NaCl:MnCl_2$ two pieces were obtained,one of them was analyzed and the other subjected to the thermal treatment and used for microscopy.An objection to this sequence is that

the piece analyzed has not been subjected to the same linear cooling as the one observed in the microscope.

It is known, since the work of Yacamán et. al (42), that if NaCl: $MnCl_2$ crystals are heated in air then a film of manganese oxide forms at the exposed surfaces. Thus it is natural to inquire how much manganese has been lost through oxidation, for this amount is equal to the difference between the measured concentration (in an untreated sample) and the net amount of Mn available for the formation of the $6NaClMnCl_2$ phase (in the heat treated sample).

In order to avoid this problem, in the present experiments the measured concentration is that of a mirror face of the sample observed in the microscope and which was produced by cleavage after the heat treatment. For instance if the MnO film is about 100 Å thick (58) then the amount of Mn lost is of the order of 50 ppm, for crystals of the sort employed in this research.

A detailed study of the effect of an annealing on the Mn concentration profile of NaCl: $MnCl_2$ has been reported by Riveros and Cabrera (59). Although the main purpose of this study was to show how the Mn oxide formation could provide a technique for the measurement of the diffusion coefficient of Mn in NaCl, their results show that for a diffusion coefficient of the order of 10^{-8} cm/sec^2 and for annealing times of the order of $5x10^5$ sec (the length of the longest time used in the present research) the NaCl crystal loses about a 15% of the impurities. However this calculation is based on the assumption that the effect of a linear cooling is in respect to impurity loss equivalent

to an anneal (at a temperature such that the diffusion coefficient is equal to the mean diffusion coefficient for the linear cooling case. This calculation is also an over simplification in that it gives the net loss, actually a better estimate is one based on the amount of Mn in the bulk (i.e. away from the surfaces); in the present case the bulk concentration is about the same as the original one (i.e before treatment).

From the preceding discussion it is clear that the effect of the Mn oxidation is likely to be important only if the region studied is close to the surfaces (by close it is meant; in the present case at 2 μm or less from the surface).

In the experimental context, it is very unlikely that precipitates very close to the exposed surface have been taken into account for it is precisely in this region where the carbon films most easily collapse during mounting. However the two film technique introduced in chapter 2 (samples III) is potentially useful in the sense that it can be used not only to ascertain the orientation of the precipitates (such is the use of this technique in the present research) but also in that it permits the study of precipitates very close to the exposed surface.

4.4 Size Distribution of Precipitates.

As shown in chapter 3, the size distribution for the precipitates has the following characteristics:

1) The larger the initial Mn concentration, the larger the mean side of the precipitates (figures 3-14).
2) The larger the initial Mn concentration, the larger the "spread" in size of the precipitates (table 3-2).

3) The slower the cooling, the larger the mean precipitate size.

4) The slower the cooling rate, the larger the spread in precipitate size.

5) Only for the smallest Mn concentrations used and the fastest cooling (C = 300 mppm T = 11°C/h) the distribution curves show the characteristic "bell shaped" form predicted by the LSW theory. In this case it was found that the curves can not be satisfactorily fitted by the theoretical curve for interface diffusion processes; but reasonable fits were obtained for the bulk - controlled and dislocation controlled diffusion processes.

That for slower cooling rates the precipitates are larger can be understood as follows: the slower the cooling the closer the system is to thermodynamical equilibrium, thus the amount of Mn in the lattice (in solid solution) is smaller since the equilibrium concentration is less than the actual one. Thus by the Gibbs-Thompson equation, the precipitates must be larger since the smaller C the larger R.

Concerning the size distribution curves, the fact that the spread in size gets larger for the slowest cooling rates can be understood on the basis that the slower the cooling the larger the time the system is at temperature high enough for ripening to take place. Since the half width of the LSW curves (in terms of particle size) varies as "Rc" (Rc - critical radius) and since Rc varies as "t" (t=time), (this is true for the case of diffusion through dislocations but analogous results are obtained in the other case). The half - width of the curve must increase with t; and hence the spread increases with concentration.

As pointed out by Jain and Hughes (25) in general there exists the possibility that there is not one, but several, independent ripening systems. In this case the distribution curves should be a superposition of several LSW curves. The fact that the size distribution curves obtained experimentally show in most cases several peaks suggests that several LSW systems are present. This is turn is related to the question of the homogenity of the spatial distribution of the precipitates. Although no noticeable departure from an homogeneous distribution was found, several examples of "clusters" of precipitates were found and it is possible that these clusters contribute to the formation of independent ripening systems.

The results of this reasearch differ from those by Jain and Hughes (25) in that in the present case the best fits were obtained for bulk and dislocation diffusion processes, on the other hand the general features of the observed distribution curves are analogous.

4.5 Step Structures and the Precipitates.

In chapter 3 attention is drawn to the facts that:

1) The cleavage steps always (or nearly always) bend in a neighbourhood of the precipitates. This bending is such that the steps tend to become aligned with the boundary of the precipitates.

In symbols, if "a" is a unit vector along the [100] direction corresponding to the side met by the cleavage first,

if a' is constructed from a by a $\pi/2$ clockwise rotation, then the unit vector along the step and in the direction of the advancing cleavage front can be expressed as $V = \alpha a + \beta a'$. If $\alpha < 0$ then the step bends in the "a" direction, if $\alpha < 0$ then it bends the opposite direction.

2) The region where the cleavage front meets the precipitate first is characterized by the presence of a step-like boundary. This boundary is usually not present on the sides where the crack leaves the precipitate. It is also sometimes absent on three of the precipitate sides when $V \parallel [100]$ (figure 3-31). In some instances the boundary is present on all four sides of the precipitate.

3) Where steps were found, inside the precipitate area, they tended to arise from the corner where the crack met the precipitate first. These steps then continued in a radial way (figure 3-30).

4) The region where the crack left the precipitates was usually characterized by the emergence of a large number of pairs of steps. These steps emerged normally to the precipitate side where they originated, but they recovered the original cleavage direction after a distance of a few microns. When $V \nparallel [100]$ the pairs annihilate each other. These line pairs are similar to the V-shaped patterns found elsewhere on the crystal surfaces and also found in our crystals (39).

5) Structures composed exclusively of steps were found, they are the patterns called "Irregular Structures" in

Figure 4-1 To illustrate the fact that steps start bending at point A where cleavage front (broken lines) touches the precipitates.

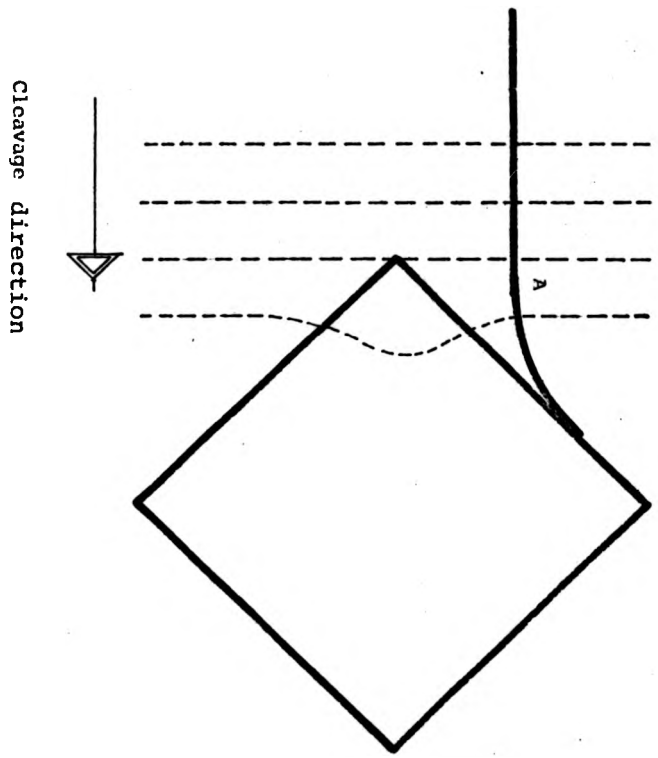

chapter 3. These are characterized by the facts that they appear only in doped crystals, they are composed of steps similar to the V-shaped pairs found elsewhere on the crystal (also in pure specimens but they are highly localized, have an overall square shape aligned as the precipitates and their size is of the same order as that of the precipitates. They appear with a density some 15 times smaller than that of the precipitates. For these reasons these structures are believed to be related to the precipitates . (Figure 3-37).

As the cleavage front approaches the precipitate, the cleavage steps bend in a way that suggests that the cleavage front is dividing into two diverging directions. In general it was found that the steps start bending very close to the precipitate (some 400 Å apart from it); although the exact direction of the cleavage crack entering the precipitate can not be known accurately, since the cleavage steps are not perfectly straight. The evidence obtained indicates that the bending starts at a point such that (assuming a plane cleavage-crack front) part of the cleavage crack has already entered the precipitate (figure 4-1). If this is true, the fact that the steps bend can be explained in terms of the acceleration or retardation the crack suffers upon entering the precipitate. The evidence suggests that outside the precipitate the cleavage proceeds quite undisturbed, although there is the possibility that the stress field of the advancing crack interacts with the precipitate at long distances. For instance, as the cleavage crack approaches the precipitates

chapter 3. These are characterized by the facts that they appear only in doped crystals, they are composed of steps similar to the V-shaped pairs found elsewhere on the crystal (also in pure specimens but they are highly localized, have an overall square shape aligned as the precipitates and their size is of the same order as that of the precipitates. They appear with a density some 15 times smaller than that of the precipitates. For these reasons these structures are believed to be related to the precipitates . (Figure 3-37).

As the cleavage front approaches the precipitate, the cleavage steps bend in a way that suggests that the cleavage front is dividing into two diverging directions. In general it was found that the steps start bending very close to the precipitate (some 400 Å apart from it); although the exact direction of the cleavage crack entering the precipitate can not be known accurately, since the cleavage steps are not perfectly straight. The evidence obtained indicates that the bending starts at a point such that (assuming a plane cleavage-crack front) part of the cleavage crack has already entered the precipitate (figure 4-1). If this is true, the fact that the steps bend can be explained in terms of the acceleration or retardation the crack suffers upon entering the precipitate. The evidence suggests that outside the precipitate the cleavage proceeds quite undisturbed, although there is the possibility that the stress field of the advancing crack interacts with the precipitate at long distances. For instance, as the cleavage crack approaches the precipitates

image forces can be expected to operate. These forces can arise from the fact that there is a boundary separating two media whose elastic constants are different. Another possibility is that the stress field of the cleavage crack interacts with the elastic field produced by the semi-coherent precipitate; or that it interacts with the fields of the misfit (boundary) dislocations. The available evidence does not allow a choice to be made between these alternatives. In practice all these mechanisms might operate simultaneously; but the evidence obtained in the present research indicates that the effect of the precipitates on the advancing cleavage front is quite small at large distances from the precipitate.

Under the hypothesis that cleavage proceeds faster inside the precipitates, a qualitative picture can be given for the decoration structures associated with the precipitates. Figure 4-2 shows schematically this "model". Consider first the case where the side of the precipitate is nearly parallel to the cleavage direction; in this case the steps remain undisturbed till the cleavage front touches the precipitate (figure 4-3). Then the cleavage proceeds faster inside the precipitate and the cleavage front has the appearance shown in figure 4-2, outside, the cleavage steps bend in such a way that they remain normal to the local cleavage front. The case of oblique incidence is analogous (figure 4-4). A faster cleavage propagation in the precipitate region produces a bending of neighbouring steps. Figures 4-5, 4-6 show examples of this two modes of interaction, figure 4-5 for the parallel incidence case and figure 4-6 for the (general) oblique incidence case.

This simplified model also explains other observed features:

1) After the cleavage front has passed over the precipitate, it recovers its original direction. Hence it explains why steps away from the precipitate and after it have the original cleavage direction.

2) The model also explains why the V-shaped pairs of lines that arise on the far side of the precipitate bend and become aligned with the original cleavage direction. For these steps arise in a region where the local direction of the cleavage crack is normal to the precipitate side and away from the precipitate the crack direction is again the original one.

3) The fact that, on the V-shaped pairs refered to in (2), the lines bend in such a way that they anihilate can be accounted for, since the local directions of the cleavage for each line do not coincide and hence they show a different radius of curvature that causes the emergence and anihilation of the steps.

4) If the crack inside the precipitate advances faster, then the cleavage front should have the shape sketched in figure 4-2. From this it is seen that the steps inside the precipitate should advance in a radial way. Figure 4-7 shows an example of this.

5) Consider again the case in which the precipitate side coincides with the direction of the cleavage front motion. Figure 4-8 shows this situation. Along the sides 2 and 3 of the figure, the local direction of cleavage is close to that of the precipitate side. Now, if there are along

Figure 4-2: To illustrate the behaviour of the step in the precipitate area. If cleavage front (broken lines) curves due to an acceleration, then the steps diverge as sketched.

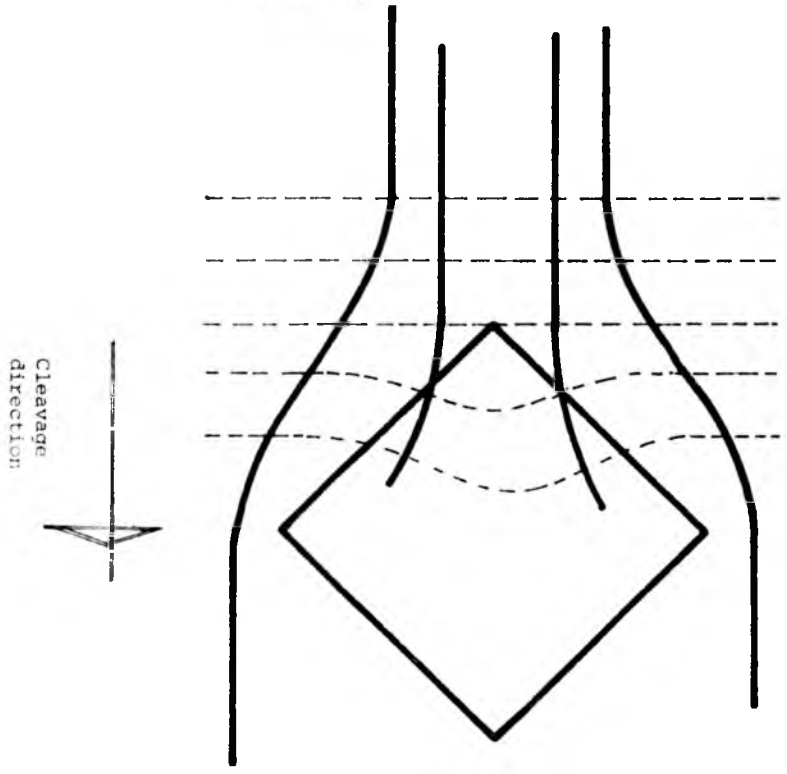

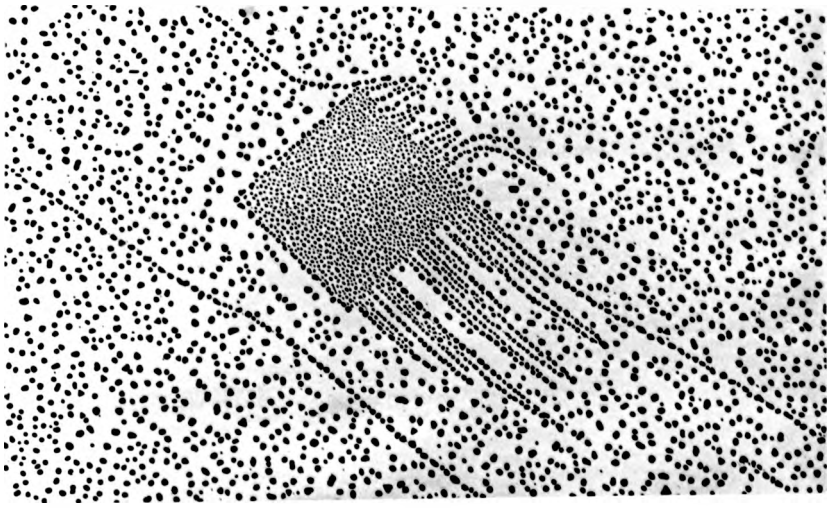

4-3 Sample 99, showing general characteristics for crack propagating close to [100] . (84000X)

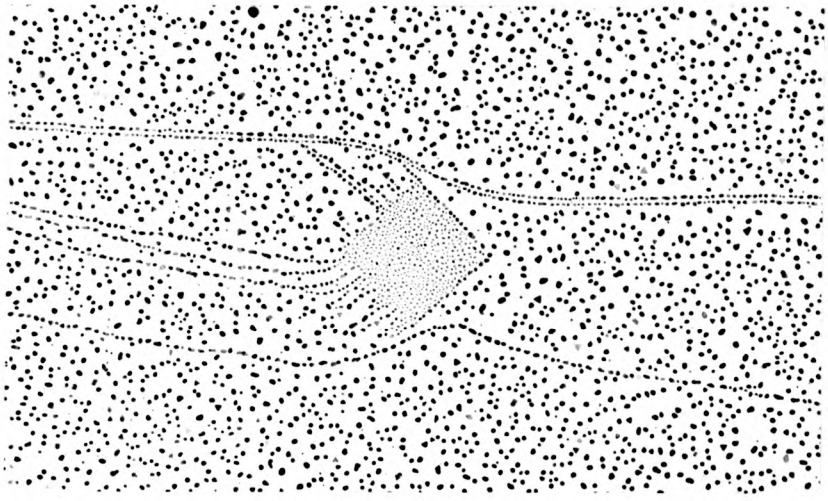

4-4 Sample 99, illustrating the way in which steps interact with the precipitate for crack advancing approximately along [110] (84000X)

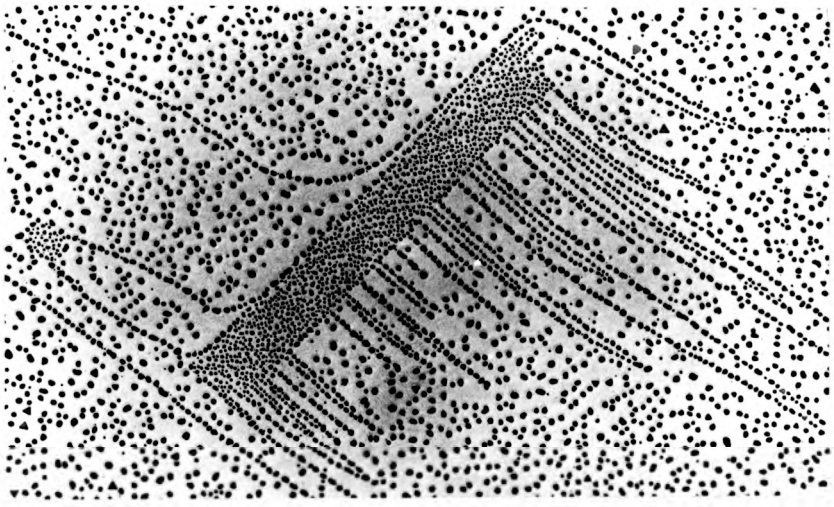

4-5 Sample 99, an elongated precipitate showing the interaction of cleavage steps with the precipitate (84000X)

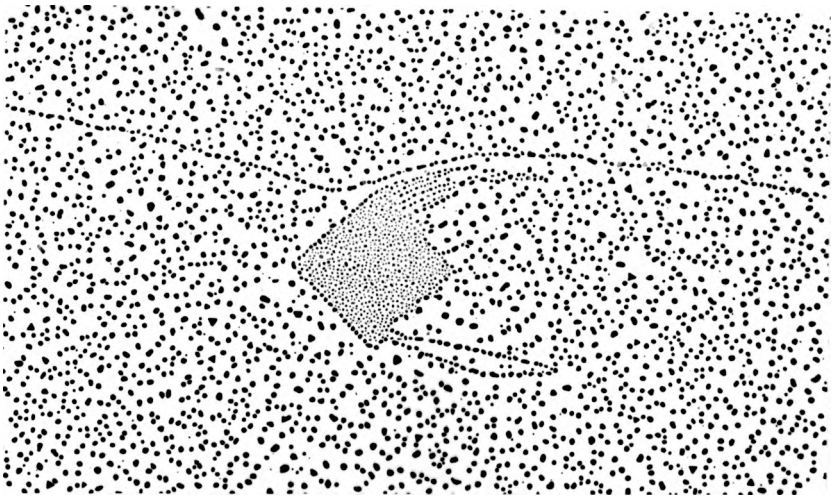

4-6 Sample 99, illustrating step-precipitate interactions (84000X)

This simplified model also explains other observed features:

1) After the cleavage front has passed over the precipitate, it recovers its original direction. Hence it explains why steps away from the precipitate and after it have the original cleavage direction.

2) The model also explains why the V-shaped pairs of lines that arise on the far side of the precipitate bend and become aligned with the original cleavage direction. For these steps arise in a region where the local direction of the cleavage crack is normal to the precipitate side and away from the precipitate the crack direction is again the original one.

3) The fact that, on the V-shaped pairs refered to in (2), the lines bend in such a way that they anihilate can be accounted for, since the local directions of the cleavage for each line do not coincide and hence they show a different radius of curvature that causes the emergence and anihilation of the steps.

4) If the crack inside the precipitate advances faster, then the cleavage front should have the shape sketched in figure 4-2. From this it is seen that the steps inside the precipitate should advance in a radial way. Figure 4-7 shows an example of this.

5) Consider again the case in which the precipitate side coincides with the direction of the cleavage front motion. Figure 4-8 shows this situation. Along the sides 2 and 3 of the figure, the local direction of cleavage is close to that of the precipitate side. Now, if there are along

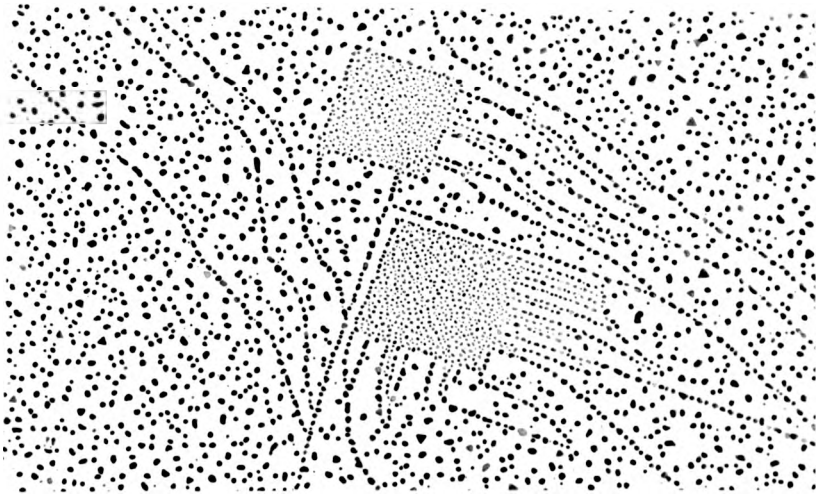

Figure 4-7 Sample 99 illustrating the behaviour of the steps inside the precipitate area. (84000X)

Figure 4-8: Schematic illustration of the interaction between the cleavage front and the precipitates for the nearly [100] crack propagation direction.

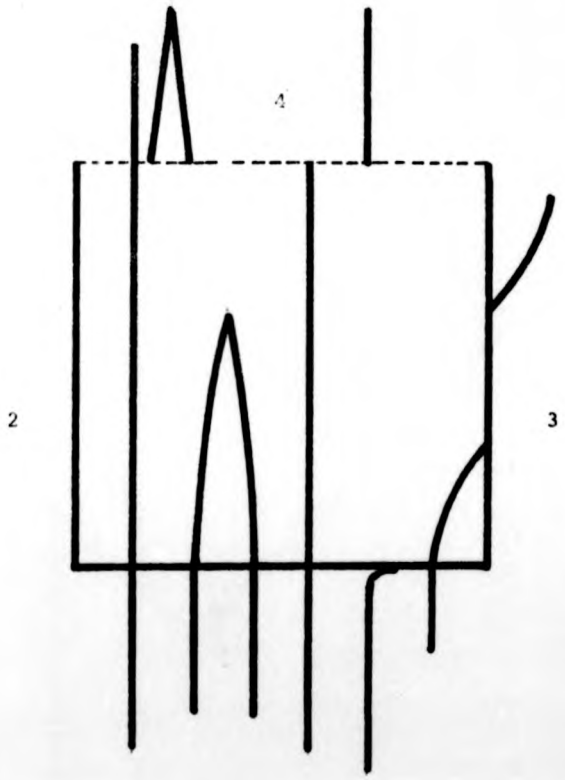
4
2
3
1

Figure 4-9: Schematic illustration of cleavage-precipitate interaction in the case where the cleavage proceeds in a direction different from [100].

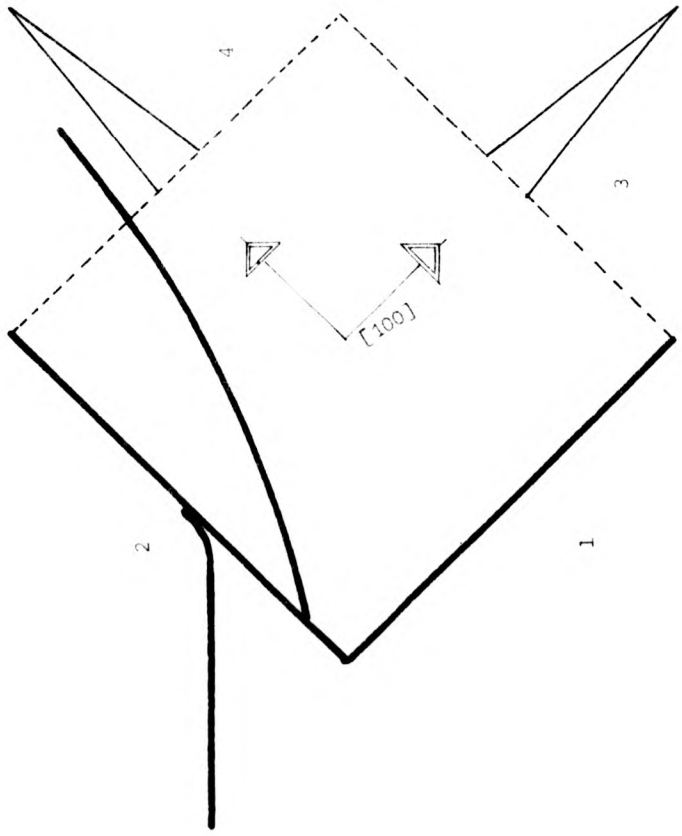
4
3
[100]
2
1

this boundary dislocations cutting the (001) plane with a screw component, then the steps generated by these dislocations will lie in the $[\bar{1}00]$ direction contributing to the boundary of the precipitate.

The steps generated on face 1 run till they cross face 4 (they will not cross faces 2 and 3 for there the direction of the crack is nearly parallel to the precipitate sides). Some steps will annihilate each other before reaching face 4; others will be annihilated by a dislocation on face 4 of opposite sign to that which formed the step; and some steps will emerge. The number of steps formed on face 1 and emerging on face 4 is likely to be small in view of the fact that those that seem to emerge from side 4 annihilate each other in distances of the order of the precipitate side itself. In view of the radial-nature of the cleavage front inside the precipitate most of the steps are expected to end in sides 2 and 3 and thus contribute to the precipitate sides there.

In this model as the cleavage front reaches side 4 it must slow down to adjust its speed to that of the cleavage front outside. Here it cuts more dislocations (or it generates them, it is possible that the cleavage is slowed down by plastic deformation it produces on side 4) which form the V shaped pairs observed.

6) The picture remains essentially the same for the case of oblique incidence, but in this case (fig. 4-9) sides 1 and 2 behave like side 1 of the previous case and 3 and 4 behave like 4. Along 1 and 2 the local crack direction will be that of the precipitate side and hence the steps will contribute to the boundary. Along 3 and

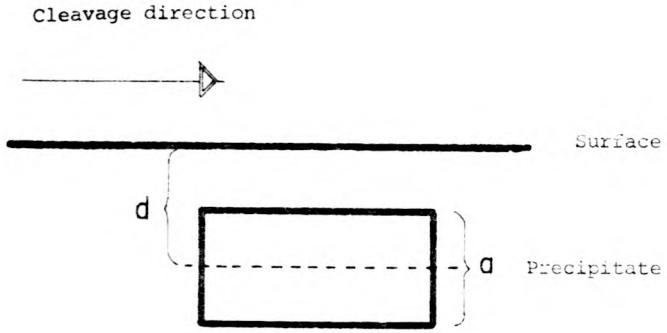

Figure 4-10: Schematic representation of a precipitate close to the cleavage surface. There are believed to be recognisable for the "irregular structures".

4 there is usually no boundary but a large number of steps emerge. (figure 3-34).

7) For an oblique incidence, the speed of propagation of the crack inside the precipitate is expected to have a larger component in the direction of the original incoming front. This explains why of the 2 sides with steps emerging, the one whose normal is closer to the original cleavage direction has more steps. Roughly speaking most of the retardation of the front is expected to take place at such a side. This in turn suggests that the velocity of the crack inside should be considered to be rather a sum $\{100\} + \{010\}$ with a larger component in the direction closer to that of the original crack since $\{100\}$ and $\{010\}$ are expected to be the energetically favoured cleavage directions in the Suzuki Phase. This is consistent with the assumed division of the crack outside the precipitate.

The consideration in 5,6 and 7 above can not account completely for the presence of the (decorated) steps boundary. Other mechanisms should be considered, for instance the fact that the sides of the precipitate are along $[100]$ suggests that slip steps (generated in the fashion described, for instance, by Robins et al. (38)) could also contribute to the boundary. A complete account of all observed structures will not be possible, till the detailed structure of the NaCl-Suzuki phase interface is elucidated.

The fact that steps are generated in the precipitate area indicates clearly the presence of dislocations at the NaCl-Suzuki phase interface. Concerning the existence of these dislocations

two mechanisms for their production may be considered, which are expected to operate simultaneously. The first of these is the generation of dislocations by the cleavage process itself; the other is the generation of boundary dislocations at the interface to relieve the mismatch. General evidence for the first mechanism has been shown by Robins et al.(38) (for Mgo) whereas for the presence second mechanism there is direct electron microscope evidence (19) as well as gold decoration evidence (53). Hirth et al. have shown that the spacing between perfect lattice dislocations necessary to account for the mismatch is of the order of the precipitate side itself; so it has been proposed that the NaCl-Suzuki phase boundary is formed by an array of partial dislocations, these dislocations would have a Burgers vector such that they relieve the local stress produced by the anion displacements (chapter 1).

On the experimental side, the measured step distances inside the precipitates behave with respect to precipitate size, in the way expected for the process of loss of coherency (63). Hence it can be concluded that, in the present case, most (if not all) of the cleavage steps found inside the precipitate area are due to the boundary.

4.6 Irregular Structures.

The so called irregular structures have characteristics such that it may be concluded that they are associated with the Suzuki precipitates in the crystal. The question of what is this relationship is more difficult to answer and it is the purpose of this section to discuss some possibilities.

In general terms it can be thought that the Suzuki phases are revealed by two processes:

1) The structure of the Suzuki phases is such that the Gold is nucleated with greater density. The physical processes responsible for this are presumably of an electrical character (36).

2) The interaction between the cleavage and the dislocation structures produces steps, and these are known to be preferential sites for nucleation (24).

On the other hand, the fact that the volume fraction (V_S/V_T) occupied by the precipitates and the area fraction (A_S/A_T) are equal (9) means that the Gold decoration process is revealing basically those precipitates that intersect the cleavage face (see appendix 1). Based on these considerations, a possible mechanism for the formation of the "irregular structures" can be given as follows:

1) The irregular structures correspond to precipitates close to the cleavage surface but not intersecting it. According to remark I above, the random-like nucleation in the Suzuki phase regions could be ultimately due to an electrical interaction, but because these phases are neutral it is conceivable that the interaction is of dipolar character and hence of short range (going as $1/(\text{distance})^6$). Thus one would expect that those precipitates close (but not cutting it) to the cleavage surface do not produce a uniform distribution of nuclei, but instead present the decoration structures found in precipitate precipitate free regions.

2) Since the irregular structures are composed of zig-zag and V-shaped steps resembling the zig-zag and V-shaped structures in precipitate-free regions or in pure samples (38, 39, 50), it is thought that they arise as a result of either an

interaction of the cleavage front with dislocations (interface dislocations for instance, (19,23)) or as an enhanced plastic deformation due the fact that the NaCl crystal is in fact much thinner in a region just above the precipitate.

If this mechanism is correct since the size of the irregular structures is about the same as that of precipitates but appears some 15 times less frequently, they would correspond to precipitates whose distance from the surface (measured from their upper face) is between 0 and some "a" / 30 where "a" is the mean precipitate size. (figure 4-10, figure 3-7).

Another possibility is that the irregular structures correspond not to the Suzuki phases but to precipitates of the equilibrium phase $MnCl_2$ (or 2NaCl - $MnCl_2$). In fact such phases have been observed in X-ray studies of the NaCl: $MnCl_2$ system (see appendix 2).

4.7 The Dislocation Nature of the Interface.

As it can be seen from the micrographs , a large number of steps emerge from the precipitates. This has been interpreted as an indication of the incoherence between matrix and precipitate (9) and the steps are believed to arise from the dislocations cutting the cleavage surface.

It has been pointed out (63) that the matrix precipitate misfit can be accomodated by perpendicular sets of dislocations with Burgers vector

$$b = 1/2 \quad [110]$$

or

$$b = [100]$$

with the dislocation lines pointing in the $[110]$ and $[010]$ directions respectively. Of these possibilities the first one would be favoured due to a smaller core energy (63).

However, the spacing between steps calculated on the basis of these dislocations does not agree well with the observed spacings. Typically the calculated distances indicate about one dislocations per precipitate whereas there can be as many as 30 steps emerging from an average precipitate.

This has led to postulate a partial interface dislocation model. As explained in chapter 1, the clorine ions are displaced in the Suzuki phase whith respect to their positions in the NaCl matrix. Along the $\langle 110 \rangle$ rows of Cl^- these displacements assume the form of alternating expansions and contraction by $\sqrt{2}\,\delta a_s$ where δa_s is the fractional displacement of the ions.

Thus if perfect interface dislocation dissociate into partials with Burgers vectors $\sim \sqrt{2}\, a_s$ both local and long range strains will be relieved.

Ledge spacing measurements in NaCl: Mn, NaCl: Fe and NaCl: Cd give some support to this model (63). If the gold nuclei decorating the surface are small ($\sim$ 20 Å) a large number of steps can be revealed in the precipitate areas; close to the interface they appear uniformly spaced. The mean distance between

steps for large precipitates conforms to the expectations from the model and it increases as the precipitate size decreases as expected from loss - of coherency considerations.

This dislocation network around the precipitates has been observed by Yacamán et al. (19) by direct electron microscopy of NaCl : Mn. Their findings have been briefly described in Chapter 1; they found dislocation lines "disappearing" upon entering the precipitate and it is now believed (63) that this represents the loss of contrast due to the dissociation into partials.

In the present research most of the steps inside the precipitate area can not be seen, due to the fact that the gold nuclei are relatively big. Actually a compromise must be made; if the gold nuclei are very small more steps can in principle be resolved (i.e. steps separated by small distances) but the overall configuration looks very much like a uniform array of random nuclei; if the gold nuclei are big (and also if there is some coalescence) closely spaced steps can not be resolved but the pattern allows a clear identification of the steps. Clearly the optimum nuclei size depends on the information sought.

The present experiments were designed so that a few steps could be seen and followed having in mind to study the crack propagation in the various regions ofthe surface.

CHAPTER 5

CONCLUSIONS AND SUGGESTIONS FOR FURTHER WORK

5.1 Introduction

The observations described in this research can be divided into three main groups:

1) Morphological observations.

2) The size and distribution of precipitates.

3) The step structures associated with the precipitates.

5.2 Morphological Observations

In the present research the Suzuki precipitates $6NaClMnCl_2$ have been observed by means of the gold decoration technique.

The observed features are essentially in the form of square and rectangular regions inside of which the gold has been nucleated with a greater density and smaller nucleus mean diameter than elsewhere.

The fact that the precipitates show square and rectangular sections is in agreement with earlier studies (21). For the experimental conditions used here the precipitates show a predominatly square section, an analysis of the "shape" distribution of the precipitates shows that 88% are cubes 11% are parallelepipeds with two equal sides and 1% are parallelepipeds of unequal sides.

No correlation was found between the shape of the precipitates and the presence of grain boundaries.

The sides of the precipitates were found to be aligned along $\langle 100 \rangle$ directions, in agreement with other studies (21,9,26).

This was ascertained in three ways: 1. Comparing the sides of the precipitate with surface features of known orientation, such as slip steps. 2. Comparing the bright field images of the precipitates with the diffraction pattern of the gold and using the fact gold grows on NaCl with certain preferred orientations and 3. Comparing the direction of the precipitate side with the "edge" of the crystal; the edge was made visible by coating simultaneously with carbon the crystal face with the decorating gold and an adjacent face.

Structures composed of steps only were also found and which have not been reported before; since they appear only in doped specimens, are localized and with an overall cubic appearance they are believed to be related to the Suzuki precipitatates. It is postulated that these structures are caused by precipitates close to (but not cutting) the cleavage surface; these structures are believed to arise from an enhanced plastic deformation in the region between the precipitate face and the surface or from the cutting and moving of interface dislocation.

5.3 The Size and Distribution of Precipitates

The spatial distribution of the precipitates was found to be, in general, homogeneous and no indications of a possible preferential nucleation at grain boundaries were found. In some instances "clusters" of precipitates were found, in some of which the precipitates were aligned but no correlation between these clusters and boundaries was found; the direction of alignment of these clusters did not agree in general with that of any low index direction. Instances of "overlapping" precipitates were also found. The mean precipitate side was also found to increase upon

decreasing the cooling rate. All these results are in qualitative agreement with those found by Kahweit for slowly cooled supersaturated solutions.

The size distribution of the precipitates was analyzed only for the fastest cooling rate used (11°C/h) and for the samples with lowest Mn concentrations the curves show the expected bell shaped appearance; for faster coolings or higher Mn concentrations the curves show several peaks. In the case of those samples with bell shaped distribution an attempt was made to adjust the theoretical distribution curves presented by Jain and Hughes (25) based on the Lifschitz-Shlezov-Wagner Theory (60). In disagreement with the findings of Jain and Hughes, the experimental curves are not compatible with a slow surface reaction mechanism; but the fit was found to be satisfactory for bulk-diffusion and dislocation-diffusion processes, the data obtained favour equally well both of these possibilities. In chapter 3 the size distribution curves for 10 samples of various Mn contents and cooled at different rates were presented.

5.4 The Step Structures Associated with the Precipitates

The cleavage steps interact in various ways with the precipitates. They can meet the precipitate and merge with its boundary, sometimes they cross the precipitate completely; they show changes in their directions in a neighbourhood of the precipitate; when they are in the interior of the precipitate areas they follow radial-divergent directions; new steps emerge from the precipitates.

These interactions show that whatever produced the square (or rectangular) structures that have been associated with the precipitates,they were present before cleavage and are not a decoration artifact.

The fact that cleavage steps can join the boundary of the precipitates proves the step character of the boundary itself.

These interactions give also support to the idea that there is a dislocation network surrounding the precipitates and that the cleavage proceeds faster inside the precipitate areas. A simple model has been proposed to explain the observed features in terms of an acceleration of the cleavage front in precipitate areas.

5.5 Suggestions for further work.

a) Experiments of the sort considered in this research can be done using various dopant-hostmatrix combinations. In this way several important parameters can be varied, such as: 1) the lattice misfit between matrix and precipitate (it is even possible that in some systems the precipitates be coherent). 2) the local misfit due to the anion displacements (since the displacements depend on the relative ionic radii) 3) From 1) and 2) it seems that, since the ledge structures associated with the interface depend on its dislocation nature; studies with different dopants and/or matrices might give more information concerning the structure of the interface. In particular it seems interesting to check the model for the interface proposed by Hirth et al. (63) by measuring the precipitate ledge spacing against precipitate size for various systems.

b) Using shadow decoration techniques it is possible to improve the sensitivity of the decoration towards observing steps. Furthermore, the relative signs of the steps can be determined. Thus it seems worth studying the step structures around the precipitates with this technique; for instance some models assume that the interface dislocations alternate in the sign of their screw component normal to the cleavage plane, and thus the correspond-

ing ledges should alternate in sign.

Another use of this technique is that, since it produces very little nucleation on terraces, the ability to detect and follow steps on the precipitates is much improved and studies as the present one considering crack propagation in precipitate areas can be expanded.

c) X-ray studies are also potentially useful. With X-rays several important pieces of evidence can be obtained such as:

1) the existence of a Suzuki phase
2) the presence of the stable phase
3) the anion displacements
4) the solvus for the various phases

Again, it is suggested that these studies be made for various matrix-dopant combinations.

d) The direct electron microscopy of the precipitates can yield information in various areas. Firstly it can be used to confirm the presence of precipitates in various systems. Secondly; given that it is possible to observe dislocations and to measure their Burgers vectors, this seems a most promising area regarding the determination of the structure of the interface.

It has been suggested (62) that using weak beam conditions it might be possible to resolve the partials into which the interface dislocations have been postulated to split. Experimentally the difficulties are that a low temperature stage is needed (to slow down the radiation damage and permit a conveniently long observation time) and that a goniometer is required to produce the required tilting; it is quite difficult to design stages with both facilities.

e) The Suzuki phases offer the opportunity of studying the nucleation of gold onto substrates which have an ordered array of defects (20); and hence it is possible to use the precipitate areas as substrates to study the influence of point defects on both nucleation and epitaxy. In chapter 1 some speculations and results (some of them contradictory) in this area have been mentioned, and it is suggested that systematic nucleation studies be conducted onto Suzuki phase forming systems to test them. In particular, attention should be paid to the question of whether the Suzuki phases promote epitaxy or not.

It is suggested that these experiments be done under ultrahigh vacuum conditions to minimize the possible influence of contaminants.

f) In chapter four it has been suggested that the so-called irregular structures correspond to precipitates close to the cleavage surface. The proximity of the precipitate to the surface would cause plastic deformation in the crystal whose decoration remnants would be observed as irregular structures (composed mainly of V-shaped patterns).

This idea can be tested by means of the two-film techniques described in chapter 2 (a technique that has also been used independently by Wainer (55) Upon decorating two faces of the same crystal it is possible to see if a precipitate close to the surface (and revealed on one of the decorated faces) corresponds to an irregular structure (as revealed on the other decorated face).

Furthermore, with this technique it is also possible to study the "depth" of the decoration procedure for precipitates, by "depth " here it is meant the maximum distance from the surface at which a precipitate is detected by the decoration.

g) The experiments thus far described concerning the size distribution curves are "static" in the sense that they give a picture of the distribution at a given time. However, the process of Ostwald ripening is time dependent.

For these reasons it is suggested that experiments be made to follow the evolution in time of the distribution curves.

These experiments can be carried out by annealing for various times crystals previously quenched from a high temperature (the purpose of the quenching is to get a supersaturated solid solution). If after the anneal the crystal is quenched to room temperature and decorated, the distribution curves will correspond to the given t (length of the anneal) and T (temperature at which the sample has been annealed). Obviously T has to be chosen to correspond to a temperature at which precipitation takes place at a detectable rate and must be smaller than the temperature at which the thermal resolution of the precipitates commences.

Thus isothermal experiments of the sort proposed can be used to test the ripening theories in greater depth. For instance, the mean particle size $\bar{R}$ goes, in the Lifschitz - Wagner-Slezov theories including its extention by Jain and Hughes (25)

as $\bar{R} \propto t^{m}$

where $n = 1/2$ for surface controlled processes

$n = 1/3$ for bulk diffusion controlled processes

$n = 1/4$ for the case of diffusion through dislocations.

APPENDIX 1

ON AREA AND VOLUME FRACTIONS

In chapter two it was stated that the volume fraction Vs/Vt and the area fraction As/At occupied by the precipitates are given by

$$(1) \quad \frac{Vs}{Vt} = \frac{As}{At}$$

(here Vs and Vt are the volume occupied by all the precipitates and the total volume of the crystal respectively, and As and At refer to the areas of the precipitates and of the whole crystal respectively).

It is the purpose of this appendix to show that this equation is correct indeed and to show some of its consequences. This problem is not only important as a justification of some procedures followed in chapter two and three; but it is also interesting in that, despite of its simplicity, it has been a matter of disagreement between some authors. For instance in the work by Kahn (9) equation 1 is used as it stands whereas in the work by Kirk, Kahn and Pratt (21) equation "2" is used instead:

$$(2) \quad \frac{V_s}{V_T} = \left(\frac{A_s}{A_T}\right)^{3/2}$$

Kahn (9) presented a proof of eq. 1 which is simple and general in the sense that it applies to any precipitate shape; his proof is as follows:

Consider a crystal cubic in shape and with side L. Let As be as before, and At = L^2. If As does not depend on the position of the crystal section being observed, then the total volume occupied by the Suzuki phase is

$$(3) \quad V_s = \int_0^L A_s \, dz = A_s \cdot L$$

where Z represents the position of the planes (see figure 1) on which the precipitates have total (cross sectional) area As.

Equation 3 immediately implies "1" since

$$\frac{V_s}{V_T} = \frac{A_s \cdot L}{V_T} = \frac{A_s \cdot L}{L^3} = \frac{A_s}{L^2} = \frac{A_s}{A_T}$$

That As does not depend on "Z" is a good hypothesis provided that the symmetry of the crystal has not been altered in some way; for instance if the "Z" direction coincides with the growth axis of the crystal then there might be a "Z" dependence of A due to the distribution coefficient for Mn in NaCl. However, even in this case, equation 1 is still valid provided the average of As(Z) over $[0,L]$ is used, i.e.

$$\langle A \rangle = \frac{1}{L} \int_0^L A_s(z)\, dz$$

in which case

$$\int_0^L A_s(z)\, dz = V_s = L \langle A \rangle$$

and

$$\frac{V_s}{V_T} = \frac{\langle A \rangle}{A_T}$$

A simple interpretation can be given to formula 1 in the case of precipitates of cubic shape and uniform side "a". In this case (which is not far from the actual case, as seen in chapter four) given a surface At the number of precipitates that are observed is given by

$$(4) \qquad N = \int_{-a/2}^{a/2} \rho A_T\, dz = \rho A_T a$$

Where ρ is the density of precipitates and it is assumed to be constant. That thus result is correct follows from the fact that when one surface is examined only those precipitates located at distances $d \leq a/2$ from the surface, cut it and can be revealed by the replication process; figure Ap. 1-2 shows this schematically.

Then the fraction area is simply

$$\frac{A_s}{A_T} = \frac{Na^2}{A_T} = \frac{\rho A_T a^3}{L^2} = \rho a^3$$

but $$\frac{V_S}{V_T} = \frac{a^3 \int \rho_v dv}{V_T} = \rho_v a^3$$

and equation (1) follows.

The important point in this proof is that there exists a length Λ (= a in the case just analyzed) that represents the "depth" of the observational technique; or, in other words, that only precipitates at distances $d \leq \Lambda/2$ from the surface will be observed. In the present research it is contended that the right choice for Λ is $\Lambda = a$, meaning that a precipitate will be observed if and only if it cuts the surface; physically this means that a precipitate not cutting the surface (or not being very close to it) will not be able to affect the gold decoration because: 1. The gold atoms arrive on NaCl. 2. The Suzuki phase being electrically neutral, it can affect the gold nucleation only through dipolar contributions to the electric field; and the dipolar field fades away rapidly with the distance.

In some other areas, choices different from $\Lambda = a$ can be used; for instance in surface physics the question "how many particles are there at the surface?" really means "how many particles are there on the first layer?". In this case $1/\rho$ has the meaning of volume per particle and $\rho_v^{-1/3}$ is the mean distance between particles; so the choice $\Lambda = \rho_v^{-1/3}$ is justified in these instances and

$$\frac{A_S}{A_T} = \frac{a^2 \rho_v A_T \Lambda}{L^3} = a^2 \rho_v \rho_v^{-1/3} = a^2 \rho_v^{2/3}$$

whereas

$$\frac{V_S}{V_T} = \frac{\rho_v L^3 a^3}{L^3} = \rho_v a^3$$

so

$$\frac{V_S}{V_T} = \left(\frac{A_S}{A_T}\right)^{3/2} \qquad (5)$$

which is the equation used by Kirk et.al. Hence it can be concluded that in the present research equation 1 is the right one and that

equation 5 neglects the fact that only precipitates cutting the surface can be observed.

It is interesting to rephrase the previous considerations in terms of the surface density ρ_S of precipitates, from equation 3 using λ instead of "a" it is obtained

$$N = \rho_V A_T \lambda$$

so

$$\rho_S = N/A_T = \rho_V \lambda \quad (6)$$

the choice $\lambda = a$ gives

$$\rho_S = \rho_V a$$

whereas $\lambda = \rho_V^{-1/3}$ gives $\rho_S = \rho_V \rho_V^{-1/3} = \rho_V^{2/3}$ (7)

and it is immediately recognised that eq. (7) is the usual "rule of thumb" for relating surface and volume densities. The conclusion reached here is that equation 7 should not be used carelessly, and in particular will lead to wrong answers in problems with a well defined "depth of observation"; but of course eq (7) will work perfectly well in problems involving point defects only provided one is certain that the observational technique will detect the particles up to the "first layer".

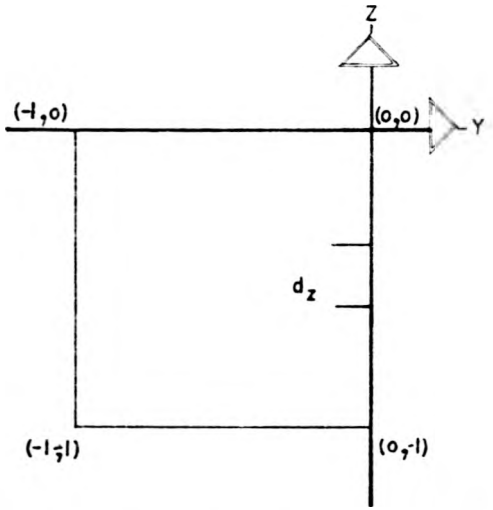

Figure A-1: Geometry used in the proof of equation 3; the points (0, 0), (-1, -1), (-1, 0) and (0, 1) represent the projection of the precipitate onto the y-z plane.

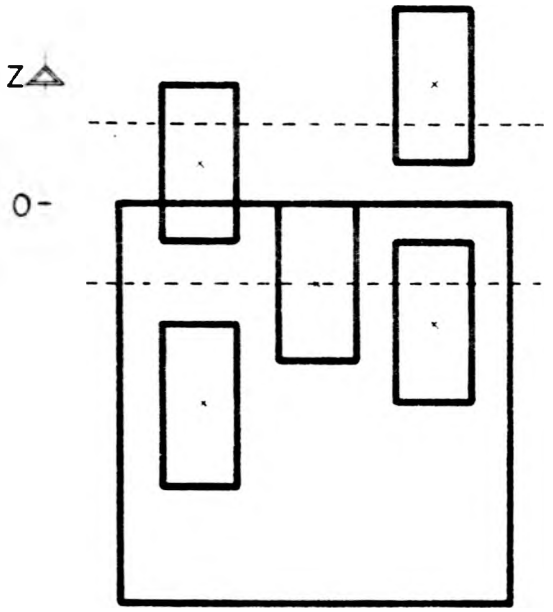

Figure A-2: Cross section of a crystal containing precipitates whose centres (X) are in the region marked by broken lines will be revealed by the replication procedure.

APPENDIX 2

THE SLOPE OF THE V_s/V_t vs C CURVE.

Starting with a crystal at 650°C, in which the Mn is completely dissolved, one has the following composition:

C_0 moles of NaCl

C_1 moles of $MnCl_2$, assume $C_1 \ll C_0$

C_1 moles of vacancies (charge compensating)

When the crystal is cooled down very slowly there is a precipitation reaction of the type

C_0 moles NaCl + C_1 moles $MnCl_2$ + C_1 moles vacancies $\rightarrow$

$(C_0 - 6C_1)$ moles NaCl + C_1 moles Suzuki phase.

The "6" comes from the fact that the Suzuki phase has the composition $MnCl_2 6NaCl$; so the reaction is just the precipitation of vacancies together with Mn and some NaCl.

Since $C_1 \ll C_0$ the approximation $C_0 - 6C_1 \approx C_0$ is valid and the volume occupied by these C_0 moles of NaCl is just $(C_0 N a^3)/4$ where N is Avogadro's number, a is the NaCl lattice spacing and the factor "4" comes from the fact that in the F.C.C. lattice there are 4 lattice points per (conventional) unit cell.

The Suzuki phase grows in a F.C.C. lattice as well, define $\alpha = b/a$ where b is the lattice parameter of the Suzuki phase. Hence $b = \alpha a$; the volume occupied by the C_1 moles is $(C_1 N b^3)/4 = (C_1 N \alpha^3 a^3)/4$ and $V_s/V_t = (\alpha^3 C_1)/C_0 = \alpha^3 C$ where C is the molar fraction of the dopant.

Hence the slope should be the cube of the ratio of the unit cell size of the Suzuki phase to that of the NaCl.

As it has been noticed before, in the text, this slope is expected to be close (but not identical) to "8". It must be remarked that the results of this appendix were obtained on the assumption that all the manganese precipitates; if a fixed amount of Mn remains in another state then a shift in the curve is expected so $V_s/V_t = \ldots C + C'_0$, where C'_0 represents the amount of Mn not in the Suzuki phase. Using the value for the unit cell obtained by Van Loon and Idjo (16) $\ldots = 1.99$, the slope of the V_s/V_t vs C curve should be 7.89, a difference of about 1.3% with respect to the reported value "8"; well within the reported experimental error.

APPENDIX 3

X-RAY OBSERVATION OF SUZUKI PHASES IN $NaCl:MnCl_2$

As mentioned in chapter 1, there have been several studies of Suzuki phases by X-ray diffraction. In the system $NaCl:MnCl_2$ there are studies by Chapman and Lilley (2), Sors (5) and Van Loon and Idjo (16). These last authors worked with Suzuki-phase crystals and found that the unit cell of the Suzuki phase is not exactly twice that of the NaCl(see chapter 1); whereas those studies on $NaCl:MnCl_2$ have been interpreted in terms of a lattice parameter exactly twice that of the NaCl matrix.

With a view to measuring the lattice parameter of the $6NaCl:MnCl_2$ in NaCl, Cano and Cordero (64) took diffractometer measurements from one of the crystals used in the present research, containing about 500 parts per million of Mn. Their results show that the Suzuki phase parameter is 11.24 $\pm$ 0.01 Å in good agreement with Van Loon and Idjo (16). Other peaks have been observed and they correspond to the 2 $NaCl:MnCl_2$ phas

The position of the peaks obtained is reproduced in table app-1

The author kindly acknowledges permission to use these unpublished results.

TABLE APP. 3

PEAK	d(A)	INDEXES
1	1.573 ± 0.001	(711) or (551)
2	1.900 ± 0.002	(531)
3	2.163 ± 0.002	(511) or (333)
4	3.399 ± 0.006	(311)
5	6.539 ± 0.017	(111)

Diffractometer measurements in a NaCl-$MnCl_2$ crystal (only peaks due to the Suzuki phase are reported). Taken from O. Cano and A. Cordero (unpublished work.)

APPENDIX 4

SOME GEOMETRICAL ASPECTS OF THE BOUNDARY BETWEEN NaCl AND THE SUZUKI PHASE

In general, to predict what the boundary between two crystals will be is very difficult given the large number of factors involved such as residual elastic strains, surface energies etc. However in some cases a purely geometrical approach due to Ballmann gives the possible boundaries between the two crystals (66-68). It is the purpose of this appendix to use this approach to predict the possible boundaries of Suzuki phases in alkali halides taking advantage of the fact that for crystals in parallel orientation the analysis is particularly simple.

Briefly Ballmann's approach consists of the following steps:
1) Only the lattices of the two crystals are considered; the basis attached to each lattice point is neglected in the first stages of the analysis and their influence is considered only afterwards. It is in this sense that the theory is "geometrical" (depending only on the spatial distribution of lattice points).
2) For any two given lattices, the O-lattice is constructed (for a description of the O-lattice see ref (68)). It is argued that the O-lattice gives the regions of good fit between the two crystals and hence gives the possible boundaries.

In what follows the notation used will be that of Ballmann (66).

The primitive cell of the alkali halide is given by the vectors a_1, a_2, a_3 defined as

$$a_1 = \frac{a}{2}\ (1,1,0)$$
$$a_2 = \frac{a}{2}\ (0,1,1)$$
$$a_3 = \frac{a}{2}\ (1,0,1)$$

with respect to a cartesian co-ordinate system, a is the lattice

parameter. If the Suzuki phase is also F.C.C. and grows in an orientation parallel to that of the matrix, its lattice is given by b_1, b_2, b_3 where

$$b_1 = \frac{a\alpha}{2} \quad (1,1,0)$$

$$b_2 = \frac{a\alpha}{2} \quad (0,1,1)$$

$$b_3 = \frac{a\alpha}{2} \quad (1,0,1)$$

and α is such that $a\alpha$ gives the lattice parameter for the Suzuki phase.

Then the matrix relating one lattice to the other is simply

$$A = \begin{pmatrix} \alpha & 0 & 0 \\ 0 & \alpha & 0 \\ 0 & 0 & \alpha \end{pmatrix} = \alpha I$$

where I is the identity matrix and it is assumed that $\alpha \neq 0$ (otherwise there is no lattice for the Suzuki phase) and $\alpha \neq 1$ (the two lattices differ in parameter).

The the O-lattice is given by all the points X^O defined by

$$X^O = (I - A^{-1})^{-1} b^2$$

where $\{b^2\}$ is the set of all lattice vectors, referred to the alkali halide matrix.

Thus

$$X^O = \frac{Ib^2}{(1-\frac{1}{\alpha})} = \gamma I b^2 = \gamma b^2$$

where γ is defined as $= \frac{1}{1-\frac{1}{\alpha}}$

Taking b^2 as a_1, a_2 and a_3 it is seen that the O-lattice is also f.c.c., it is parallel to the two lattices from which it is derived, and has lattice parameter γ.

This immediately suggests that (in the spirit of Ballmann's approach) the boundary between the matrix and the precipitate should be, in our case, composed of low index planes of the O-lattice and hence of high density, and this is in excellent agreement with the observed habits for the Suzuki phase.

In case α is a rational number, there is in addition a coincidence lattice between both lattices since $\alpha = n/m$ (for some n,m integer) and $n\, a_i = m\, b_i$ $(i = 1,2,3)$. Furthermore the coincidence lattice if f.c.c. and parallel to the original lattices with lattice parameter na.

Upon consideration of the "real" crystals (i.e. introducing the basis at each lattice point of both lattices) a constriction appears on the value of α; for as seen in chapter one the Suzuki phase has (100) planes that are NaCl-like. Thus α can not depart very much from 2 so there is good match between the NaCl-like planes of the Suzuki phase and the (100) planes of the NaCl lattice.

This approach gives the possible boundaries, but it does not indicate exactly which one is the actual one. That the Suzuki precipitates have a (100) boundary and not a (111) boundary (the most dense plane of the O-lattice) is related to the other factors neglected in the theory (the basis, for instance). Its virtue is that it gives the regions of "good match" and hence of lowest misfit.

REFERENCES

(1) K. Suzuki J. Phys. Soc. Japan 16 67 (1968)

(2) J.A. Chapman E. Lilley Jour. Mat. Sci. 10 1154 (1975)

(3) E. Lilley J.B. Newkirk Jour. Mat. Sci. 2 567 (1967)

(4) Yal-Jammal Unpublished, quoted by A.I. Sors and E. Lilley in Phys. Stat. Sol. (a) 27 469 (1975)

(5) A. Sors. PhD Thesis Sussex University (1973).

(6) A.J. Bannaghan D.R. Hayman P.L. Pratt in "Reactivity of Solids" edited by J.S. Anderson M.W. Roberts F.S. Stone Chapman and Hall, London (1972)

(7) K. Suzuki M. Phys. Soc. Japan 10 794 (1955)

(8) A.I. Sors E. Lilley Phys. Stat. Sol. (a) 32 533 (1975)

(9) A.R. Kahn PhD Thesis University of London, England (1967)

(10) M. Hartmanova G. Vlasak Journal de Physique 37 C-7 601 (1976)

(11) G.A. Andreev M. Hartmanova V.A. Klimov Phys. Stat. Sol. (a) 41 679 (1977)

(12) R. Capelletti A. Gainotti Journal de Physique 37 C7-317 (1976)

(13) M. Locatelli Jornal de Physique 37 C7-322 (1976)

(14) M.J. Yacaman G.A. Bassett J. Appl. Phys. 47 2313 (1976)

(15) K. Toman Czech. J. phys. B 12 542 (1962)

(16) C.J.J. Van Loon D.J.W. Idjo Acta Cryst. B31 770 (1975)

(17) A.I. Sors E. Lilley Phys. Stat. Sol. (a) 27 469 (1975)

(18) I.M. Boswarva Phys. Stat. Sol. (a) 37 65 (1976)

(19) M.J. Yacaman L.W. Hobbs M.J. Goringe Phys. Stat. Sol. (a) 39 K85 (1977)

(20) D.L. Kirk R.W. Innes Thin Solid Films 28 243 (1975)

(21) D.L. Kirk A.R. Kahn P.L. Pratt J. Phys. D 8 2013 (1975)

(22) G.A. Bassett M.J. Yacaman Thin Solid Films 31 375 (1976)

(23) M.J. Yacaman J.P. Hirth Thin Solid Films 38 215 (1976)

(24) G.A. Bassett Phil. Mag. 3 1042 (1958)

(25) S.C. Jain A.E. Hughes Journal de Physique 37 C7-463 (1976) (Supplementary issue to number 12)

(26) M.J. Yacaman D.R.W. Vook 35th Ann. Proc. Electron Microscopy Soc. Amer. Boston Mass 1967 pp. 258 ed. G.W. Barley

(27) D.L. Kirk P.L. Pratt Proc. Brit. Ceram. Soc. 9 215 (1967)

(28) G.D. Watkins Phys. Rev. 113 79 (1959)

(29) H.F. Symmons J. Phys. C. Solid State Physics 3 1846 (1970)

(30) P.A. Forrester E.E. Schneider Proc. Phys. Soc. London Sect. B 69 33 (1956)

(31) J.A. Chapman E. Lilley Journal de Physique 34 C-9-455 (1973)

(32) S. Unger M.N. Perlman Phys. Rev. B 10 3692 (1974)

(33) J.E. Strutt E. Lilley Phys. Stat. Sol. (a) 33 229 (1976)

(34) J.E. Strutt E. Lilley in "Reactivity of Solids" proceedings of the 7th International Symposium on the Reactivity of Solids, Bristol July 1972 pp. 34-96

(35) J.H. Crawford Jr. J. Phys. Chem. Solids 31 399 (1970)

(36) A.A. Chernov L.I. Trusov Sov. Phys. Cryst. 14 172 (1969)

(37) Niedermayer Private Comm. to M. J. Yacaman

(38) J.L. Robins T.H. Rhodin R.L. Gerlach J. Appl. Phys 37 3893 (1968)

(39) L. Levi Phil. Mag. 28 427 (1973)

(40) H. Bethge Phys. Stat. Sol. 2 3 (1962) and Phys. Stat. Sol. 2 775 (1962)

(41) L.W. Hobbs Harwell report AERE-R-7929 Oxfordshire England (1975)

(42) M. J. Yacaman A. Gomez G.A. Bassett Thin Solid Films 35 37 (1976)

(43) A. Oberlin M. Hucher Colloques Internationaux du Centre National de la Recherche Scientifique 152 407 (1965)

(44) H. Bethge Surf. Sci. 3 33 (1964)

(45) J. Serna L. Bru Anales de la Real Sociedad Española de Física y Química A 64 309 (1968)

(46) P.B. Hirsch A. Howie R.B. Nicholson D.W. Pashley M.J. Whelan in Electron Microscopy of Thin Crystals Butterworths (London) (1965)

(47) M.J. Yacaman A. Gomez Rodriguez Phil. Mag. 32 13 (1975)

(48) M. Kahlweit Progress in Sol. State. Chem. 2 151 (1965)

(49) D.C. Baird in Experimentation ed. Prentice Hall. Inc. New Jersey U.S.A. (1962)

(50) C.T. Forwood A.J. Forty Phil Mag. 11 1067 (1965)

(51) S.J. Burns W.W. Webb Jour Appl. Phys. 41 2073 (1970) and 41 2086 (1970)

(52) C.B. Duke L.S. Cota Araiza in "Surface Structure: Determination by electron diffraction and emission". Proceedings of the "Escuela Latino Americana de Fisica" Universidad Nacional Autonoma de Mexico, Mexico July 1974

(53) L. de Wainer Thin Solid Films 21 S-31 (1974)

(54) Z. Hornbogen Nucleation of Precipitates in Solid Solutions. In Nucleation Ed. Zetllemoyer, Marcel Dekker (1975).

(55) H. Riveros, Private Communications .

(56) J. Serna, L. Bru. Surface Science 12 369 (1968).

(57) M. José Yacamán, E. Pedrero Nieto. Jour Cryst. Growth 7 259 (1976).

(58) E. Cabrera, H. Riveros. Proceedings of the 15th meeting of the Sociedad Mexicana de Física, Morelia,Mich. México. November 1972, p.99

(59) I. M. Lifschitz, V.V. Slezov Sov. Phys. Jet p. 38 331 (1959) and J. Phys. Chem. Solids 19 35 (1961).

(60) C. Wagner, Z. Electrochen 65 581 (1961).

(61) M.J. Yacamán. Private Communications.

(62) M.J. Yacamán. Private Communications.

(63) J. P. Hirth, M.J. Yacaman and A. Gomez, to be published in Phil. Mag. (1978)

(64) O. Cano, A. Cordero (Unpublished; internal report Solid State Physics Department, U.N.A.M. , 1977).

(65) L. de Wainer PhD Thesis. University of Warwick 1977.

(66) W. Bollmann. Crystal defects and Crystalline interfaces Springer Verlag New York. Heidelberg. Berlin 1970.

(67) W. Bollmann. Phil. Mag. 16 363 and 383 (1967).

(68) D.A. Smith, R.C. Pond. Int. Met. Rev. Review 205 June 1976.